

Vitreo-retinal eye surgery robot : sustainable precision

Citation for published version (APA):

Meenink, H. C. M. (2011). *Vitreo-retinal eye surgery robot : sustainable precision*. [Phd Thesis 1 (Research TU/e / Graduation TU/e), Mechanical Engineering]. Technische Universiteit Eindhoven.
<https://doi.org/10.6100/IR717725>

DOI:

[10.6100/IR717725](https://doi.org/10.6100/IR717725)

Document status and date:

Published: 01/01/2011

Document Version:

Publisher's PDF, also known as Version of Record (includes final page, issue and volume numbers)

Please check the document version of this publication:

- A submitted manuscript is the version of the article upon submission and before peer-review. There can be important differences between the submitted version and the official published version of record. People interested in the research are advised to contact the author for the final version of the publication, or visit the DOI to the publisher's website.
- The final author version and the galley proof are versions of the publication after peer review.
- The final published version features the final layout of the paper including the volume, issue and page numbers.

[Link to publication](#)

General rights

Copyright and moral rights for the publications made accessible in the public portal are retained by the authors and/or other copyright owners and it is a condition of accessing publications that users recognise and abide by the legal requirements associated with these rights.

- Users may download and print one copy of any publication from the public portal for the purpose of private study or research.
- You may not further distribute the material or use it for any profit-making activity or commercial gain
- You may freely distribute the URL identifying the publication in the public portal.

If the publication is distributed under the terms of Article 25fa of the Dutch Copyright Act, indicated by the "Taverne" license above, please follow below link for the End User Agreement:

www.tue.nl/taverne

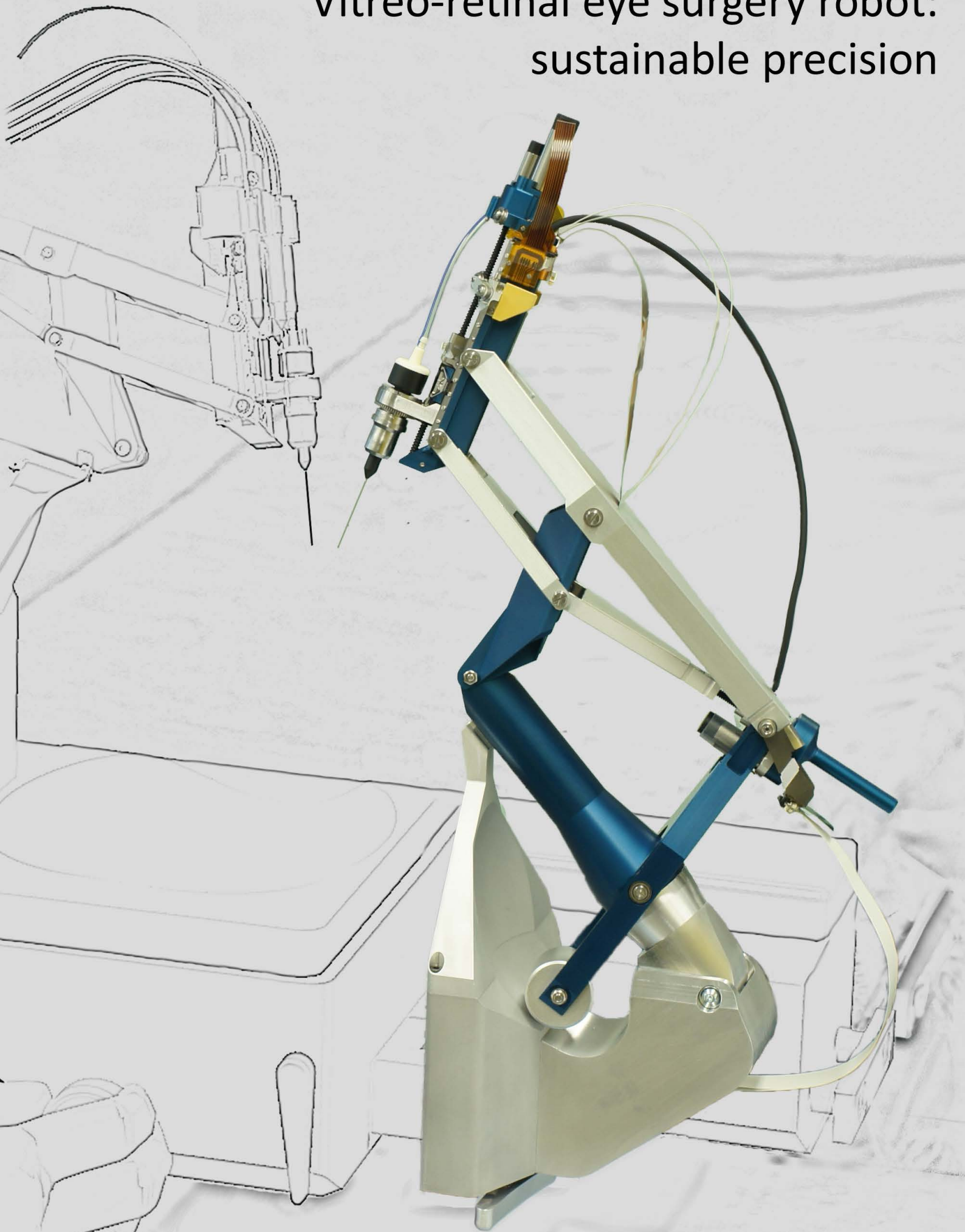
Take down policy

If you believe that this document breaches copyright please contact us at:

openaccess@tue.nl

providing details and we will investigate your claim.

Vitreo-retinal eye surgery robot: sustainable precision



Thijs Meenink

Vitreo-retinal eye surgery robot: sustainable precision

Thijs Meenink



This research was financially supported by the IOP Precision Technology program of the Dutch Ministry of Economic Affairs.

Vitreo-retinal eye surgery robot: sustainable precision

by H.C. M. Meenink

Eindhoven: Technische Universiteit Eindhoven, 2011 - Proefschrift

A catalogue record is available from the Eindhoven University of Technology Library.

ISBN: 978-90-386-2800-4

NUR: 978

Cover design: Thijs Meenink

Reproduction: Ipskamp Drukkers B.V., Enschede, The Netherlands

Copyright ©2011 by H.C.M. Meenink, All rights reserved.

Vitreoretinal eye surgery robot: sustainable precision

PROEFSCHRIFT

ter verkrijging van de graad doctor
aan de Technische Universiteit Eindhoven,
op gezag van rector magnificus, prof.dr.ir. C.J. van Duijn,
voor een commissie aangewezen door het College voor Promoties
in het openbaar te verdedigen
op maandag 31 oktober 2011 om 16.00 uur

door

Hildebert Christiaan Matthijs Meenink

geboren te Steenderen

Dit proefschrift is goedgekeurd door de promotoren:

prof.dr.ir. M. Steinbuch

en

prof.dr. M.D. de Smet

Copromotor:

dr.ir. P.C.J.N. Rosielle

Summary

Vitreo-retinal eye surgery encompasses the surgical procedures performed on the vitreous humour and the retina. A procedure typically consists of the removal of the vitreous humour, the peeling of a membrane and/or the repair of a retinal detachment. Vitreo-retinal surgery is performed minimal invasively. Small needle shaped instruments are inserted into the eye. Instruments are manipulated by hand in four degrees of freedom about the insertion point. Two rotations move the instrument tip laterally, in addition to a translation in axial instrument direction and a rotation about its longitudinal axis. The manipulation of the instrument tip, e.g. a gripping motion can be considered as a fifth degree of freedom.

While performing vitreo-retinal surgery manually, the surgeon faces various challenges. Typically, delicate micrometer range thick tissue is operated, for which steady hand movements and high accuracy instrument manipulation are required. Lateral instrument movements are inverted by the pivoting insertion point and scaled depending on the instrument insertion depth. A maximum of two instruments can be used simultaneously. There is nearly no perception of surgical forces, since most forces are below the human detection limit. Therefore, the surgeon relies only on visual feedback, obtained via a microscope or endoscope. Both vision systems force the surgeon to work in a static and non ergonomic body posture. Although the surgeon's proficiency improves throughout his career, hand tremor will become a problem at higher age.

Robotically assisted surgery with a master-slave system can assist the surgeon in these challenges. The slave system performs the actual surgery, by means of instrument manipulators which handle the instruments. The surgeon remains in control of the instruments by operating haptic interfaces via a master. Using electronic hardware and control software, the master and slave are connected. Amongst others, advantages as tremor filtering, up-scaled force feedback, down-scaled motions and stabilized instrument positioning will enhance dexterity on surgical tasks. Furthermore, providing the surgeon an ergonomic body posture will prolong the surgeon's career.

This thesis focuses on the design and realization of a high precision slave system for eye surgery.

The master-slave system uses a table mounted design, where the system is compact, lightweight, easy to setup and equipped to perform a complete intervention. The slave system consists of two main parts: the instrument manipulators and their passive support system. Requirements are derived from manual eye surgery, conversations with medical specialists and analysis of the human anatomy and vitreo-retinal interventions.

The passive support system provides a stiff connection between the instrument manipulator, patient and surgical table. Given the human anatomical diversity, pre-surgical adjustments can be made to allow the instrument manipulators to be positioned over each eye. Most of the support system is integrated within the patient's head rest. On either the left or right side, two exchangeable manipulator-support arms can be installed onto the support system, depending on the eye being operated upon. The compact, lightweight and easy to install design, allows for a short setup time and quick removal in case of a complication. The slave system's surgical reach is optimized to emulate manually performed surgery.

For bimanual instrument operation, two instrument manipulators are used. Additional instrument manipulators can be used for non-active tools e.g. an illumination probe or an endoscope. An instrument manipulator allows the same degrees of freedom and a similar reach as manually performed surgery. Instrument forces are measured to supply force feedback to the surgeon via haptic interfaces. The instrument manipulator is designed for high stiffness, is play free and has low friction to allow tissue manipulation with high accuracy. Each instrument manipulator is equipped with an on board instrument change system, by which instruments can be changed in a fast and secure way. A compact design near the instrument allows easy access to the surgical area, leaving room for the microscope and peripheral equipment.

The acceptance of a surgical robot for eye surgery mostly relies on equipment safety and reliability. The design of the slave system features various safety measures, e.g. a quick release mechanism for the instrument manipulator and additional locks on the pre-surgical adjustment fixation clamp. Additional safety measures are proposed, like a hard cover over the instrument manipulator and redundant control loops in the controlling FPGA. A method to fixate the patient's head to the head rest by use of a custom shaped polymer mask is proposed.

Two instrument manipulators and their passive support system have been realized so far, and the first experimental results confirm the designed low actuation torque and high precision performance.

Table of contents

Summary	v
Table of contents	vii
Chapter 1 Introduction	1
1.1 Robotics	1
1.1.1 Health care robotics	2
1.1.2 Surgical robotics	3
1.2 Eye surgery	5
1.3 EyeRHAS project	8
1.4 Master-slave system	10
1.5 Outline of the thesis	12
Chapter 2 Design requirements	13
2.1 General design requirements	13
2.1.1 Safety	13
2.1.2 Added value	15
2.1.3 Operating room layout	16
2.2 Vitreo-retinal eye surgery	17
2.2.1 Visualization with microscope and endoscope	19
2.2.2 Vitrectomy	20
2.2.3 Membrane peeling	24
2.2.4 Repair of retinal detachment	25
2.2.5 Cannulation	26
2.2.6 Forces involving ocular surgery and haptic performance	27
2.3 Human anatomical diversity	28
2.4 Robotic assisted eye surgery	30
2.4.1 Handheld tools	30
2.4.2 Robotic slave systems for eye surgery	32
Chapter 3 Surgical setup	35
3.1 Passive pre-surgical adjustment concepts	35

3.2	Design of the pre-surgical adjustment setup	40
3.2.1	X and Y adjustment	41
3.2.2	Short Z-arm	45
3.2.3	Tall Z-arm	50
3.2.4	Stiffness and eigenfrequencies	55
3.3	Instrument manipulator orientation	57
Chapter 4 Instrument manipulator		59
4.1	Requirements of the instrument manipulator	59
4.2	Concepts of manipulating Φ and ψ	60
4.2.1	Double rotor mechanism	60
4.2.2	Curvature rail mechanisms	61
4.2.3	Parallelogram mechanism	62
4.2.4	Concepts to manipulate θ and Z	63
4.3	Design characteristics of the instrument manipulator	64
4.4	Θ -Z manipulator	68
4.4.1	Θ -module	68
4.4.2	Bistable instrument clamp	69
4.4.3	Z manipulation	71
4.4.4	Onboard instrument change system	75
4.5	Manipulating Φ	80
4.5.1	Φ -drive	81
4.5.2	Ψ manipulation	81
4.6	Instrument manipulator stiffness and eigenfrequencies	87
4.7	Wiring and electronics of the instrument manipulator.	90
4.8	Realized manipulator	93
Chapter 5 Patient fixation, sterilization and safety.		95
5.1	Additional safety considerations	95
5.2	Sterility	97
5.3	Patient fixation	97
5.3.1	Eye fixation	98
5.3.2	Head fixation	98

Chapter 6 Conclusions and recommendations	101
6.1 Conclusions	101
6.2 Recommendations	103
Nomenclature	105
References	109
Appendix A Anatomical terms of location	115
Appendix B Calculations of the θ-manipulator	117
B.1 Resistance to manipulate Θ	117
B.2 Θ -bearing calculation	118
Appendix C Calculations of the Z-manipulator	121
C.1 Finite element analysis of the 2-DoF Z-carriage suspension	121
C.2 Finite element analysis of the 2-DoF Z-nut suspension	122
C.3 Relation between forces during an instrument change	123
Appendix D Analysis of the parallelogram mechanism	125
D.1 Finite element analysis of the parallelogram mechanism	125
Samenvatting	129
Dankwoord	131
Curriculum Vitae	133

Chapter 1

Introduction

Robotic systems are widely used. Most robotic systems have pre-programmed robots to perform repetitive tasks. Medical robots demand more versatility and a specific design for certain applications. Eye surgery, or in particular, vitreo-retinal eye surgery, is an application where a robotic system can assist the surgeon. This robotic system is desired to be a master-slave system, where the slave system performs the actual surgery, controlled by the surgeon at the master. As such, it can bring stability to enhance the surgeon's surgical skills, while the surgeon's knowledge and experience can still guide the process. This chapter gives some background information on robotics and describes some specific applications in medicine and vitreo-retinal eye surgery. The aim and approach of this thesis will also be discussed. The last section provides the outline of this thesis.

1.1 Robotics

Robots have been broadly introduced in many areas. They are most commonly used production processes, where pre-programmed robots do repetitive and/or accurate tasks in a consistent fashion. Initially, robots were designed to take over labour and thereby save labour costs. Robots have various advantages over humans:

- they are potentially faster,
- potentially cheaper,
- operate more accurately,
- can be used in hazardous environments,
- are able to handle heavy and large components,
- are able to get a consistent result,
- do not need (lunch/coffee) breaks and can be in service 24/7.

For example, multiple robots are used in the car production process to lift and position body panels, while other robots weld them together. Further on, at the assembly line,

robots lift and position heavy passenger doors or seats and mount them to the chassis. These industrial robots are designed for general multipurpose use. A specific end-effector tool and pre-programmed instructions make them suitable for one or a few dedicated tasks.

It is not possible for these systems to work in a dynamic environment, as it would require autonomous work on the part of the robot. An example of research on an autonomous robotic system is described in [71]. The focus of that paper is on the perception of doors and handles and what is needed to open and close them. These are some of the requirements for a personal robot to enter and function in a human living environment. The use of autonomous robotic systems does not imply that humans will soon become superfluous. Autonomous robots are not able (yet) to make complex decisions, like humans do.

Contrary to general robots, medical robots require more advanced robotic skills; they must be more versatile (e.g. adaptable to inconsistent situations) and at the same time specifically designed for a single application. Here, there is a trend going in two directions of:

- 1) health care robotics, to assist the patient, elderly or invalids,
- 2) surgical robotics, to assist the surgeon.

In the following two sections these trends are presented in more detail.

1.1.1 Health care robotics

Where pre-programmed robots are not able to make their own decisions, health care robots do need to adapt to their environment to fulfill the needs of the patient [28][72][82][86]. In societies facing an ever aging population, these care robots are designed to lower nursing costs and fulfill the increasing demand in care. Care robots must be capable of performing a variety of tasks like opening a door, switching on the light or get the patient a drink. Therefore, they must have multiple degrees of freedom (>6) and a multipurpose end-effector. Tasks can be applied by e.g.: a remote control or voice control. A learning ability is desired, as the environment might change and the demand to perform new tasks increase.

An example of such a robot is the Amigo robot created in the international RoboEarth project [82][86]. Here, the robot can learn skills from e.g. its own experience or by human feedback. Skills and other learning components are shared and stored online, hence sister robots can use and share the experience previously gained. In Figure 1.1, the amigo robot supplies a bottle of water taken from a fridge, to a patient in a hospital bed.



Figure 1.1/ The amigo care robot supplying a bottle of water to a patient [86].

1.1.2 Surgical robotics

Surgical robotics demand another type of robotic system. Here, the intent is to use and enhance surgical knowledge and skills [80]. The surgeon remains in control and the robotic system is an assistive tool. A master-slave system is a typical design for such a robotic device. Here, the slave system handles the surgical instruments/tools, while being controlled by the surgeon, through the master console. Such systems are called tele-operated robots. Although most interventions would require the surgeon to be in control, one of the first commercially available surgical robots (1994) was a pre-planned CAD/CAM robot (RoboDOC®), for robotic hip replacement surgery [17][62].

Figure 1.2 shows a current commercially available surgical master-slave system, the DaVinci® system by Intuitive Surgical [36], with on the left the surgeon console (master) and a patient-side cart (slave) in the middle. This system is designed for minimal invasive surgery (MIS), using long slender instruments (≈ 300 mm, $d = 8.5$ mm) to enter the human body via small incisions, often fitted with a trocar. MIS allows surgery to be performed with less trauma to the patient, reducing hospital stay, and the chance of complications. Compared to open surgery, MIS demands additional operating skills. Because instruments are manipulated outside the body, their movements inside the body are inverted and scaled by the instrument pivoting point (at the insertion site). Moreover, to reach the instruments the surgeon must make non-ergonomic movements to control them. The Da Vinci® surgeon console deals with these issues. It supplies a comfortable and ergonomic working position and enhances dexterity by scaling movements and controlling the tip of the instrument inside the body. A similarity between the hand movements and movements of the instrument tip

seen on vision system, in combination with the natural hand-eye instrument alignment, gives an intuitive way of working.

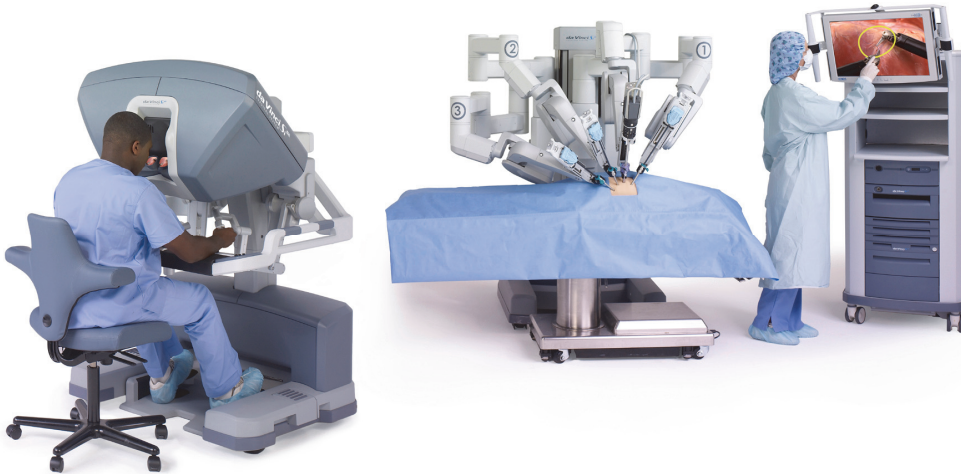


Figure 1.2/ The Intuitive Surgical Da Vinci® master-slave system, currently the most used robotic system in the operating room. In the middle, the slave part operates the patient, controlled by the surgeon at the master on the left [36].

In spite of the advantages of the Da Vinci® system, surgeons indicate that it is also desirable to have (i) a table mounted slave to ease table adjustments during surgery, (ii) instruments with additional degrees of freedom to extend organ approach capabilities, (iii) force feedback to re-introduce some sense to improve safety for tissue manipulation and reduction of operating time and (iv) a more compact slave design to ease approaching the patient and the field of surgery [7]. This is achieved with the *Sofie* robot (Figure 1.3), designed and realized at the TU/e [7].

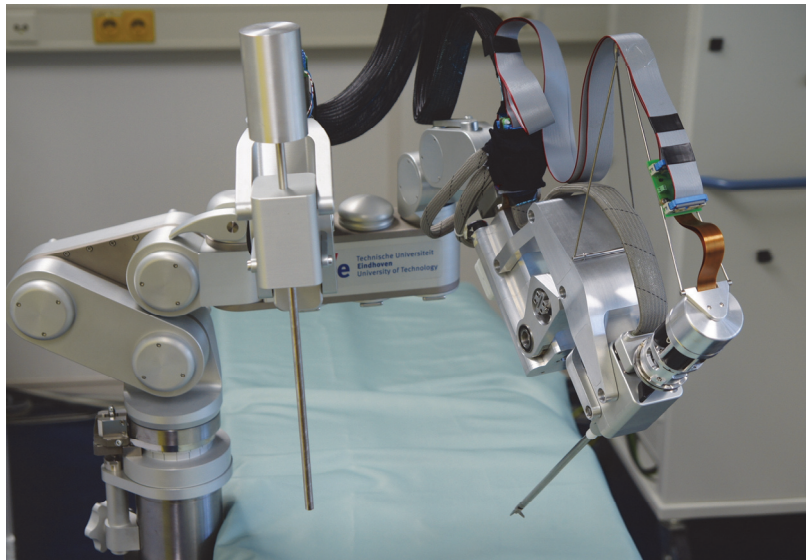


Figure 1.3/ Slave part of the Sofie robot, as designed and realized at the TU/e [7].

Eye surgery is performed using MIS-like instrument movements and also uses a non ergonomic body posture. Surgical procedures are performed without force feedback, yet in vitreo-retinal surgery for example, inappropriate manipulation of fragile and

highly specialized retinal structures can lead to their damage or loss. Force feedback and downscaled instrument movements would increase the surgeon's surgical accuracy [15]. It could allow him to perform delicate tasks such as microcannulation, which are difficult if not impossible to do manually [79]. Therefore, a master-slave system would also be highly useful for vitreo-retinal eye surgery.

1.2 Eye surgery

Eye surgery can be performed on both the inner and the outer side of the eyeball. External eye surgery on the rectus muscles controlling eye movement can correct strabismus (crossed-eye). Refractive surgery is often external, only affecting the cornea (LASIK¹ for example) or can be intraocular. Intraocular surgery can involve anterior eye structures (refractive cataract, or glaucoma surgery) or the posterior part (vitreoretinal surgery). By far, the majority of eye surgical cases are performed on the anterior part of the eye. It represents about 80% of all eye surgical interventions. While surgery to the anterior part is more commonly practiced, surgery to the posterior part is typically the most difficult and demands special surgical skills and expertise. Therefore, to become a vitreo-retinal surgeon, additional training is required beyond that of a normal ophthalmic surgeon. Most vitreo-retinal surgeons start their career in their mid 30's and end it somewhere in the late 50's. This is a relatively short time given the expertise required to excel in this field. Their skills could be enhanced and extended by use of a robotic system.

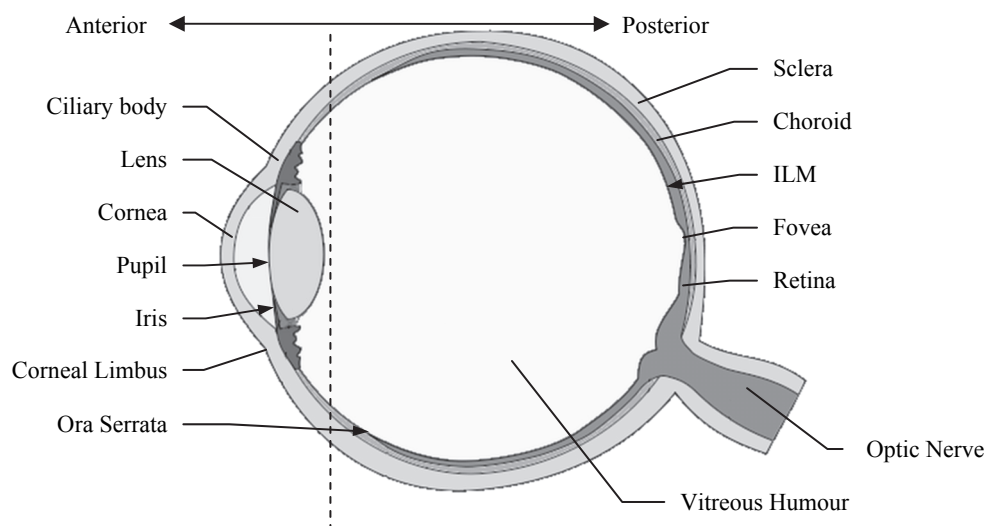


Figure 1.4/ Anatomy of the human eye. Surgery can be performed to the anterior as well as the posterior side of the eye. An explanation of the medical terms can be found in the nomenclature.

As the name implies, vitreo-retinal eye surgery relates to the vitreous humour and the retina. To make an image, light enters the eye through the cornea and the pupil. It is

¹ Laser-assisted in situ keratomileusis

focused by the lens and projected onto the retina. The retina generates an electrical impulse, partially integrates it into a vague image and sends this information via the optic nerve to the brain, which finally resolves the image. The pupil acts as the aperture on a camera. It limits the amount of light entering the eye to the amount needed to generate an image. While light is needed to generate an image, it also can damage retinal structures when too much of it is focused onto the retina [91].

Vitreo-retinal surgery is performed not-unlike MIS (Figure 1.5). Instruments enter the eye through surgeon made scleral openings, often fitted with a cannula. Instruments are about 30 mm in length, with a diameter of 27 up to 20 Gauge (respectively 0.42 to 0.81 mm). Small scleral openings induce less trauma which is desirable as it reduces the recovery time and reduces the chance of infection [64][67][68]. By using instruments with a diameter less than 23 gauge and using certain incision techniques [69], post operative suturing is not necessary further enhancing recovery [67].

To fully benefit from the advantages of small gauge surgery, it is preferred to apply the least amount of force on the scleral openings during surgery and thus, minimize the stress on the sclera. Therefore, instruments must be manipulated about the scleral openings, where it acts as a pivoting point and all degrees of freedom must intersect. This leaves four degrees of freedom to manipulate, three rotations (Φ , Ψ and Θ) and a translation in axial direction (Z). The manipulation of the instrument tip, e.g. a gripping motion can be considered as a fifth degree of freedom. Because instruments are manipulated on the outside of the eye, the pivoting insertion point inverts lateral movements (Φ and Ψ rotation) as well as scales the movement depending on the insertion depth of Z .

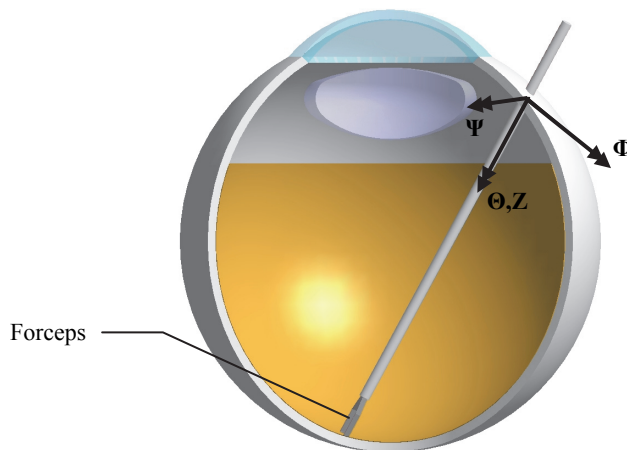


Figure 1.5/ An instrument can be manipulated in four degree of freedom (three rotations: Φ , Ψ and Θ and a translation in axial direction: Z) through the surgeon made scleral opening. The closing of for example a forceps is the fifth degree of freedom.

Before surgery starts, the patient is covered by a sterile drape (Figure 1.6). The drape has a transparent window, with an adhesive lower surface. The window is placed onto the eye. After it is cut open, eyelid retractors hold both this plastic foil and the eyelids open, creating an access to the surgical area, which is sealed from the rest of the

patient. It also prevents fluids (for example to moisten the eye) from seeping under through the drape, instead flowing over the drape into fluid collecting bags on the side. If possible only a local anesthetic is used to immobilize the eye and suppress pain.

The surgeon is sitting at the top end side of the surgical table in line with the patient's head (Figure 1.6). A microscope provides stereoscopic visual feedback, which gives a ≈ 5 to 25 times magnification of the operation area. Sterilization of the microscope is not possible and therefore it is covered with sterile plastic bags and caps. The microscope is provided with a second ocular at the side. There, an assistant can follow the surgery and anticipate the actions of the surgeon providing him with a new instrument or moistening the eye. During surgery, the surgeon rests his hands lightly on the patient's forehead. This allows the surgeon to orient himself in 3-dimensional space, as well as provide him added security as he is able to perceive any patient movement early. If the patient moves, the surgeon can quickly react by withdrawing the instruments.



Figure 1.6/ Project initiator: surgeon M.D. De Smet at vitreo retinal surgery. The surgeon is sitting at the top end side of the patient (covered by sterile drapes). The microscope gives a magnified, stereoscopic view of the operation area.

Characteristically, the manipulation of delicate intraocular tissue is required. By resting the hands on the patient's forehead, the shortest eye-instrument-hand force loop and the highest accuracy is achieved. The surgeon of course can only use two

instruments at any given moment. Often, one is an illumination probe, which leaves only one instrument for tissue manipulation. Forces are below the human detection limit of 0.06 N, which means that surgeons must rely on visual feedback only. The use of a microscope is of great importance, but forcing the surgeon in a static and non-ergonomic body posture.

Summarized, vitreo-retinal surgery is characterized by:

- small and inverted instrument movements, depending on the Z-insertion,
- manipulation of delicate, micrometers thick intraocular tissue,
- instrument forces, which are below the human detection limit (visual feedback only),
- a maximum number of two instruments simultaneously,
- a static and non ergonomic body posture.

1.3 EyeRHAS project

Several different robotic systems are able to assist a vitreo-retinal surgeon (Section 2.4), but none of these systems are suitable for a complete intervention or able to cover all the issues mentioned in the previous section. None is commercially available. Therefore, the *Eye Robot for Haptically Assisted Surgery* (EyeRHAS) project was started in 2006. The project was initiated by M.D. de Smet (UvA AMC) and is a collaboration of UvA AMC, TNO and TU/e. The project's goal was to create a working model of a master-slave system with force feedback for vitreo-retinal eye surgery. Figure 1.8 gives a schematic overview of the project layout and its subsystems.

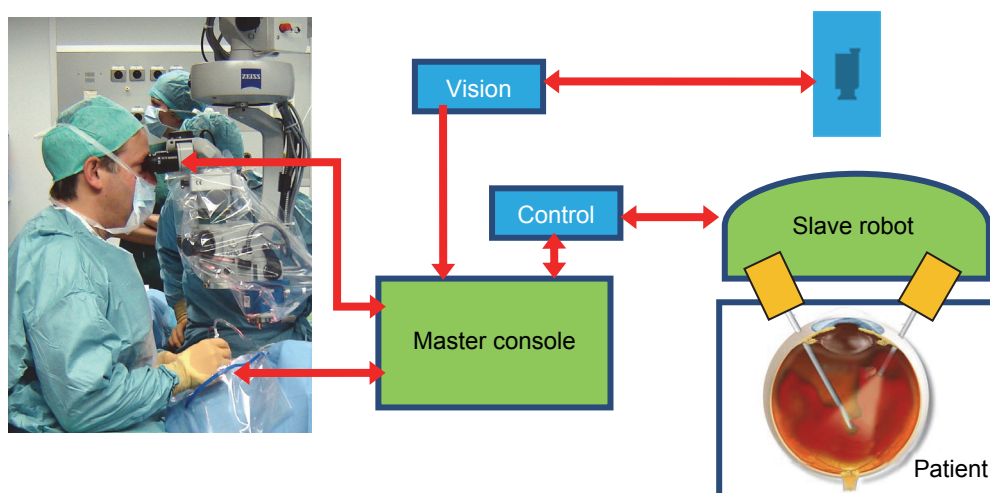


Figure 1.7/ A schematical overview of the EyeRHAS project. The goal is to realize a technology demonstrator of a master-slave system, to perform vitreo-retinal eye surgery. The system will have force feedback and will enhance the surgeon's dexterity. The project is financially supported by IOP precision technology program and is a collaboration of UvA, TNO and TU/e.

Four subsystems cover the EyeRHAS project.

- 1) The master console, where the surgeon controls haptic interfaces, which provide the motion input for the instrument manipulators of the slave system. This master with force feedback and scaling of hand motions extends existing surgical skills to perform surgery on the vitreous humour and the retina. The design and realization of the master console was the successful PhD research of R. Hendrix recently completed also at the TU/e [33].
- 2) The slave system performs the actual surgery by way of instrument manipulators that directly handle the instruments. For bimanual surgery, at least two instrument manipulators are required of high accuracy and which can reach the major parts of the posterior inner eye. The slave must be adjustable to fit the requirements of the patient head and must be equipped to perform a complete intervention. Furthermore, it provides the information for force feedback. The design and realization of the slave system was designed as a second PhD research project and is the subject of this thesis.
- 3) Control comprehends the electronics and software between the master and slave hardware. This subsystem consists of the power supplies, motor amplifiers, data acquisition and control hardware with appropriate control algorithms and safety features. At least a bilateral control scheme is required for the position tracking and force feedback between master and slave.
- 4) With a master-slave system there can be an increase in distance between surgeon and patient. This means that the surgeon may choose to not use the binocular of the microscope. Implementation of an alternative system for the visual feedback is covered in the fourth subsystem: vision.

Summarized, the combination of these subsystems allows numerous advantages over manually performed surgery, like:

- hand tremor filtering,
- filtering of sudden movements (shock, like a shiver or cold),
- downscaled movements,
- upscaled force feedback,
- putting the system on hold,
- possible new interventions,
- automation of simple tasks,
- additional safety features can be incorporated ,
- pre-surgical practice or simulation of intervention in a virtual environment,
- surgeons do not necessarily have to be in the same room as the patient,
- using multispectral imaging and today's high resolution, high contrast 3D-monitors, additional tissue information might be obtained and used in real time.

1.4 Master-slave system

The goal of this thesis is to design and realize the slave part of the EyeRHAS technology demonstrator to perform vitreo-retinal surgery.

Figure 1.8 shows a typical representation of a master-setup for vitreo-retinal surgery. Like manually performed surgery, the surgeon is sitting at the top end side of the surgical table. The master-slave system uses a table mounted design (Figure 1.8), where the design is set to be a compact, lightweight, easy to setup system and equipped to perform a complete intervention. The slave system consists of two main parts: the instrument manipulators (IMs) which handle the instruments and their passive support system.

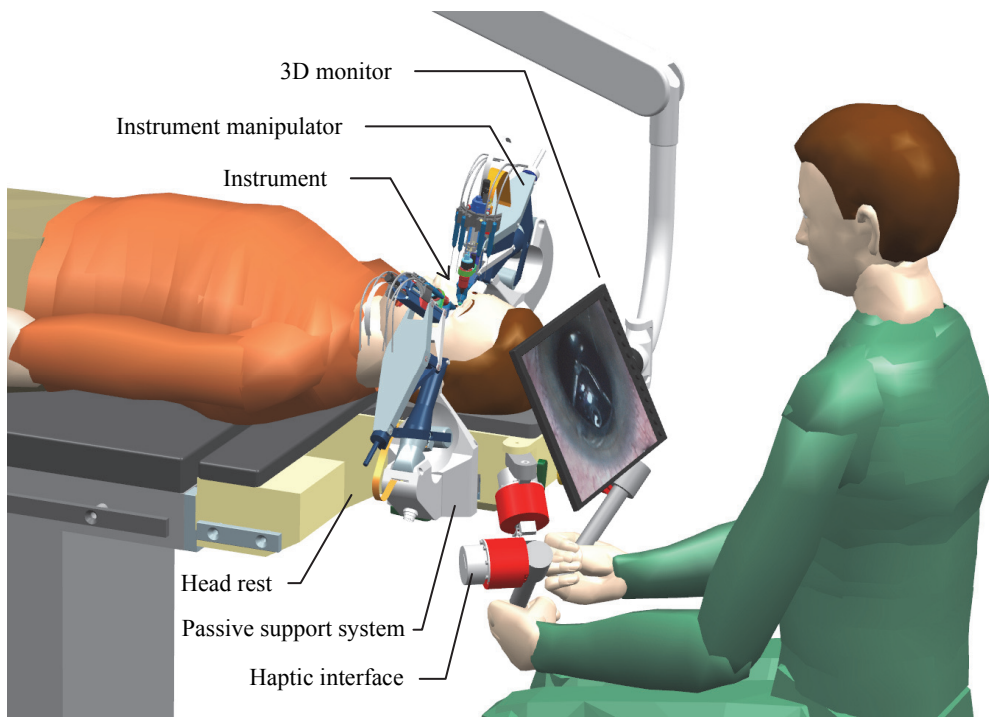


Figure 1.8/ Schematic representation of a master-slave setup for vitreo-retinal eye surgery. The instrument manipulators handle the instrument, controlled by the surgeon via haptic interfaces.

For bimanual operation of the instrument, at least two instrument manipulators are used. Additional instrument manipulators can be used for non-active tools e.g. an illumination probe or an endoscope. During surgery, various instruments are used interchangeably, therefore, each instrument manipulator is equipped with an on board instrument change system. Instruments can be changed in a fast and secure way. The instrument manipulator is designed for high stiffness, is play free and has low friction to allow a high accurate tissue manipulation and an accurate force measurement as feed back to the haptic interfaces. The slave system's surgical reach is optimized to emulate manually performed surgery. The compact design near the instrument allows easy access to the surgical area, and it leaves room for the microscope and peripheral equipment.

The passive support setup provides a stiff connection between the instrument manipulator, patient and surgical table. Given the human anatomical diversity, pre-surgical adjustments are required to allow the instrument manipulators to be positioned over each eye (Figure 1.8). Most of the support system is integrated within the patient's head rest. On either the left or right side, two exchangeable manipulator-support arms can be installed onto the support system, depending on the eye being operated upon. A compact, lightweight and easy to install design, allows for a short setup time and quick removal in case of a complication. The compact and table mounted design, also allows direct patient access, leaves legroom for the surgeon and allows foot-switches to be used as desired.

Integrated into the setup shown in Figure 1.8 is the master console [33]. The main components of the master console are two haptic interfaces [34] controlled by the surgeon and a vision system e.g. a 3D-display for visual feedback. A comfortable and intuitive working environment was designed allowing manipulations of the haptic interfaces to simulate movements of the instrument tip inside the eye. Therefore the geometry of the degrees of freedom are placed as indicated in (Figure 1.5). All degrees of freedom in the master are optimized mechanically, back drivable and equipped with an electric motor to provide a very accurate force feedback and position input for the instrument manipulators. Early functional tests of the master system coupled to an endoscopic slave system confirmed that its use was intuitive [7][33].

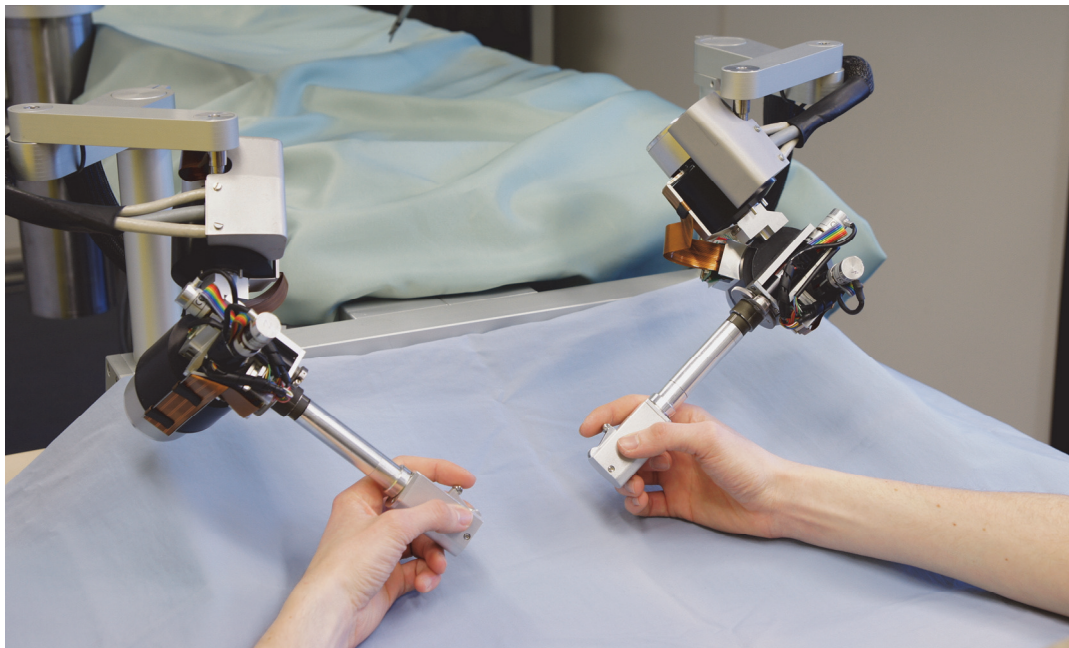


Figure 1.9/ Two haptic interfaces for bimanual instrument control as realized for the EyeRHAS project [33].

1.5 Outline of the thesis

The requirements for the slave system are formulated in Chapter 2. These requirements are derived from discussions with surgeons, observations in the operating theater and analysis of vitreo-retinal eye surgery. This is followed by an overview of existing systems for vitreo-retinal eye surgery.

In Chapter 3, several concepts and considerations of the slave setup, c.q. the pre-surgical adjustment system are discussed. While all concepts are table mounted, differences exist in the approach from the table to the eye. Concepts vary in compactness, stiffness and access to the eye. One concept is selected and discussed in detail. At the end, the most optimal instrument manipulator layout is discussed in detail

The instrument manipulator is discussed in Chapter 4. First different concepts are discussed of which one is selected. Similar to Chapter 3, the design and realization of this concept is described in detail.

In Chapter 5 some safety considerations are pointed out. The fixation of the patient's head is discussed in considerable detail.

Conclusions and recommendations are given in Chapter 6.

Chapter 2

Design requirements

In this chapter, the design requirements are discussed. Requirements are derived from discussions with vitreo-retinal specialists, visits to the operating theater and the literature. First, general design requirements are discussed, based on safety and added value. Second, vitreo-retinal surgery is discussed, from which some of the performance requirements are derived. Then, requirements are discussed, to make the slave robot suitable for use in humans given their anatomical diversity. In the last part, other robotic systems for vitreo-retinal surgery are discussed. Characteristics are coded by an R for requirement, an S, V and P for respectively: safety, added value and performance. With these codes the characteristics and requirements are referred to in the subsequent chapters.

2.1 General design requirements

2.1.1 Safety

In order to design a medical system which is intended to be commercially available, it has to meet local regulations, e.g. CE for Europe. Regardless of the purpose of the medical device, one single requirement stands above all: it must be safe! This applies not only for the patient, but for the surgical staff as well.

Mechanical safety is the basic requirement for a robot. Most early papers mention, redundant components e.g. sensor/end-switches, mechanical constraints, fault detection systems and control strategies to achieve this goal [24][26][27][29][40][81]. Taylor et.al. [81] points out four basic safety requirements for robotic surgery. Although initially set up for an orthopedic bone machining robot, these requirements hold true for most surgical robots, they are:

- the robot should never “run away”,

- the robot should never exert excessive force on the patient,
- the robot's cutter (or instrument tip) should stay within a pre-specified positional envelope,
- the surgeon must be "in charge" at all times.

Kazanzides [40] indicated that a surgical robotic system must be either *fail-safe* or *fault-tolerant*. A fail-safe system is allowed to fail, as long as failure causes it to enter a safe state. In contrast, a fault-tolerant system must continue to operate even in the presence of failures.

Although various safety properties are proposed, there aren't yet specific standard safety guidelines for medical robotics [13][26][40]. It is nevertheless prudent to apply good engineering design concepts and by necessity satisfy all regulatory requirements and general medical device standards such as NEN 14971, 60601-1-6 and 62366. To obtain for example CE approval, every aspect must be documented and various tests must be performed. In relation to the latter, a certain number of clinical trials must also be performed to prove the system's safety and in turn, must be documented. This implies that the intended goal, a working demonstration model, does not necessarily need to meet CE regulations. It is chosen only to set some fundamental safety requirements which relate to the mechanical design. These are presented below.

- RS1** Instruments are manipulated in a minimally invasive fashion. Their degrees of freedom must intersect at the entry point to the eye, creating a pivoting point. During surgery, this pivoting point may not drift and must be constrained passively. This leads to intrinsic safety, where in case of system malfunction the medical parts cannot exert force onto the scleral openings.
- RS2** The instrument manipulators must be gravity balanced, by which the degrees of freedom cannot drift, in case of malfunction (e.g. power loss).
- RS3** Backdrivable instrument manipulators allow the inactive degrees of freedom to be manually overruled.
- RS4** Interactions with the instrument manipulator during surgery may not lead to excessive drift. Ideally, a force of 1 N may not lead to an inaccuracy of over 10 μm (related to RP3). Thus the stiffness must be at least 100 N/mm.
- RS5** Common biocompatible materials must be used for parts which could show wear, so that particles excreted cannot harm the patient. For example: stainless steel AISI 420, AISI 316 or titanium when metals are required and PPSU, POM or UHMWPE for plastics [9].
- RS6** Easy removal of both the instrument manipulator and the passive support system, will contribute to a fast transition to manual surgery, where the first few minutes are crucial in case of a complication.

Some additional safety aspects are not (yet) set as a requirement, for example highly accurate instrument manipulation contributes to the ease of use by the surgeon or the ability of measuring forces helps detecting excessive force applied on the patient or a given tissue.

2.1.2 Added value

The second most important requirement is to make the surgical robot commercially attractive. This holds true when such a system has added values over manually performed surgery [13].

Performing surgery more quickly, efficiently and with less personnel, directly affects surgical costs. It reduces labour costs and possibly allows more patients to be operated per day. This consequently shortens waiting lists. Requirements to perform surgery as quickly as possible are presented below.

- RV1** High accuracy tissue manipulation, to make surgical tasks easier and possibly faster. This is quantified in the Section 2.2.
- RV2** Changing instruments rapidly via e.g. an automated instruments change system, preferable onboard of the instrument manipulator.
- RV3** Short installation and removal time. This implies an easy to setup system, which is compact, has a low mass and is easy and quick to adjust. Here, a single staff member must be able to install modules, by holding them single handed and control the installation and fixation by the other. Max. 2 kg is considered to be allowed for easy module handling.
- RV4** Obviously, a short instrument manipulator preparation time is desired as well.

Shorter recovery time has an indirect commercial added value, as patients on sick leave cost money and healthy working people gain money with respect to health insurance and hospital stay. Moreover, amongst others, it requires fewer medications to control inflammation and infections, shorter hospital stays and less nursing staff etc., which implies less medical costs. Robotic surgery can contribute by more accurately manipulating tissues (RV1) that require surgery and leave healthy tissue unharmed.

Robotic surgery, by the passive constraints on the pivoting points at the scleral entrance controlling forces acting on the scleral openings (RS1), may limit damage to the tissue. In the last decade, vitreo-retinal interventions are performed more and more frequently without the need for scleral sutures. In sutureless surgery, wound construction is optimized and self sealing (Section 2.2). Optimized wound construction results in rapid healing and less chance of infection. It is required that:

- RV5** vitreo-retinal robotic surgery is performed sutureless.

New interventions which are not/hardly possible manually, may lead to more surgical procedures, thus can be commercially attractive from a hospital view point. While this may increase the future value of the system, the initial focus of this project is to develop a robotic system for use with conventional instruments and for existing vitreo-retinal procedures. Novel procedures which extend slightly beyond the limits of current surgery are also considered such as the cannulation of retinal veins.

RV6 The instrument manipulator must be suitable for conventional vitreo-retinal procedures, extended with procedures performed in a similar fashion, which are hard to perform manually.

Better surgical quality leads to less complications, more successful interventions and should directly affect the recovery time and quality of life. Requirements comprise RV1-RV6.

2.1.3 Operating room layout

Based on current operating room arrangements, a surgical layout for the placement of the master device is suggested in [33]. It proposes that a table mounted console at the top end, is preferred over a floor standing or ceiling mounted system. This allows the position of the surgical assistant as well as peripheral equipment to be maintained and in arms reach. It is required to fit the slave system in this layout as well, the two main reasons being the surgical ergonomics and the mechanical design of the slave.

With respect to the ergonomics, a table mounted slave does not claim floor space or space which is necessary for a comfortable seating position. An ergonomic surgical body posture can be supplied and the floor is free for the usual foot switches. The surgeon's legs can be situated under the surgical table. For the surgeon, this ensures access to the patient and the possibility to use the microscope as in manual surgery. This feature could be seen as an added security in case robotic surgery should not provide adequate control on the operative situation or in conditions of training. A switch from robotically assisted surgery to manual surgery under these circumstances would imply an easy transition, when the patient is within arms reach of the surgeon.

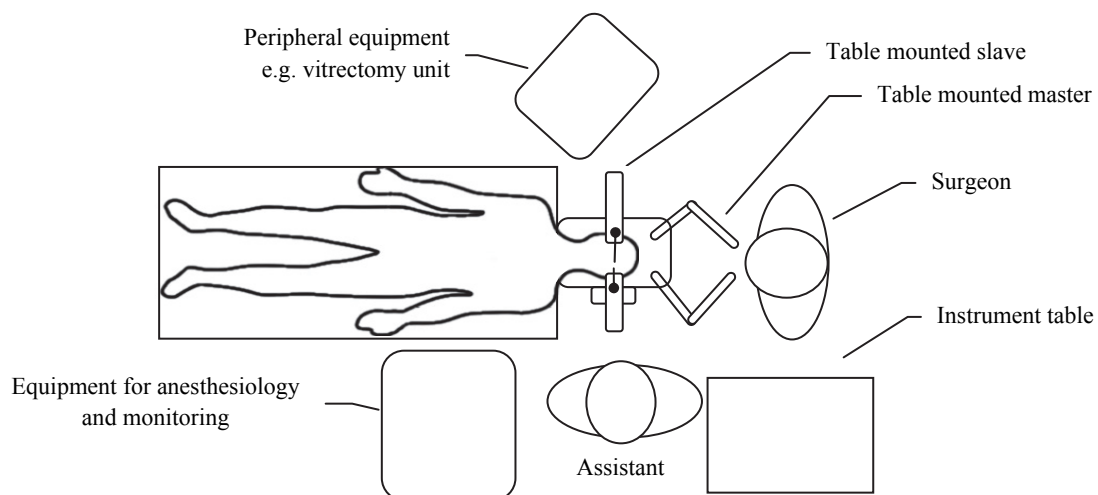


Figure 2.1/ A typical operation room layout for eye surgery. It is preferred to maintain the current operating room layout, where the patient and peripheral equipment is within arms reach. A table mounted slave system is compact and contributes to this.

From a mechanical point of view, a table mounted slave system minimizes the eye-instrument force loop, increasing the possibility for highly accurate instrument

manipulation. However, contrary to a ceiling mounted or a floor standing system, it may not as easily be driven or swung away when the operating room must be used for non-ocular surgery. Therefore, an easy to install, lightweight and compact system must be designed, where installation time as well as the time to uninstall is only a few minutes. Requirement RS6 and RV3 relate to this, moreover:

- RV7** the slave system must be table mounted,
- RV8** the slave must be compact to facilitate its use in current operating room settings,
- RV9** the lowest number of degrees of freedom are desired to position the instrument manipulator,
- RV10** straight forward adjustable degrees of freedom contribute to easy adjustment.

2.2 Vitreo-retinal eye surgery

The system's performance requirements are determined by a range of procedures performed during vitreo-retinal surgery. As representative of the types of manipulations done during surgery, three typical interventions were considered: vitrectomy, membrane peeling and retinal detachment. Often a combination of these tasks is carried out. In addition, retinal vein cannulation is discussed.

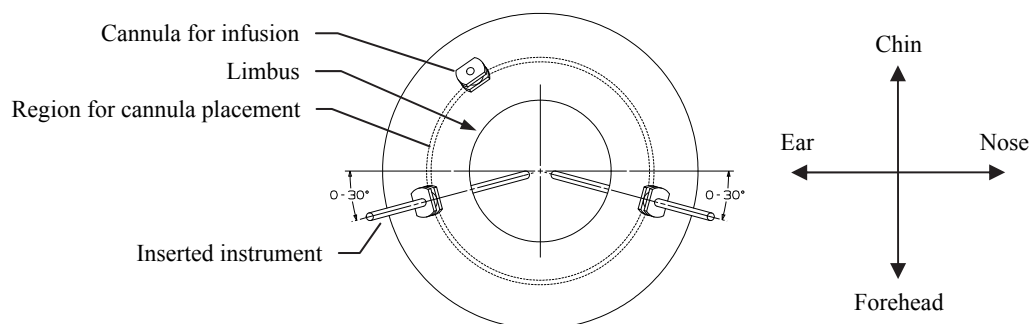


Figure 2.2/ The typical instrument layout during manually performed vitreo-retinal surgery for the left eye. Cannula placement is only possible at a distance of 3-4 mm from the corneal limbus. The placement depends on the preferred area to reach and the surgeon's preferred way of working.

A surgeon uses two instruments simultaneously, which requires two scleral openings commonly fitted with a cannula (or trocar). One instrument is inserted at the nasal side and the other at the outer lateral side (Figure 2.2). This layout provides a large working area and a natural simultaneous operation for the left and right hand. The incision placement can vary from opposing each other, up to 30° with respect to the transverse plane (Figure 2.2). This depends on the preferred area to reach and the preferred way of working of the surgeon. A third opening is made for an infusion, also often fitted with a cannula. Additional openings are sometimes made in the sclera

to position a lighting system. In the context of robotic assisted surgery, it is conceivable that additional instruments would be inserted through additional openings. For the robot, it is desired to have a similar layout to surgery performed manually, as it provides the largest working area and provides an intuitive and familiar way of working, therefore:

RP1 at least two instrument manipulators must be available to allow bimanual surgery.

Cannulas

Cannulas (or trocars) are mostly used with the smaller sized instruments: 27, 25 and 23 gauge (respectively: 0.42, 0.51 and 0.61 mm in diameter). Without cannulas, the small openings tend to close [23][67][69] and as a result, are hard to find and re-enter when changing an instrument. Moreover, cannulas reduce stress and trauma induced instrument insertion and manipulation. Cannulas are placed prior to any surgery.



Figure 2.3/ Example of a 23 Gauge (0.6 mm) stiletto with cannula attached onto the shaft, for one-step cannula placement.

The cannula is placed by use of a stiletto (one-step cannula placement [22]). Here, the cannula is pre-fitted onto the shaft of the stiletto. First, the incision is made by the trapezoidal cutting section at the tip. Thereafter, the stiletto is inserted fully until the cannula is placed correctly. While removing the stiletto, the cannula is left behind at the sclera.

To prevent penetration of the retina or ciliary body, scleral openings must be made at 3-4 mm from the corneal limbus [69] (illustrated in Figure 2.2). Special insertion techniques are proposed for sutureless surgery using a two-stepped beveled incision, providing an optimal wound construction and recovery (e.g. Zorro or Rizzo technique [67][69]). The proposed technique starts with an oblique angle of about 45° (Figure 2.4) with respect to the normal vector of the eyeball (at insertion). Once the blade is engaged in the sclera about the length of the cutting blade, it is turned perpendicular to the scleral surface and inserted further into the eye in the direction of the optic nerve until the trocar reaches the surface of the sclera. The tunnel of the scleral opening may either be parallel to the corneal limbus, or it can run a posterior-anterior course [67]. At the latter, when the stiletto's blade surface is facing upwards, the

incision is made parallel to the scleral fibers (Figure 2.4). As such, the fibers are mostly spread apart and not completely torn apart.

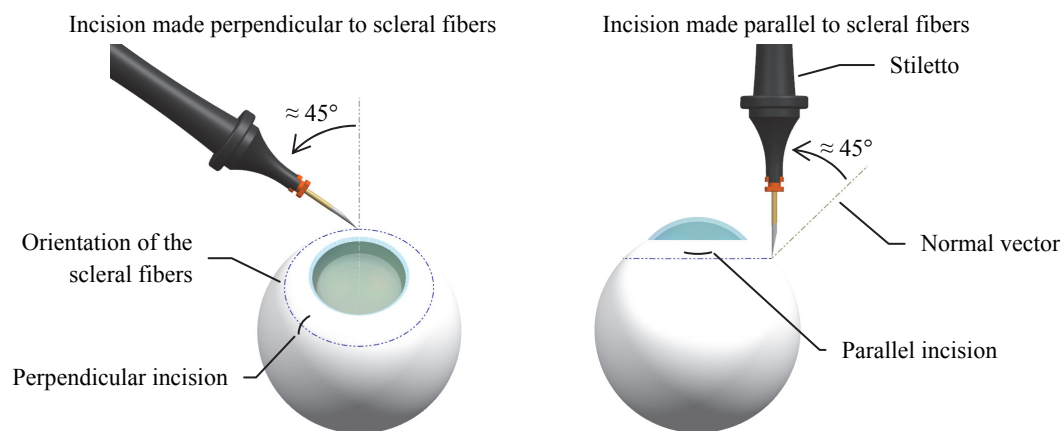


Figure 2.4/ Oblique incision techniques. Left, the scleral tunnel is made parallel to the corneal limbus, by which the incision is made perpendicular to the scleral fibers. On the right, the tunnel is made in an anterior-posterior orientation, where the incision is made parallel to the scleral fibers.

After surgery, massaging the wound is sufficient to close the wound and provide a sufficiently watertight closure. It is self sealing thanks to the inner ocular pressure, and provided that the initial wound has not been extended by stretching or tearing around the edges of the cannula. In most cases additional sutures to provide a water tight closure are not necessary. Robotic surgery can contribute to an optimal insertion by:

- RP2** Automated cannula placement, for sutureless insertion techniques. More specifically, the incision angle must be 45° with respect the normal vector of the eyeball at the point of insertion.

In the following, four vitreo-retinal interventions are discussed, on which the respective performance requirements are based. All discussed interventions can be performed by sutureless surgery (< 23 Gauge).

2.2.1 Visualization with microscope and endoscope

During vitreo-retinal surgery, vision provides the most important sensory feedback, since the sense of touch is lacking as most forces are below the detection limit [30]. The use of a microscope provides stereo vision and has no limitations with respect to image quality. A 2D endoscope has the ability to visualize regions that cannot be reached by the microscope e.g. the far peripheral retina or the subretinal space of a retinal detachment. Furthermore, it allows visualization in the posterior cavity, when normal visualization through the lens is compromised [74][75]. However, the image quality provided by current endoscopes is inferior to that of a microscope.

Microscope

The microscope uses large glass elements, to gather as much light as possible for visualization. The enlargement of the image and the focusing system for objects close to the lens requires a large column of lenses. This makes the microscope bulky and tall (see Figure 1.6). To look through the ocular, surgeons have to reach out, which is counter to an ergonomic seating position. For eye surgery, the microscope can switch focus, between the fundus inside and the sclera outside the eye. This is realized by a zoom and focus function or by a wide angle fundus observation system, which is placed in one hand movement between the microscope and the eye. Because microscopes are expensive and they are available to use in the current operating room setting, for robotic surgery, it is required to be able to use them in combination with the slave manipulator, in an unobstructed way.

Endoscope

The endoscope is used like other vitreo-retinal instruments. It is similar in construction to an endo-illuminator (see Section 2.2.2). Currently, endoscopes for eye surgery have a diameter of 20 Gauge (0.9 mm), by which their scleral openings are not suitable for sutureless surgery. The small diameter brings limitations with respect to image quality. Each pixel has its own optical fiber, up to date, the image resolution is limited to 20-30K pixels. Nevertheless, the sight from within the eye and the viewing angle of 110° , allows intraocular zones to be visualized and assessed that cannot be seen or are difficult to reach with the microscope [16][25]. The current endoscopes are based on technology developed in the 1980's. There have been no advances made in the last decades. In time, limitations in design, image quality and size reduction will probably improve. At manual surgery, the surgeon controls the endoscope with one hand, leaving only one hand to manipulate an actual instrument. Robotic surgery could significantly improve endoscopic surgery by providing a third instrument manipulator to safely hold the endoscope in the eye and provide an appropriate orientation and distance from the retina. Such a manipulator could be a simplified version of manipulator that handles the surgical instruments.

RV11 The slave robot must be suitable for surgery by use of: a microscope as well as an endoscope. This implies a compact slave design where the surgeon can reach the eye pieces of the microscope. There must be room for the microscope and its light envelope and/or a third (simplified) endoscope manipulator. The instrument manipulator must be suitable to handle an endoscope.

2.2.2 Vitrectomy

Removing the vitreous humour (or vitreous in short) is called vitrectomy and is performed at the onset of all retinal procedures. It is the most commonly performed

step in vitreo-retinal surgery. The vitreous is a transparent substance, which fills the posterior chamber of the eye. It mainly consists of water (96%), protein (3%) and salt (1%). A tangled network of collagen fibrils and hyaluronic acid (both biopolymers) give the vitreous humour viscoelastic properties [9][57].

The latter, makes moving instruments through the vitreous very difficult. Traction on the viscoelastic gel, can also lead to the formation of tears in the retina (as the gel pulls on the retinal surface). Such tears can lead to retinal detachments, a serious complication, which if allowed to occur and left untreated, can lead to blindness. Therefore, vitrectomy is not only performed in case of a complication, but also preventively [67]. Via an infusion, the removed vitreous is replaced by a balanced salt solution. The infusion controls the inner ocular pressure and maintains the shape of the eye. The balanced salt solution allows an easier and more accurate movement of instrument.

With aging, the vitreous separates from the retinal surface. Its separation can lead to a number of complications in the eye, examples of which are: vitreous hemorrhage and the formation of a macular hole. Vitreous hemorrhage is caused by a retinal vein bleeding into the vitreous humour. This blurs the vitreous and prevents light from reaching the retina. Macular holes form as the vitreous shrinks with age [2], leading to traction on the macula and formation of a hole.

Vitrectome

Vitrectomy is performed by use of a vitrectome (Figure 2.5). The vitrectome simultaneously cuts the vitreous and sucks the cut particles away. It consists of two coaxial tubes. The outer tube is fixed to the body of the handle and has a port opening along its cylindrical surface, adjacent to its (closed) tip (Figure 2.5, left image). The inner tube is actuated axially and acts like a guillotine. It cuts the vitreous, when its tip moves past the outer tube's opening. Actuation is done pneumatically, with a cutting rate up to 2500 cuts per minute [22]. Aspiration is done via the inner tube. The tube extends towards the rear end of the vitrectome, where fluid is aspirated via a hose.

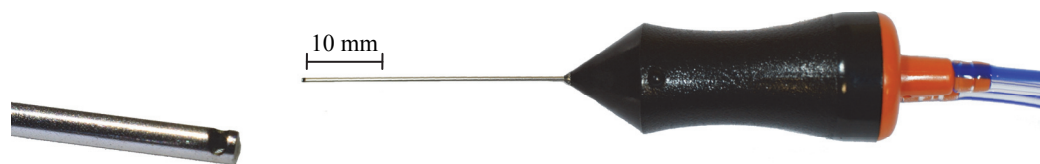


Figure 2.5/ Example of a 23 Gauge vitrectome mostly used to remove the vitreous humour. Via a port opening on the side of the tip, the vitreous is cut and sucked away.

Vitrectomy does not particularly require the highest accuracy. However, as the vitreous fills the complete posterior cavity, it does require a large reach. On average, the eye has a lateral diameter of 24.2 mm and an axial length of 23 mm [5][14].

Anatomically, the lateral diameter does not vary much. However, the axial length can measure up to 31 mm in highly myopic eyes [19][55][85] (measured from the tip of the cornea, to the opposite end of the eyeball). This requires an instrument length of at least 28.5 mm (determined from the scleral opening, to the rear of the eye). The reach on the rotation sideways (Φ and Ψ , see Figure 1.5), has in practice two limitations. Firstly, it is desirable that the Φ and Ψ rotations are limited to $\pm 45^\circ$, to protect the sclera against a too large deformation. Secondly, direct contact between the shaft of the instrument and the lens is unwanted, as damage can result in a cataract.

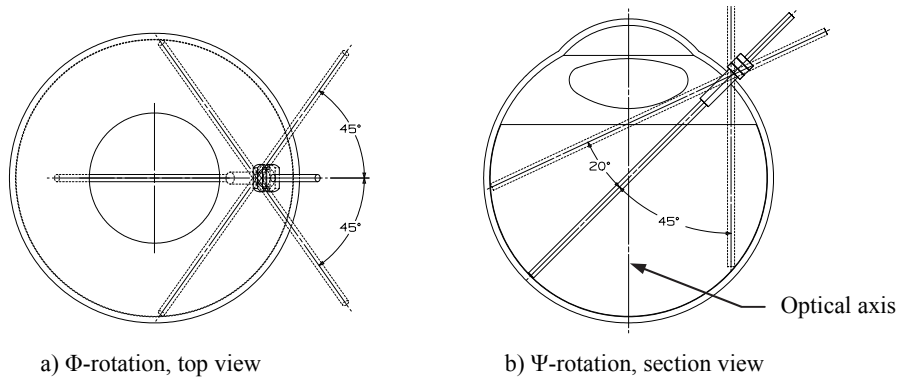


Figure 2.6/ Range of motion for a rotation around the principal Φ and Ψ axis.

Figure 2.6 gives an overview of the working area for the two principal axes of rotation. The nominal instrument angle varies between $43\text{--}48^\circ$ with respect to the optical axis as it depends on the distance between cannula and limbus (3-4 mm). Here, an angle of 45° is used.

Based on these figures, the working reach becomes $\Phi = \pm 45^\circ$ and $-20^\circ < \Psi < 45^\circ$. However, as it is desired to allow surgery at the side of the lens, it is preferred to extend the Ψ reach to $-35^\circ < \Psi < 45^\circ$. In Θ -direction, it is required to be able to cut vitreous at each side of the instrument. Here, the reach must be at least $\Theta = 360^\circ$.

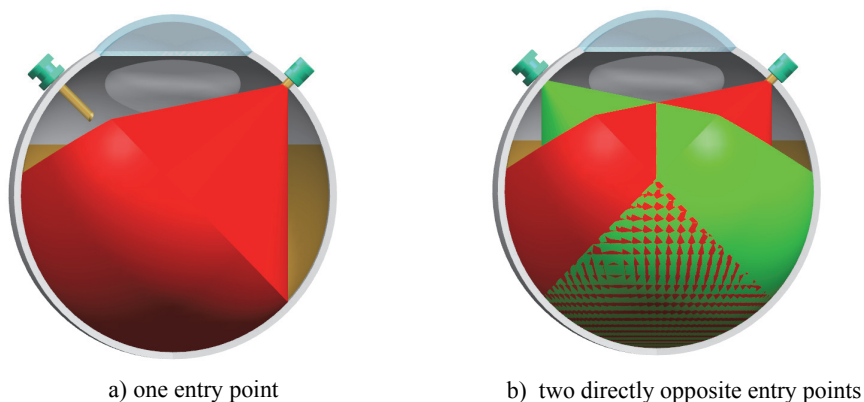


Figure 2.7/ The reach of a instrument, by use of: a) one instrument, b) two instruments (right instrument indicated in red and left in green). The reach is restricted by the lens and a maximum instrument angle of 45° with respect to a radial axis at the insertion point.

The part that cannot be reached by the right instrument in Figure 2.6, is mostly covered by the left instrument as illustrated in Figure 2.7. Nevertheless, there are peripheral regions that cannot be reached by both instruments. Performing vitrectomy to those regions is less important, as they do not interfere with the central vision.

Endo-illuminator

To perform vitreo-retinal surgery and in particular a vitrectomy, an endo-illuminator is used to view the intraocular structures and the instruments. Via an optical light fiber, light is transferred from an external light source to the tip of the endo-illuminator (Figure 2.8). The shaft of the illuminator, where it enters the eye is composed of a protective metal tube that surrounds the fiber.

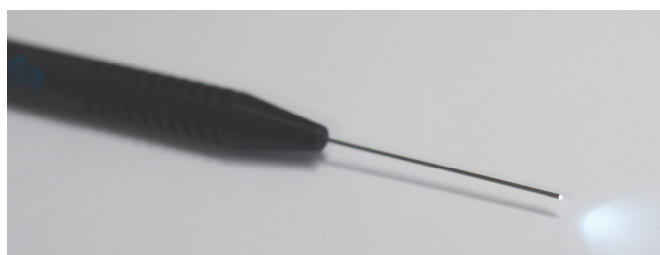


Figure 2.8/ Endo-illuminator with straight tip. Light is transferred via an optical light fiber.

The endo-illuminator can also be used to provide an additional visual depth cue. Here, light comes from the side of an instrument and creates a shadow onto the retinal surface (Figure 2.9-b). As a result, a better depth estimation can be made when the instrument/vitrectome approaches its shadow, thus the retinal surface. This depth cue cannot be realized by the light source inside the microscope (or endoscope). Here, the emitted light follows the same path, as the light that is reflected back towards the surgeon. As a result, the instrument's shadow is behind the instrument itself and moves along with it, as can be seen in Figure 2.9-a.

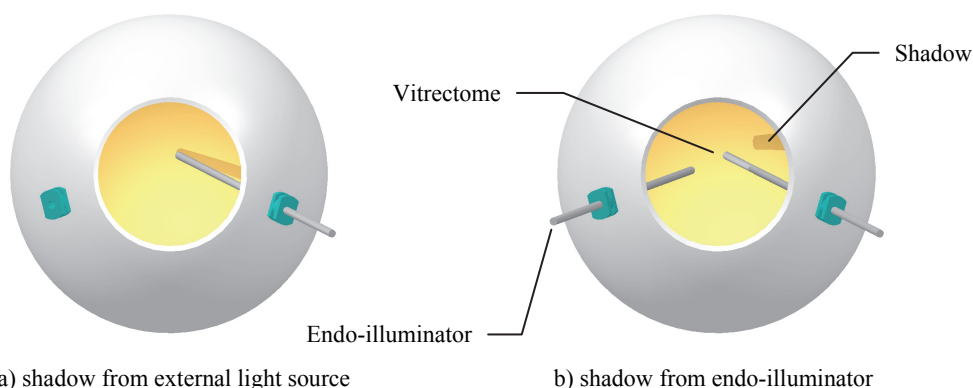


Figure 2.9/ Shadow as created by: a) an external light source (microscope) and b) an endo-illuminator. The endo-illuminator creates an additional side shadow, by which depth can be estimated better.

2.2.3 Membrane peeling

Membrane peeling is the removal of a membrane on the surface of the retina. There are two types of membranes: the internal limiting membrane (ILM) and an epiretinal membrane (ERM). ILM is a natural tissue layer between the retina and the vitreous humour (Figure 1.4). Often, it needs to be peeled off from the retina, as it contributes to: amongst others a macular hole [2]. ILM peeling improves the visual and anatomical recovery of a macular hole treatment [46][92].

An epiretinal membrane is a sort of scar tissue that can form on the retina. It can be caused by vitreous detachment but is more commonly observed associated with other diseases such as diabetes. Retraction of the membrane causes misalignment of the photoreceptors, and as a result, blurred vision [42].

The removal of an ILM requires the same operating techniques and instrumentation as epiretinal membrane removal. As both type of membranes are nearly transparent, they are first stained with a special dye (e.g. Brilliant-Blue®, MembraneBlue® or ILM-Blue®) to make them more distinguishable from the underlying retina. This fluid is injected in the vitreous cavity, after allowing it to stain the membrane for a short while. The excess dye is then removed by aspiration (sometimes by use of the vitrectome). A pick and forceps are the specific instruments required for the removal of a membrane.

Forceps and pick

The technique used to remove a membrane is surgeon specific. Some prefer only to use the forceps (Figure 2.10), grasping the membrane directly on the surface of the retina. Some prefer a pick (Figure 2.11) to create an edge that is easier to grasp. In addition to difference in technique, there are different types of forceps. Difference in forceps relate to straight or curved tips, a radial or axial gripping approach, the length of the gripper, and the type of grip. Figure 2.10 shows forceps with serrated jaws.



Figure 2.10/ Epiretinal forceps with serrated jaws. The forceps are operated by squeezing the buttons on the side of the handle body.

The forceps consist of an inner shaft, with on one end the forceps jaws. On the other, it's fixation to the handle body. The closing motion of the jaws is realized by an outer tube, which is translated axially over the wedge shaped geometry at the start of the gripper jaws. The outer tube is actuated by squeezing a button (or two simultaneously as in Figure 2.10) positioned on the side of the handle body. The specific mechanism

is dependent on the manufacturer. Since the outer tube is translated and the inner shaft is fixed to the handle body, there is no shortening of the instrument during actuation.

The pick is a simple straight shaft, with a tip bent radially. The radial length of the tip is inside the shaft's diameter during insertion via the cannula. The axial end of the bended tip is smoothed, not to damage the retina.



Figure 2.11/ A pick is often used to create a starting point, to peel off an epiretinal membrane.

Epiretinal membrane peeling is mostly performed in the macular region. This area is responsible for central vision and has a diameter of approximately 5mm. The macula is within reach of the vitrectomy procedure. Membrane peeling in the macula does not require a large reach, but it requires high accuracy. The thickness of an epiretinal membrane can grow, from zero up to a few hundred micrometers. This might be a reason, why literature is not precise about the average thickness of these membranes: 80 μm [89] and 120 μm [48]. The thinnest membranes are respectively 35 μm and 80 μm . To grasp these thin membranes, the required accuracy is somewhat lower and is set to be at least 10 μm at the tip (considered for an instrument that is inserted 25 mm).

2.2.4 Repair of retinal detachment

The retina, which lies at the inside of the posterior wall, may occasionally become detached from the underlying choroid, a layer of blood vessels. Retinal detachment is mostly initiated by traction from the vitreous. It can appear during surgery, due to traction caused by vitrectomy, or naturally, by the shrinkage of the vitreous humour. Most retinal detachments go together with a retinal break or tear. Retinal detachments and breaks can appear over the complete retina, all the way up to the ora serrata.

During surgery, the retina is placed back in its normal anatomic position, and the area around the tear is treated in such a way that it will form a permanent scar, after which it cannot re-detach. A vitrectomy is executed first, to release the traction. The retina is repositioned from the inside by injection of a heavy fluorinated liquid, air, gas (SF_6 or C_3F_8) or silicone oil. The retina is sealed to the choroid by use of a cryoprobe or by laserprobe. Both techniques cause a scar reaction to seal the break, but have a different approach. The first is used externally, creating a frozen spot onto the sclera, directly over the retinal defect. The second is used like other vitreo-retinal instruments, via the cannula. By use of the laser, a spot on the retina is extremely heated, causing a burn that sticks the retina and the choroid together. The endolaser is similar in

construction to the endo-illuminator (Section 2.2.2). The difference is that the optical fibre is connected to a laser source. For prolonged tamponade until the seal around the break heals sufficiently, gas or oil are the preferred approaches. Both press the retina into place and prevent fluid from collecting under the retina.

2.2.5 Cannulation

Sometimes, it is desired to inject pharmacologic agents directly in a specific location. In the eye, direct injection in a retinal vein for example would require direct cannulation. Retinal vein cannulation is hard to execute manually [3][77], as veins are typically 50-500 μm in diameter and the tip of the micropipette is typically 20-50 μm . For certain applications, such as the injection of plasminogen activator or [79], once positioned, the catheter must be held in place in the vein for 25 up to 45 minutes.

Studies show, that well trained ophthalmologists are able to position an instrument with an accuracy of 133 μm (RMS error) on average [66]. They are capable of keeping it positioned at an accuracy of 49 μm (RMS). This implies that the tip of the micropipette would drift up to 2.5 its diameter (on average), hence cannulation is only possible in larger retinal veins. A robotic system does not suffer from physical fatigue and tremor and can assist a surgeon in achieving and holding a cannula within a retinal vein for a prolonged period of time [54].

Requirements with respect to instrument movements

Requirements concerning instrument reach and accuracy, determined from vitreo-retinal procedures, are presented in Table 2.1. These are presented with respect to the motion of the instrument tip and the degrees of freedom. The positioning resolution is set an order more accurate. Speed, also presented in Table 2.1, is not an issue in vitreo-retinal surgery, as all movements are delicately performed. Here, it is chosen to be able to retrieve the instrument from the eye in about 1 second.

Table 2.1/ Performance requirements with respect to instrument motion (RP3).

RP3	Tip	Φ	Ψ	Z	Θ
Reach		$\pm 45^\circ$	$\pm 45^\circ$	32 mm	+ 360°
Accuracy	10 μm	40 μrad	40 μrad	10 μm	30 mrad
Resolution	1 μm	4 μrad	4 μrad	1 μm	20 mrad
Speed	0.025 m/s	1 rad/s	1 rad/s	0.025 m/s	2π rad/s
Acceleration	0.1 m/s^2	4 rad/s^2	4 rad/s^2	0.1 m/s^2	8π rad/s^2

The accuracy of the Θ rotation is inferior to the other degrees of freedom, as the radius on which it applies is (max.) 0.3 mm for a straight shaft instrument. The Θ accuracy is based on a curved instrument that is extended 3 mm radially.

The bandwidth is determined on the human bandwidth of motion and sense. Manipulations with the human hand have a bandwidth of about 10 Hz [10], including reflexive actions. During surgery, motions are more delicate and are up to 2 Hz [31]. The sense of force feedback with respect to the haptic interfaces at the master, require a higher bandwidth. Here, kinesthetic and proprioceptive force sensing go up to about 30 Hz [11]. According to [41], the best performance for size identification is reached at a force bandwidth of 40 Hz or higher. By these requirements, the bandwidth for the haptic interfaces is set to be at least 60 Hz [33]. To support this:

RP4 the instrument manipulators must have at least the bandwidth of the haptic interfaces, thus is required to be at least 60 Hz.

2.2.6 Forces involving ocular surgery and haptic performance

To provide the surgeon with an accurate haptic feedback, it is desired to measure forces at the point of interest: at the instrument tip. Measuring forces at the tip is also performed in [37]. Here, three strain measuring fiber bragg gratings are integrated in a 25 gauge pick. It is used to measure the force of peeling a membrane. However, adding force sensing abilities in the shaft of an instrument would imply a complete redesign of the instrument range, along with the factory to produce them. From an economical perspective, this is undesired, as multipurpose instruments will not benefit cost efficient disposables. The next best possible solution is:

RP5 to place a force/torque sensor inside the instrument manipulator, as close as possible to the instrument.

For cost efficiency, a commercially available force/torque sensor is preferred.

In vitro measurements, by use of a surgical instrument equipped with a single axis (axially) force sensor, show that 75% of all forces during vitreo-retinal surgery are below 7.5 mN [30][39]. Only 19% of the well trained ophthalmologists tested were able to feel forces at this level. In a subsequent study [38], more advanced in vivo tests were performed to quantify forces that appear during vitreo-retinal surgery. Here, a more advanced instrument was used, equipped with a tri-axial force sensor (X, Y, Z). Three different procedures were tested: membrane peeling, vessel puncture (cannulation) and vessel dissection. On average their respective force in X/Y direction was: 55 mN, 25 mN and 20mN (RMS). In Z direction this was: 375 mN, 75 mN and 575 mN (RMS). Furthermore, in Z direction, the force range measured: 3140 mN for membrane peeling, 490 mN for vessel puncture and 5870 mN for vessel dissection. The first and the latter are measured in a pulling action. Of course, vessel puncture is measured in a pushing action. The lateral force range measured up to 500 mN. The values in Z direction seem very high. In this thesis, surgical forces are considered being somewhat lower. From live surgery, it was noticed that the highest force appeared during scleral penetration. For 23 Gauge, this force is about 2 N [63].

From the above, the force/torque range to measure and to actuate the instrument can be derived. These are presented in Table 2.2, with respect to the instrument tip and the degrees of freedom.

As torque to actuate Θ is very low, the required torque is estimated as presented in Table 2.2. During surgery, most tissue manipulation is performed on the surface opposing the insertion point. Therefore, the required force sensing accuracy per degree of freedom is determined to an instrument insertion of 25 mm.

Table 2.2/ Force and torque range, to measure and actuate (RP6).

RP6	Tip	Φ	Ψ	Z	Θ
Range	+/- 2 N	50 mN	50 mN	+/- 2 N	50 mN
Accuracy	1 mN	0.025 mNm	0.025 mNm	1 mN	0.025 mNm
Actuation force/torque		12.5 mNm	12.5 mNm	6 N	0.2 mNm

2.3 Human anatomical diversity

Human anatomical diversity requires pre-surgical adjustments to position the instrument manipulator’s remote center of motion (RMC), at the location where the scleral openings are desired. It appears that the adjustments relate to the variety in anatomical shape of the human head, not to the shape of eye. The variety in shape of the eye [14], concerning the lateral diameter of the eyeball ($D1$, Figure 2.12) and diameter of the corneal limbus ($D2$), allow the RCM’s to be placed on a circle, with a fixed diameter. This circle is determined to be 17.4 mm, based on averaged eye dimensions and safe instrument insertion (Section 2.2). In Table 2.3 a comparison is made between the distance of safe insertion (q) at the fixed circle of penetration and the anatomical variety of the human eye ($D1$, $D2$).

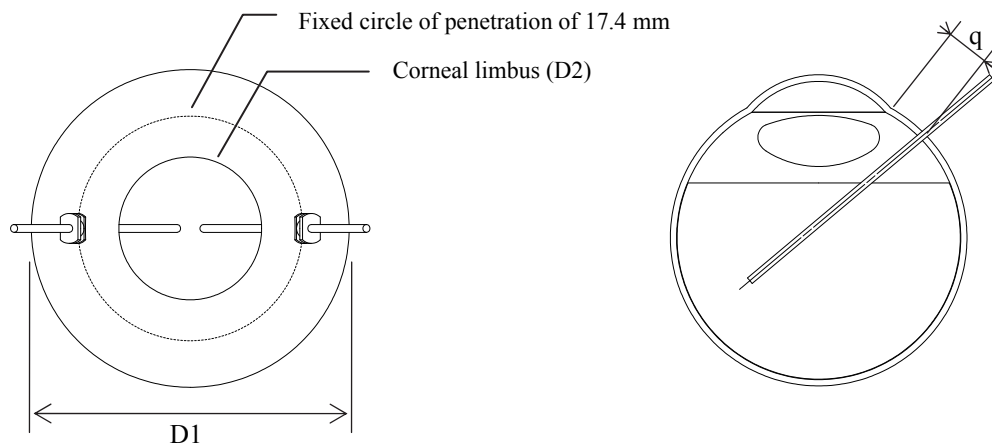


Figure 2.12/ Front view and lateral cross-sectional view of the human eye. Remote center of motions of the instrument manipulators can be placed on a fixed diameter circle to operate eyes of all sizes.

Table 2.3/ The anatomical variety of the eye compared to the permissible distance between corneal limbus and insertion.

	D1	D2	q
Average	24.2 mm	11.8 mm	3.5 mm
Large eye, largest cornea	24.7 mm	12.6 mm	3.1 mm
Large eye, smallest cornea	24.7 mm	11.0 mm	4.0 mm
Small eye, largest cornea	23.7 mm	12.6 mm	3.1 mm
Small eye, smallest cornea	23.7 mm	11.0 mm	4.0 mm

The variety in head size does demand pre-surgical adjustments. Here, at least three degrees of freedom are desired; X, Y and Z (Figure 2.13). Their reach depend on; the interpupillary breadth (X), the distance between the eye and the dorsal end of the head (Y), and the distance between the eye and the posterior-end of the head (Z). Anthropometrical measurements made by U.S. Department of Defense [20] are used to define the reach, indicated in Figure 2.13 and Table 2.4. Since the RCMs can be set at a fixed circle, three single adjustable degrees of freedom to position both instrument manipulators simultaneously will be sufficient.

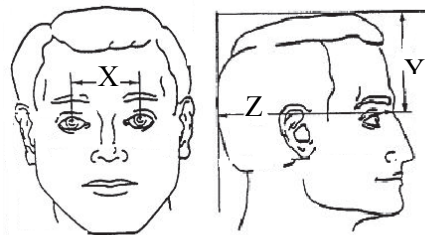


Figure 2.13/ Anthropometry of the human head. Dimensions relevant for instrument manipulator positioning.

Table 2.4/ Anthropometry of the human head and desired reach.

DoF	Min.	Max.	Desired reach
X	55 mm	74 mm	19 mm
Y	90 mm	129 mm	39 mm
Z	174 mm	214 mm	40 mm

It is desired to have additional reach, to be able to approach the eye for the larger head shapes. It is chosen not to complete the reach mechanically, but partially by way of:

RP7 Y, Z = 30mm and X = 25 mm mechanically, extended by:

RP8 additional support cushions underneath and at the dorsal side of the head, to extend the Y and Z reach to 60 mm for the smaller sized patient heads.

Neither Φ nor Ψ need to be provided by the pre-surgical adjustments, these are provided by the instrument manipulators. In addition a Θ rotation about the eye's normal axis of sight can be used to define a different insertion point. When two instrument manipulators are set in opposing positions in the transversal plane, a Θ adjustment is superfluous. The major part of the eye can be reached, which will be sufficient for most interventions, this will be explained further in Section 3.3.

2.4 Robotic assisted eye surgery

Robotic assisted eye surgery is in the field of interest for over a decade. There is a strong difference in point of view, about the implementation of such a robot. On one side, there are the handheld assistive tools and on the other the tele-operative systems (like master-slave systems). Probably, the first tele-operative eye surgical system was presented by [77] in 1983. Here, retinal vein cannulation was performed, by use of a Zeiss micromanipulator and a joystick. More recent robotic assisted studies are discussed below.

2.4.1 Handheld tools

Steady hand

A research group at the Johns Hopkins University in Baltimore, USA is handheld assistive minded. Their *Steady hand* robot was introduced in the late 90's [43] and a third generation was recently published [84]. The Steady hand is designed to extend the human's ability to perform sub-millimeter manipulation tasks. Here, the robot and surgeon manipulate a single instrument simultaneously. Via a force/torque sensor, the instrument is mounted to the robot. This system senses forces exerted by the operator on the tool and uses this information in various control modes to provide smooth tremor-free positional control, where forces are fed back and scaled 10 to 100 times. Because the Steady hand is handheld, it lacks the ability of motion scaling.

It consists of a stacked, three degrees of freedom (X, Y, Z) base, to position the instrument to the point of insertion, and a remote center of motion assembly, to manipulate the instrument. The first generation is based on a mechanically defined remote center of motion, where the Φ , Ψ and Z degree of freedom (as in Figure 1.5) are provided for instrument manipulation. The second generation applies a virtual remote center of motion [54]. Here, on top of the three degrees of freedom (DoF) base, a Φ and Ψ motion manipulator is stacked. The remote center of motion, as well as the instrument motion is defined actively by software. In the third generation [84], the Steady hand is again based on a mechanically defined remote center of motion. However, only the Φ and Ψ motion are discussed, it is unclear if and how the Z motion is implemented.

The base appears to be side-cart considered. From the base to the instrument, they chose a relatively long (approximately 300 to 400 mm) and slender remote center of motion design (approx. $d \approx 25$ mm). This way, nearly the entire robot is away from the surgical field and the instrument is easily accessible. It has a claimed accuracy of $\approx 5 \mu\text{m}$ over a reach of $\Phi, \Psi = \pm 30^\circ$ [84] ($\pm 15^\circ$ for [43] [54]).

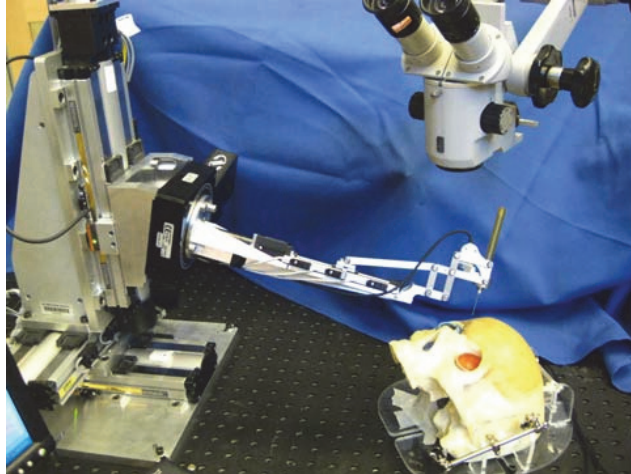


Figure 2.14/ The new Steady Hand, third generation. A handheld assistive system, both the surgeon and the robot handle the instrument simultaneously [84].

The steady hand aims for microsurgical soft tissue manipulation. The focus is on membrane peeling and vein cannulation. The latter is successfully performed on a chorioallantoic membrane of a chicken embryo [54]. Further functionality of the Steady hand for e.g. a complete intervention is not mentioned.

Micron

The micron [4] is also a handheld apparatus, but not a robotic device Figure 2.15. It is like an extended handle of the instrument, designed to compensate physiological tremor and other unwanted movements.

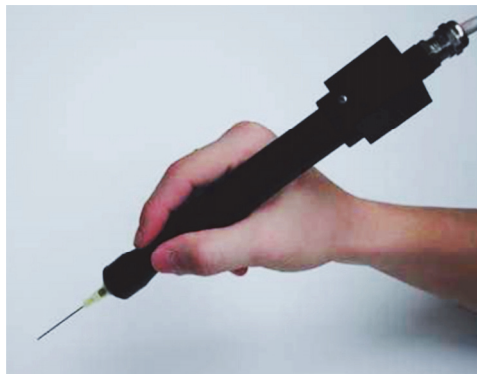


Figure 2.15/ The Micron, the instrument tip is actuated to compensate hand tremor [4].

Hand movements are measured by accelerometers and gyroscopic sensors. Tremor is filtered and cancelled by actuators with respect to the instrument tip. The main purpose is to be able to perform difficult tasks manually, like retinal vein cannulation, in a cost efficient way.

2.4.2 Robotic slave systems for eye surgery

Two microsurgical master-slave systems are realized in the late 90's: one at the Jet Propulsion Laboratory (JPL) [15][18] and one at the department of mechanical engineering of the Korea Advanced institute of Science and Technology (KAIST) [44]. Both systems claim an accuracy of 10-20 μm , motion scaling and to be suitable for ocular surgery.

Four recent robotic master-slave systems which are designed by the University of Tokyo, Japan, and Columbia University, New York, USA are discussed in more detail below. The focus is put on the slave part of these systems.

The University of Tokyo

The University of Tokyo has designed three vitreo-retinal slave systems. All slave systems share the same seven degree of freedom master module and 3-dimensional vision system.

The first slave system is a feasibility study [83] (Figure 2.16, left illustration). The instrument manipulator has a five degree of freedom (DoF) serial layout: $\Phi, \Psi = \pm 50^\circ$, $-29 < Z < 32 \text{ mm}$ and $\Theta = 360^\circ$. In [35][56][83] these DoF are called respectively α , β , δ and γ . The fifth DoF is to actuate the gripper motion of the instrument. The reach of motion is set to reach the complete vitreous cavity, which supports the statement of the reach of motion in Section 2.2.2 and RP3.

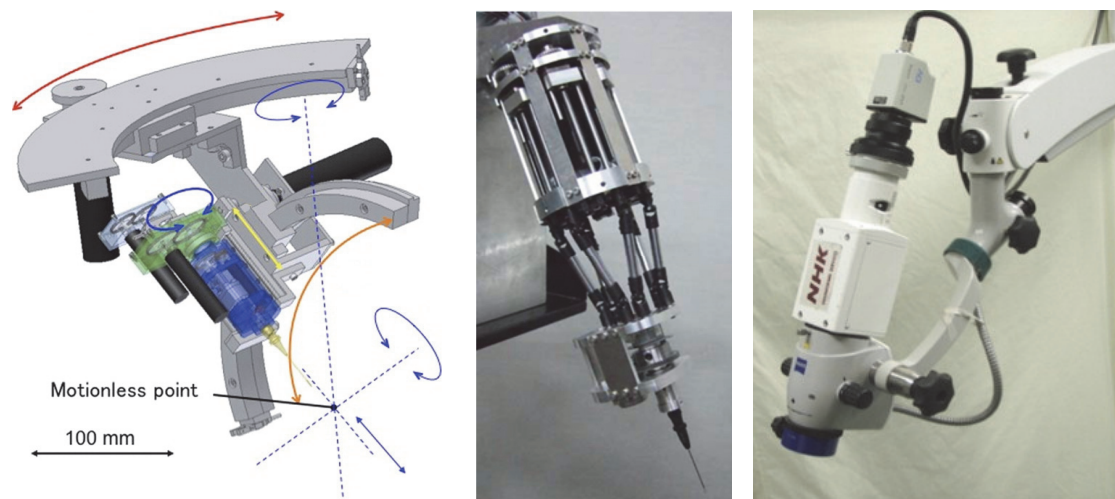


Figure 2.16/ A 3-D camera and two instrument manipulators from the University of Tokyo. Left, a serial linked system [83], in the middle a parallel system [56] and on the right a 3-D camera system [59].

The instrument manipulator is constructed of mostly commercially available products and is rather simply assembled. The two main rotations Φ and Ψ , are made by two circular ball guides, which realize a mechanical remote center of motion. Their main conclusion with respect to this slave system is that tasks can be performed 5-10 times more accurate over manually performed surgery.

A compact stereovision camera system is used [59] (Figure 2.16, right image). It has a slender design of approximately 400 mm long and 80 mm in diameter. A single high definition video camera (2010x1086 pixel resolution) captures the left-lens and right-lens image through a beam splitter. The image is projected on a screen and via a prisma-lens viewer, the three dimensional view is observed.

The second slave system has a parallel layout [56]. It consists of a two DoF end-effector mounted to a six DoF parallel manipulator (Figure 2.16, image on the middle), which in turn, is suspended to an arm of an Olympus microscope. The $\Phi, \Psi = \pm 10^\circ$ and $Z = 50$ mm DoF are done by the parallel manipulator, by which the remote center of motion is realized via software. This design differs from a Stewart platform, as manipulation is not done via linear actuators inside the rods, but by linearly displacing the base joints. The end-effector provides the axial instrument rotation ($\Theta = 360^\circ$) and makes the gripper motion.

In [56] they conclude that this system performs tasks five times as slow as a surgeon performs manually, which is mainly due to a large motion scaling by factor of 1:40. Secondly, the required accuracy of 10 μm was not achieved, amongst others that was caused by mechanical vibrations. Further, they have problems with setting up the initial remote center of motion location. Setting up the remote center of motion takes several minutes.

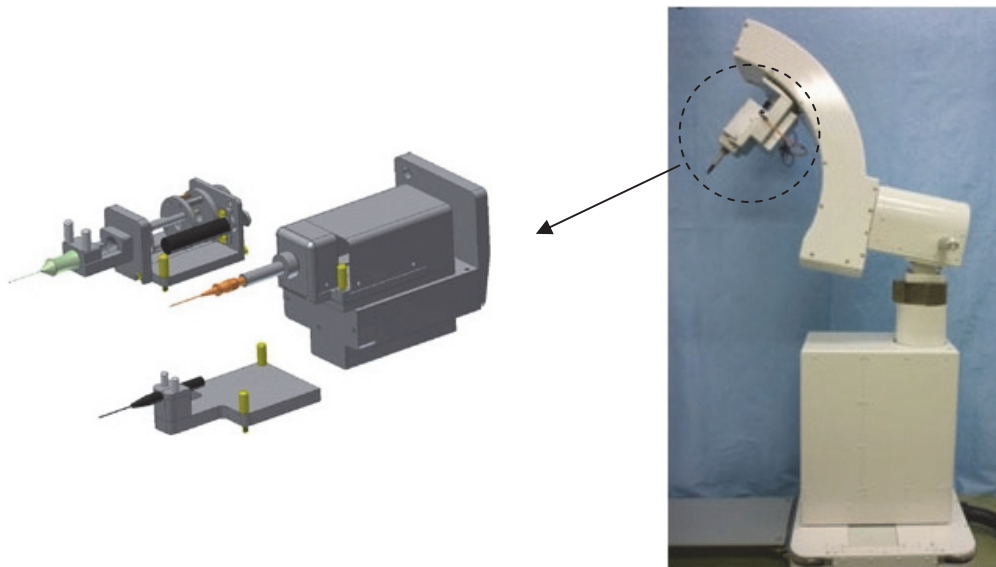


Figure 2.17/ The third robotic slave system for vitreo-retinal surgery designed by the University of Tokyo. It has a three degree of freedom instrument manipulator (right) and various tool units for different type of instruments (left) [35].

The instrument manipulator of the third slave system has again a serial layout [35]. The manipulator consists of a two DoF unit ($\Phi = \pm 90^\circ$, $\Psi = \pm 40^\circ$), with a translational stage attached ($-29 < Z < 32$ mm) (Figure 2.17, right image). Onto the translation stage, various tool units can be placed, which the DoFs depend on the type of instrument (Figure 2.17, left illustration). For example, the endo-illumination probe unit has no additional DoFs, but the forceps unit makes the rotational DoF ($\Theta = 360^\circ$)

and the gripper motion. This slave system has successfully assisted in cannulation of retinal veins down to 70 μm in diameter. The slave system measures: 390 x 410 x 1060 mm.

Columbia University

The focus of this research is on the design and evaluation of a slave that combines instrument manipulation with an orbital manipulation of the eyeball [87][88]. The slave consists of a head mounted ring with two hybrid instrument manipulators (Figure 2.18). Each manipulator is based on a six DoF Stewart platform with on top an adjustable two DoF intraocular dexterity robot. The Stewart platform is designed for an Φ and Ψ working range of $\pm 20^\circ$. With the 2 DoF dexterity robot it becomes possible to work with sideward extended instruments.

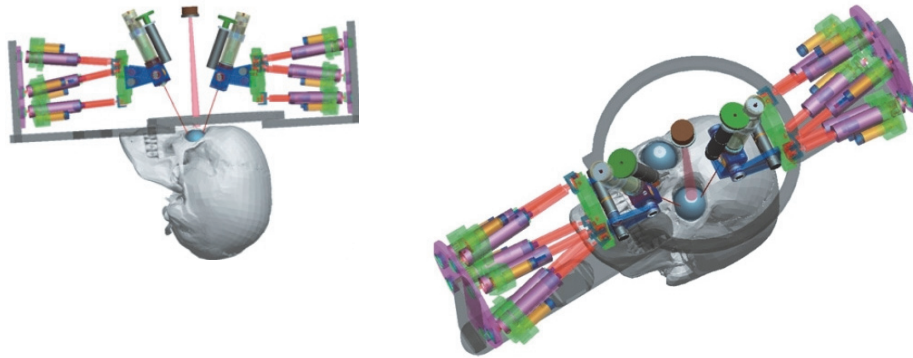


Figure 2.18/ Slave robot for bimanual surgery as designed by Columbia University [87][88].

The relevance of an instrument manipulator based orbital manipulation is to improve vision in the peripheral area of the eye, to roll the silicon oil to the correct place on the retina during the treatment of a retinal detachment and to decrease operation time.

Robotic systems as described above support the requirements stated in this chapter with respect to: instrument reach, instrument accuracy, instrument changeability, a compact and accessible design, preparation time and a design that is easy to setup.

In the next two chapters the slave system is discussed that satisfies the requirements discussed in the previous passages. The slave system is designed according to [70], for: high stiffness, low mass, play-free, low friction and as a statically determined system, which is of importance for a reproducible and predictable system behavior.

First the passive support system will be discussed, followed by the instrument manipulator.

Chapter 3

Surgical setup

The instrument manipulators, performing the surgery, are mounted to passive arms of the pre-surgical setup. The purpose of the pre-surgical setup is to position the instrument manipulators, in a fast, easy and safe way onto the eye. The pre-surgical setup is mounted to the top end of the surgical table. It is light weight, easy to install and compact to fit any current operating room. Adjustments are made easily in X, Y (coronal plane coordinates) and Z (vertical) direction and can be fixated for surgery. This chapter describes the (pre-) surgical setup. First various concepts are discussed of which one is selected and in the subsequent sections the chosen pre-surgical setup is discussed in detail.

3.1 Passive pre-surgical adjustment concepts

The slave system mainly consists of active instrument manipulators (IMs) to perform the actual surgery and a passive setup to support the instrument manipulator during surgery. Since there is a large anatomical variety (Section 2.3) of the human head, the IMs must have additional degrees of freedom, to be positioned onto the eye prior surgery. The passive setup allows pre-surgical adjustments, which are fixated during surgery.

In Figure 3.1-3.7 various possible pre-surgical adjustment setups are shown. Figure 3.1 and 3.2 show two systems (A and B) where the eye is approached from the top end side of the surgical table. Figure 3.5-3.7 show three systems (C to E) where the eye is approached laterally. All systems can be set to operate either the left or the right eye and cover the reach to be adjusted for human (head) anatomical diversity (RP7).

The basic thought of systems A and B is a single instrument manipulator frame, where the instrument manipulators and peripheral equipment is mounted to. This frame is in straight-up position for patient preparation and flipped down like a rollercoaster's safety strap, to be set over the eye. This action is illustrated for system B in Figure 3.3.

By rotating the frame for about 60° over the Ψ (longitudinal) axis the left or right eye can be selected (Figure 3.4).

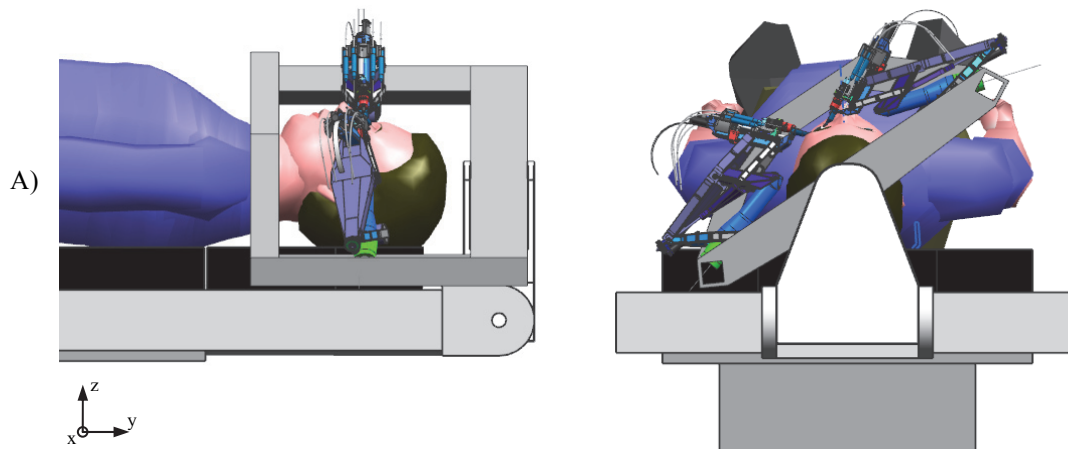


Figure 3.1/ Passive pre-surgical adjustment concept A. The instrument manipulators are table mounted, rectangular ring-shaped frame. The eye is approached from the top end side of the surgical table.

System A is mounted to the instrumentation rails parts, which run alongside the surgical table. Relatively long mounting arms are clamped over a large length to these rail parts, to gain as much fixation stiffness as possible. Pre-surgical adjustments are made under and behind the head rest. The ring-shaped instrument manipulator frame is made from rectangular tubes to create a (torsionally) stiff frame common to both instrument manipulators. The systems advantage is that a conventional surgical table, with a conventional head rest can be used. The slave system is positioned around it. Nevertheless, the distance from the rail parts of the surgical table where the slave is mounted on, to the ring pivot will not easily form a stiff mounting base. The construction is robust enough to carry the systems weight and absorbing external forces. The number of degrees of freedom (DoF) to adjust this concept are five DoFs: One to flip frame in surgical position, one DoF to select the left or right eye for intervention and finally, three to position the instrument manipulators at the eye.

A custom head rest forms the base of system B [53](Figure 3.2). The lateral X and longitudinal Y adjustments are made inside the head rest, the vertical Z adjustment is made at the top end of the head rest. For system B a u-shape frame is chosen. To realize a stiff link between the instrument manipulators, they are mounted to the end of rectangular tubes, which extend from a box-shaped structure. System B is much more compact compared to system A. However, the column behind the head rest forms an unpleasing obstruction and introduces a distance between surgeon and patient.

Figure 3.2 shows setup B with the haptic interfaces for the surgeon attached. The haptic interfaces are adjusted along in X and Y to set up the instrument manipulators, this requires shifting of the surgeons chair along. Theoretically the haptic interfaces could be fitted to the chair as an alternative but this would call for a chair frame which

would be more difficult to step out of, whereas surgeons may prefer to select their own chair. Also extensive cabling on the haptic interfaces and instrument manipulators would be on the ground. This is one of the reasons the overall system is preferred compact, with integrated cabling along fixed routes where possible. The overall number of degrees of freedom to adjust this system is similar to system A.

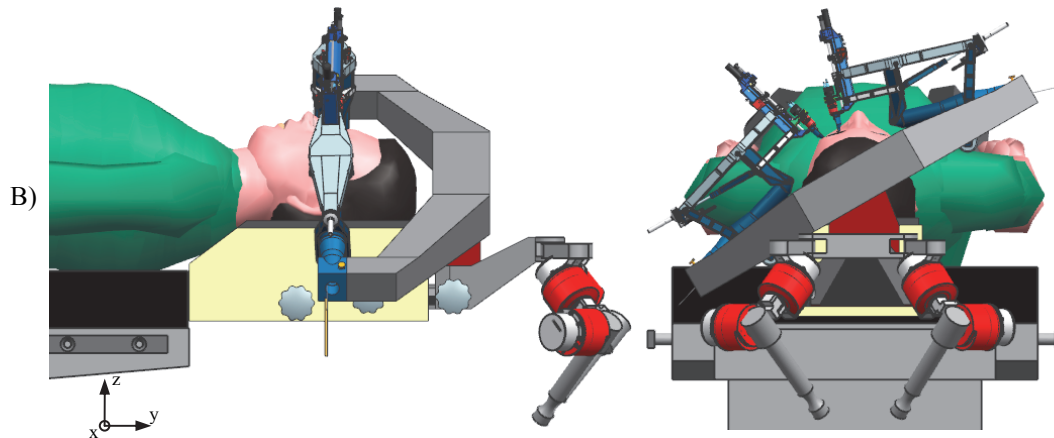


Figure 3.2/ Passive pre-surgical adjustment concept B. The instrument manipulators are fitted onto a head rest mounted U-shaped frame. The eye is approached from the top end side of the surgical table.

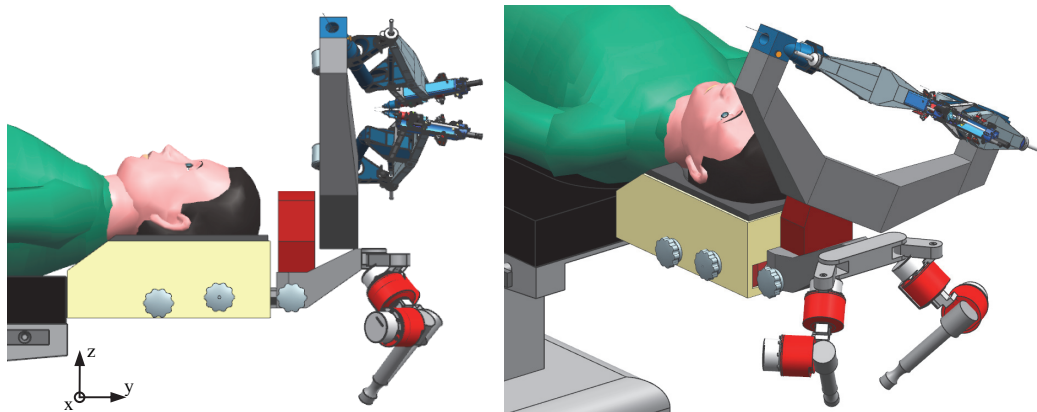


Figure 3.3/ Pre-surgical setup concept B, frame in flipped-up pre-surgical position.

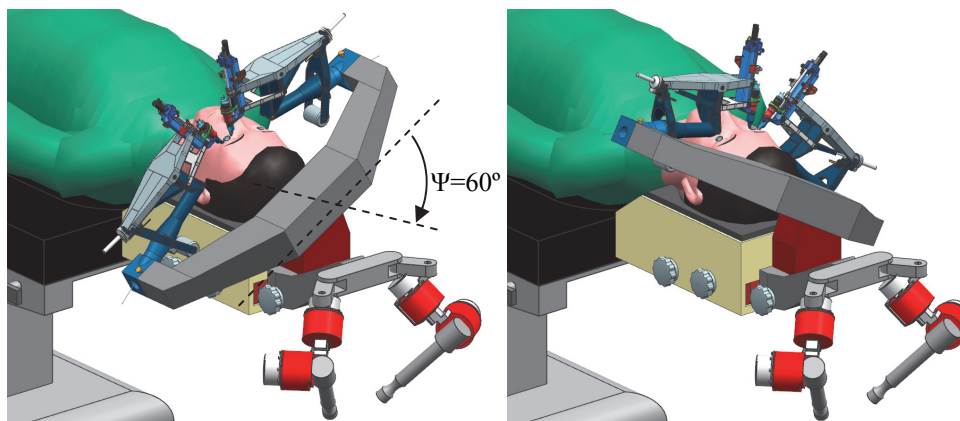


Figure 3.4/ Instrument manipulator frame rotated for left eye surgery (L) and right eye surgery (R).

Pre-surgical setup systems C, D and E (Figure 3.5 to 3.7) approach the eye laterally. This allows the master module to be mounted at the top end side of the head rest, increasing patient proximity for the surgeon. The basic principle of system C is similar to A and B. The instrument manipulators are mounted to a single frame and the complete frame is rotated to select the left or right eye. Both instrument manipulators should be flipped to an upwards position for patient preparation. All pre-surgical adjustments are made as translations inside the head rest. System C demands six degrees of freedom to be positioned onto the eye; two to flip the instrument manipulators up, one to select left or right eye for intervention and finally three degrees of freedom to position instrument manipulators at the eye.

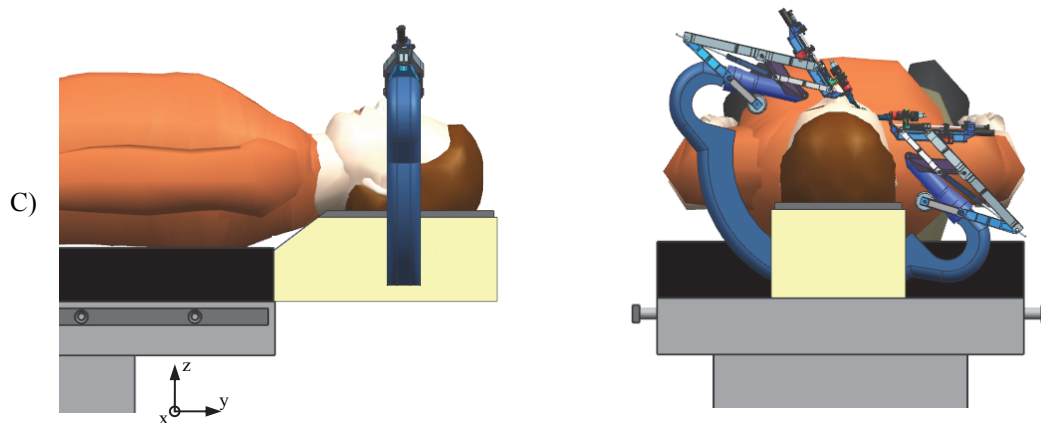


Figure 3.5/ Passive pre-surgical adjustment concept C. The eye is approached from the lateral side. The instrument manipulators are mounted to a rounded frame, adjusted inside the head rest.

System D approaches the eye by use of a linkage-arm system (Figure 3.6). Each instrument manipulators is set onto the eye separately. To define the longitudinal Y degree of freedom the arms are rotated about a (lateral) Φ -axis, located under the head rest. The resulting pre-set angle in Φ -direction is minimal and can perfectly be compensated by the active Φ -movement of the instrument manipulator. The lateral X and vertical Z degree of freedom are adjusted via two linkages and the instrument manipulator per arm. One link and the instrument manipulator should be sufficient to define a position on a (the lateral) plane and as such also onto the eye. However it is preferred to set the instrument manipulator to an angle as close as possible to the patient's head, to increase the reachable volume in the patient's eye (Section 3.3). The linkage system allows a lot of positioning freedom and covers a much wider area than required. No additional degree of freedom to flip or move the instrument manipulators away for patient preparation is necessary (like flipping up as in Figure 3.3). Unlike the other systems, instrument manipulator positioning is not uncoupled, making it hard to position (e.g. via positioning screws). The instrument manipulators must be positioned onto the eye by hand, which can cause rather inaccurately positioned scleral openings. System D demands the most degrees of freedom to be adjusted, seven; one central Φ degree of freedom, plus each arm has three degrees of freedom to position onto the eye.

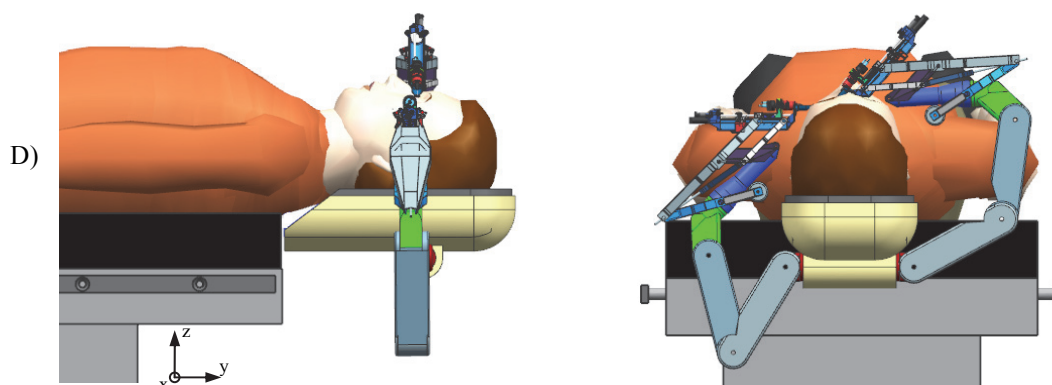


Figure 3.6/ Passive pre-surgical adjustment concept D. The eye is approached laterally, via a linkage system.

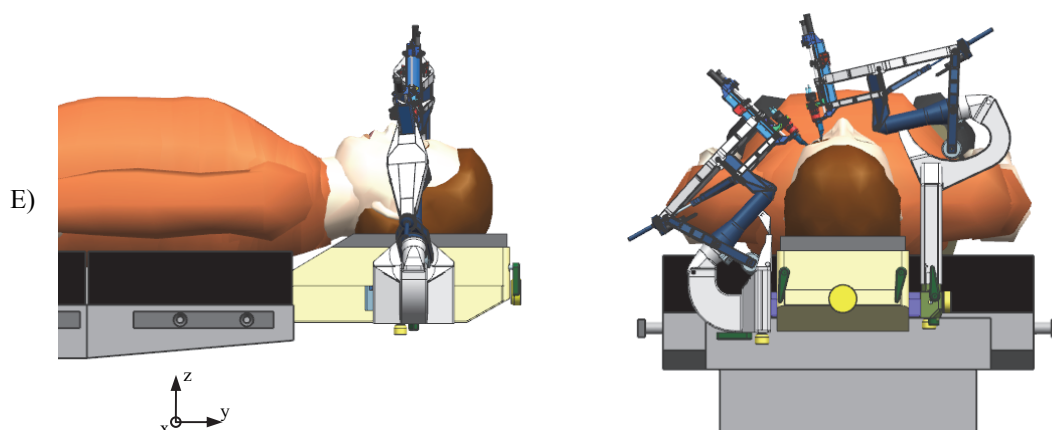


Figure 3.7/ Passive pre-surgical adjustment concept E. The eye is approached laterally. The instrument manipulators are fitted onto two different supporting arms, which can switch sides for surgery to the left or right eye.

The design of system E is proposed to be slender and not too excessively stick out underneath the head rest to ensure legroom. The distance from the head rest to the instrument manipulators is chosen to be as short as possible, to stiffen and shorten the eye-instrument manipulator force loop compared to systems A-D. This leads to a design with two specific instrument manipulator support arms (or Z-arms): one for the instrument manipulator standing aside the patient's head and the other for standing over the patient's head. As a result, the vertical Z-degree of freedom is individually adjusted per Z-arm. The X and Y degree of freedom are adjusted inside the head rest like systems B and C. The Z-arms are attached to the XY-stage and can be decoupled to change sides for surgery on either the left or the right eye. To be a successful design, the arms are modular and easy to attach and exchange. As a result, they allow fast removal in case of an emergency. Other types of instrument manipulators can also be applied e.g. simplified instrument manipulators.

Table 3.1 shows a comparison between the different pre-surgical adjustment setups in various properties. Based on the previous reasoning, setup E is chosen and will be discussed in more detail in the subsequent sections.

Table 3.1/ Pre-surgical adjustment setup summary and comparison.

	A	B	C	D	E
Degrees of freedom (RV7)	5	5	6	7	4
Stiffness estimation (RS4)	--	0	+	0	++
Compactness (RV8)	-	+	+	+	++
Diversity/modular	0	0	0	+	++
Ease to setup (RS6), (RV3)	++	++	+	--	++
Ease to fine adjust (RV10)	++	++	++	--	+

3.2 Design of the pre-surgical adjustment setup

Figure 3.8 shows an exploded view of the pre-surgical adjustment setup where five main parts can be distinguished. The Y-stage is located completely inside the head rest. The X-stage is guided through the Y-stage, for which the head rest leaves openings at both sides for the X-stage to extend out sideways. The tall Z-arm (right) and short Z-arm (left), as the respective Z-arms are called, are attached to the ends of the X-stage that extend from the head rest. The instruments manipulators (IM) are mounted to the Z-arms.

Depending on the instrument manipulator orientation the slave system is 450 up to 565 mm wide. At the short Z-arm side, the widest point is 310 mm from the surgical table's central axis (X-stage in initial position). For the tall Z-arm the widest point is 255 mm. The total width of the system nearly fits within the horizontal surface area of the surgical table (RV8), where a surgical table has a typical width of 580 mm including side rails [47]. At the top end side, the patient proximity is about 40 mm, which is close to the situation in manually performed surgery. This leaves room for the surgeon to approach as close as desired and allows arranging the operating room as preferred. When the haptic interfaces are attached to the head rest as well, the patient proximity depends on the reach of motion of the haptic interfaces and ergonomic surgical body posture [33]. Then the overall distance becomes about 600 mm. The height from the lowest point of the pre-surgical adjustment system to the back of the patients head is about 80 mm, which leaves sufficient legroom and is similar (or less) to current head rests. The total weight of the slave setup is about 8 kg, including the head rest (1,5kg) and local electronics. Both Z-arms have a similar weight of about 1.9 kg. When the operating room must be prepared from non-eye

surgery to eye surgery, the heaviest part to install is the head rest assembly of about 3.8 kg.

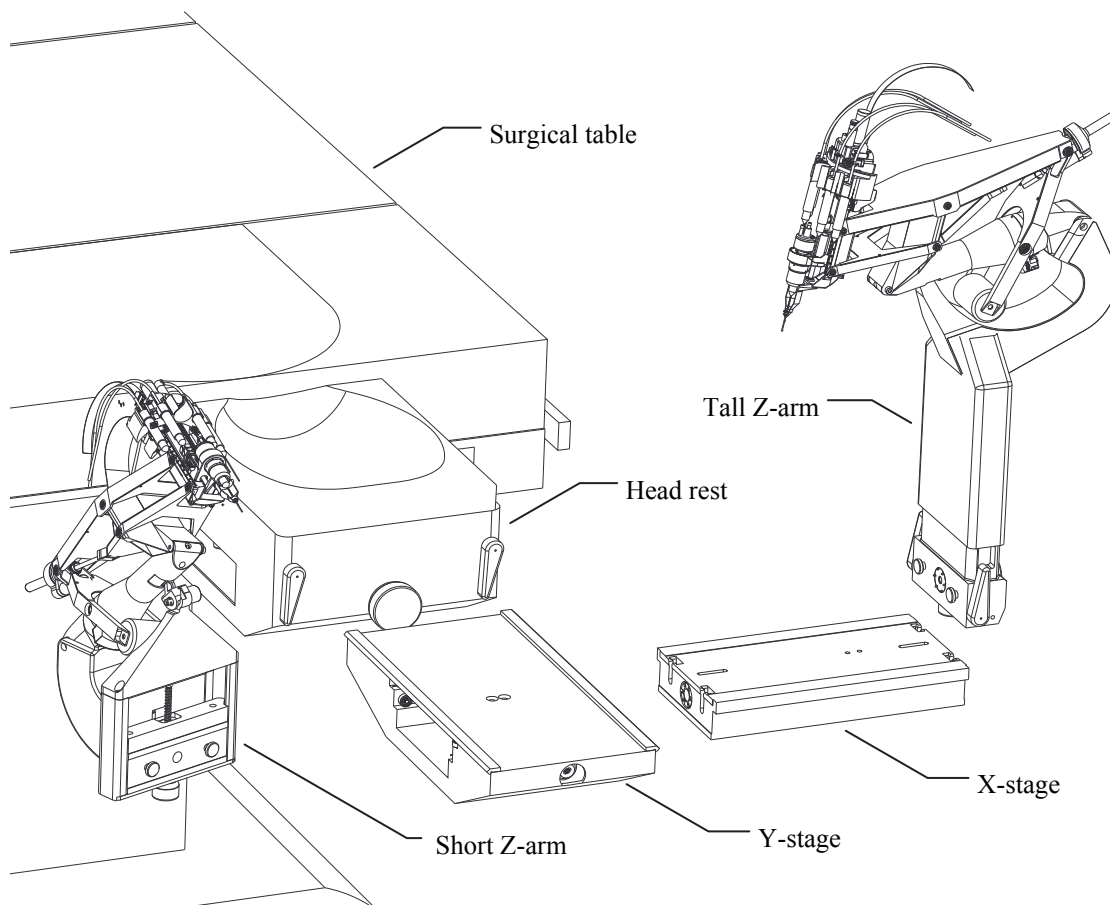


Figure 3.8/ Exploded view of the modular pre-surgical adjustment system.

For the design of the pre-surgical adjustment system similarity of actuation, guidance and fixation is applied. All pre-surgical adjustments degrees of freedom are **adjusted** manually by the use of **positioning** screws. Guide rollers combined with sliding surfaces are used for **guidance** of the degrees of freedom. By using the sliding surfaces for fixation a stiff connection can be realized without remote center of motion displacement. **Fixation** is realized by eccentric levers, pressing the sliding surfaces together with spring preload. In the following subsequent sections these functions (**positioning adjustment, guidance and fixation**) are discussed for the X and Y stages and the Z-arms.

3.2.1 X and Y adjustment

The functionality of the Y-stage is to guide, position and support the X-stage during the pre-surgical adjustment. For the X-stage this functionality is added by the fixation of X and Y DoF and it has an interface for the Z-arms to connect to. Figure 3.9 shows X and Y stage partially in exploded view.

X and Y positioning

The X and Y positioning leadscrew assemblies share similarities. The leadscrews have a diameter of 6 mm and a pitch of 5.08 mm, allowing fast movements as well as movements fine enough to position the instrument manipulators accurately. The human is able to position a screw with an accuracy less than 1° (own ability), which results in a positioning accuracy of about 0.014 mm. To minimize manipulation torque TFE (trifluorethyle) coated leadscrews are chosen and are combined with anti-backlash nuts (series LAF, Reliance [65]) to suppress free play and ensure the positioning accuracy. Figure 3.9 shows the X- and Y-stage separately.

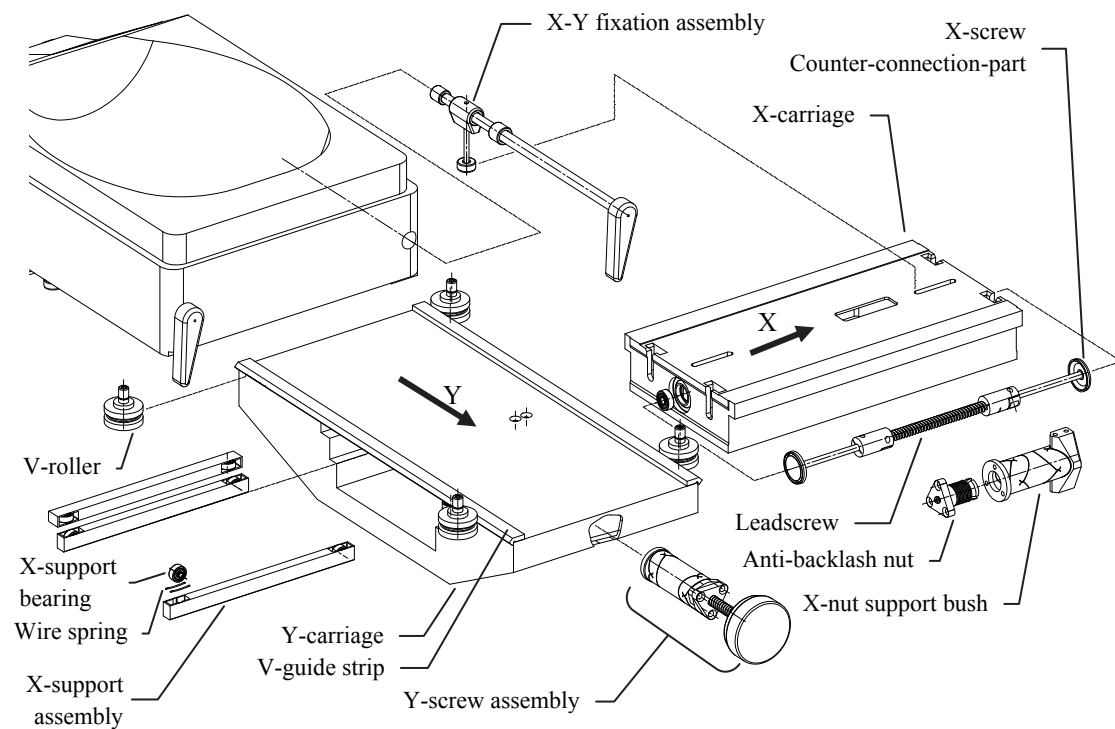


Figure 3.9/ Exploded view of the X- and Y-stage.

The Y position knob (in Figure 3.9 at the “Y-screw assembly”) is located at the dorsal end of the head rest. To the head rest the Y-screw (at the knob side) is suspended by two pre-loaded bearings in O-orientation. At the free end of the screw, an anti-backlash nut is located. The nut is statically determined mounted to the Y-carriage by means of a harmonic support bushing.

Whether mounted to the left or right side, the X-DoF is positioned by the X positioning knob located at the tall Z-arm. It can only be positioned when the tall Z-arm is installed correctly and fixated. With the installation of the tall Z-arm, a connection is made between the X-positioning knob and the X-screw connector at the X-stage, this will be discussed in Section 3.2.3 in more detail. When connected, the X position knob controls the leadscrew located inside the X-carriage. On both sides, the leadscrew is rigidly connected to the counter-connection-parts via solid couplings.

The X-screw counter-connection-parts are play-free suspended via bearings to the X-carriage. The anti-backlash X-nut is suspended to the Y-stage via a harmonic bushing (similar to situation in the Y-carriage).

X and Y guidance

Guidance in Y direction is realized by V-shaped strips and V-shaped rollers. The V-shaped strips are mounted to the upper surface of the Y-stage, four rollers are mounted to the lower surface of the head rest. Three rollers should be sufficient, when a single spring-loaded roller at the middle of one side, forces the Y-stage into two rigidly mounted rollers at the opposing side. This would result in a play-free and statically determined guide way. However, since the rollers extend beyond the height of the V-shaped strips, one could not directly be mounted over the X-stage. When this single roller is positioned out of the X-stage's reach, the roller is almost directly opposing a rigidly mounted roller at the opposite side. Resulting in a small pre-load force to the other rigidly mounted roller, by which the Y-stage can easily be dislocated. Therefore, two spring-loaded rollers are chosen, opposing the rigidly mounted rollers. Rounded strips or crownwheel roller surfaces instead of V-shaped strips are preferred, but not commercially available or suitable in this particular situation.

Through the Y-stage the X-stage is guided. The X-stage is supported via bearings in Y and Z direction. In Y direction, two spring-loaded bearings (in the Y-direction orientated X-support assembly) force the X-stage to two rigidly mounted bearings at the opposite side of the X-stage. In Z direction two similar X-support assemblies force the upper surface of the X-carrier to the lower surface of the patient's head rest.

In Figure 3.10 the X-guidance is shown, in a schematic side view.

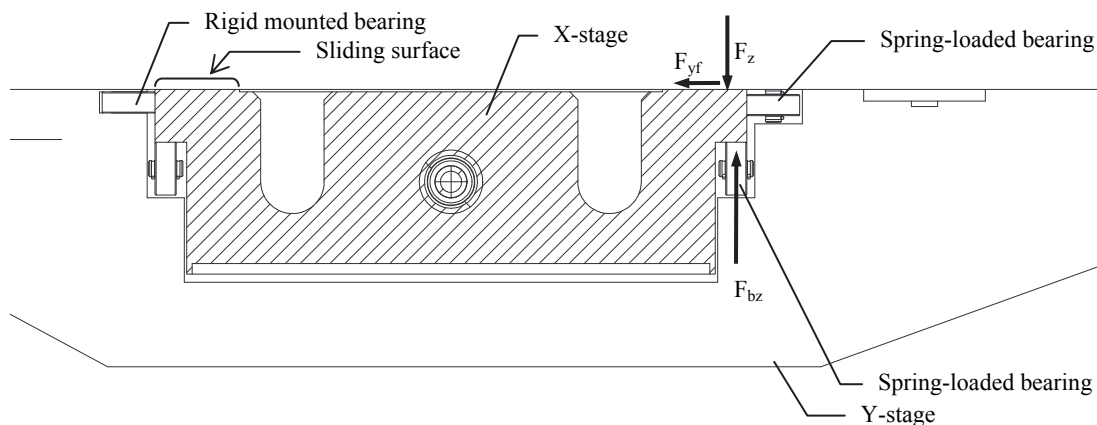


Figure 3.10/ Schematic side view of the X-guidance.

Each spring-loaded bearing is suspended by two wire springs (Figure 3.9). The bearing's extended inner axis rests onto the middle of the wire springs, the ends of the wires rest at the X-support assembly. The wire springs have a diameter of $D=0.6$ mm, a length of $L = 12$ mm and the deflection is set to $f = 0.35$ mm to realize a pre-load

force of $F_{bz} = 22$ N per bearing. The spring material is typical spring stainless steel AISI 301. Bearings with a relatively thick outer ring, are most suitable for support rollers, therefore stainless steel W623-2Z bearings are chosen

Both IM-arms are about 1.9 kg, the X-stage is 0.8 kg and if we assume additional weight considered to be 0.7 kg. The X-stage is forced upwards by $4F_{bz} = 88$ N, resulting in a contact force (between head rest and X-carriage, indicated in Figure 3.10) of $F_z = 36$ N. By an assumed coefficient of friction of $\mu_{yf} = 0.3$, the friction force becomes $F_{yf} = 10.5$ N.

Actuation torque ($T_{x,y}$) of the X and Y stage is calculated by the friction force (F_{yf} , between the X-stage and the head rest), the leadscrew lead (p_l) and the leadscrew efficiency (η_l) and is:

$$T_{x,y} = \frac{F_{yf} p_l}{2\pi\eta_l} = 13.3 \text{ Nmm} \quad (3.1)$$

A torque of 13.3 Nmm is low, similar to adjusting the volume switch on a music amplifier and therefore easily adjustable.

Fixation of X and Y

Since the X-stage is guided in X and Y direction over the lower surface of the head rest, the contact implies additional friction force and increased manipulation torque. On the other hand, after positioning, the X-stage can be forced to the head rest, without being dislocated due to free play. Hereby, the correct adjusted position is maintained. Furthermore, the shortest force loop is obtained, by introducing forces from the instrument manipulator directly into the head rest via the X-stage. Fixating the X-stage implies fixation of both X and Y degrees of freedom.

The X-stage is forced to the head rest by two X-Y clamps on eccentric shafts. The eccentric shafts are located inside the head rest near the left and right side. By fixating the X-stage as wide as possible, the highest stability is obtained. In Figure 3.11 the X-Y clamp is shown in exploded view and the location is indicated in a cut out view of the head rest.

The clamp consists of a pull rod, two Belleville springs, a push disc and a bearing housing. In lowest position the push disc has a clearance of 0.6 mm. By turning the handle upwards, the eccentric shaft pulls the X-Y clamp upwards. By an eccentric offset of $e = 0.5$ mm, the Belleville springs are deflected 0.4 mm and push the push disc with a force of 400 N to the X-stage. Force is transferred via the guide surfaces at the side of the X-stage, to the head rest (the force loop is indicated in Figure 3.11, in the right figure). In clamped situation, the eccentricity is just 10° over the most upper eccentric position, by which the spring force push the handle to an end stop. For safety, the handle is additionally locked in closed position. The eccentric shaft and bearing housing are suspended in roller bearings.

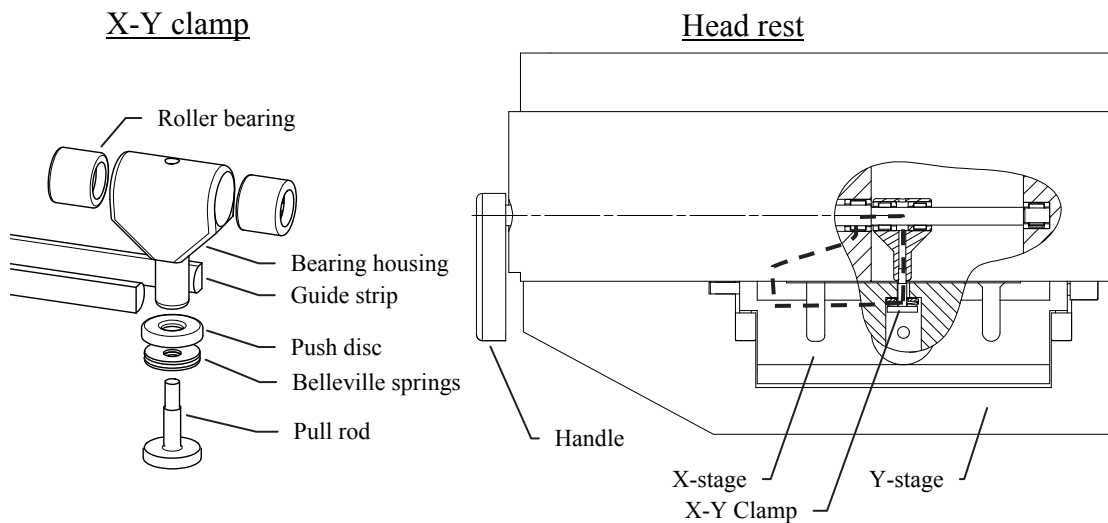


Figure 3.11/ Fixation of the X-stage. On the left in exploded view, the X-Y clamp and two guide strips. On the right, a cutout view of the head rest assembly to visualize the X-Y clamp.

While adjusting the Y direction, the X-Y clamp slides over the eccentric shaft. The clamp is pushed by the X-stage at height of 25 mm from the eccentric centerline. The contact length of the bearings is 16 mm. For this to work, the friction force of the clamp must be lower than the force applied by the X-stage (F_{xstage}). Considering a greased sliding surface with $\mu_{ecc} = 0.15$:

$$2\left(\frac{25}{16}\right)\mu_{ecc}F_{xstage} < F_{xstage} \quad (3.2)$$

In which, the left part equals the friction force, with 25/16 the ratio between the height at which acts and the width of the bearing housing. Slotted cutouts in the X-stage (see top surface of the X-carriage in Figure 3.9) and guide strips on the head rest (Figure 3.11), maintain the clamp's vertical orientation.

3.2.2 Short Z-arm

The principles of guidance, actuation and fixation for both short Z-arm and tall Z-arm are done in a similar fashion as to the X-stage.

Figure 3.12 shows an exploded view of the short Z-arm. The short Z-carriage, the neck body and carriage top form the main part of the short Z-arm. The connection part is the stationary part that is forced to the X-stage and functions as guidance for the short Z-carriage. Similar to the X-stage two guide surfaces of the carriage are guided over the connection part and six bearings of which four are pre-loaded, keep the guide surfaces aligned. Opposing the guide surface, two spring wire pre-loaded bearings (10 N each), one at each side, keep the guide surfaces in contact. Perpendicular to the guide surface, two bearings are rigidly mounted to the connection part and on their opposing side two bearings are pre-loaded (10 N each).

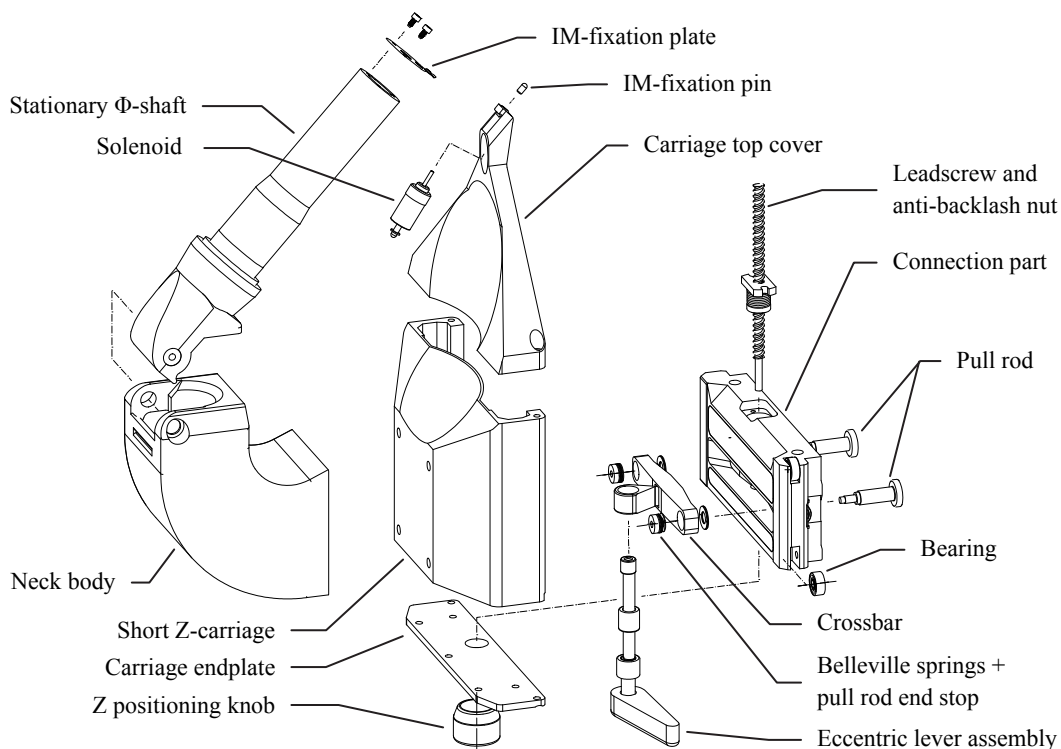


Figure 3.12/ Exploded view of the short Z-arm

Positioning of the short Z-arm

For Z actuation a TFE coated leadscrew with a diameter of 5 mm and a lead of 4.88 mm in combination with an anti-backlash nut from the LNTBF [65] series are chosen. The leadscrew is suspended by two X-orientated bearings to the carriage endplate. The nut is at the free end of the leadscrew rigidly mounted to the connection part. A LNTBF series nut consist of two relatively short separate nuts, pushed apart by a compression spring. These nuts leave a small ability of rotation over the radial axis of the leadscrew (Φ and Ψ direction). By the use of a single-side suspended leadscrew and the LNTBF-type nut at the free-end of the screw, a quasi-statically determined actuation is realized.

The weight of the moving mass (Z-direction) is supported by two coil springs hooked to the carriage endplate and the top of the connection part. This results in an up and downwards actuation torque of $T_z = 8.4 \text{ Nmm}$, by which only the friction force must be overcome.

The instrument manipulator is mounted on the stationary Φ -shaft on ball bearings. The shaft can pivot on ball bearings on the neck body. At the proximal end of the stationary Φ -shaft, an instrument manipulator fixation plate is mounted via the two upper Φ -motor fixation screws (Section 4.5.1). Starting from the initial upright slightly preloaded position (Figure 3.13-a), in which the manipulator is held by a torsion spring (not shown in Figure 3.12), the mechanism is described. Pushed

downward, the instrument manipulator clicks into surgical position (Figure 3.13-d). Here, the part of the plate which extends from the manipulator, while bending (Figure 3.13-c), slides over a rounded fixation pin at the top-end of the Z-carriage top cover. The manipulator is locked, when the plate bends back as a hole in the plate falls over the tip of the pin (Figure 3.13-c). The plate remains slightly bent, by which the hole is pushed onto the pin creating a play-free connection.

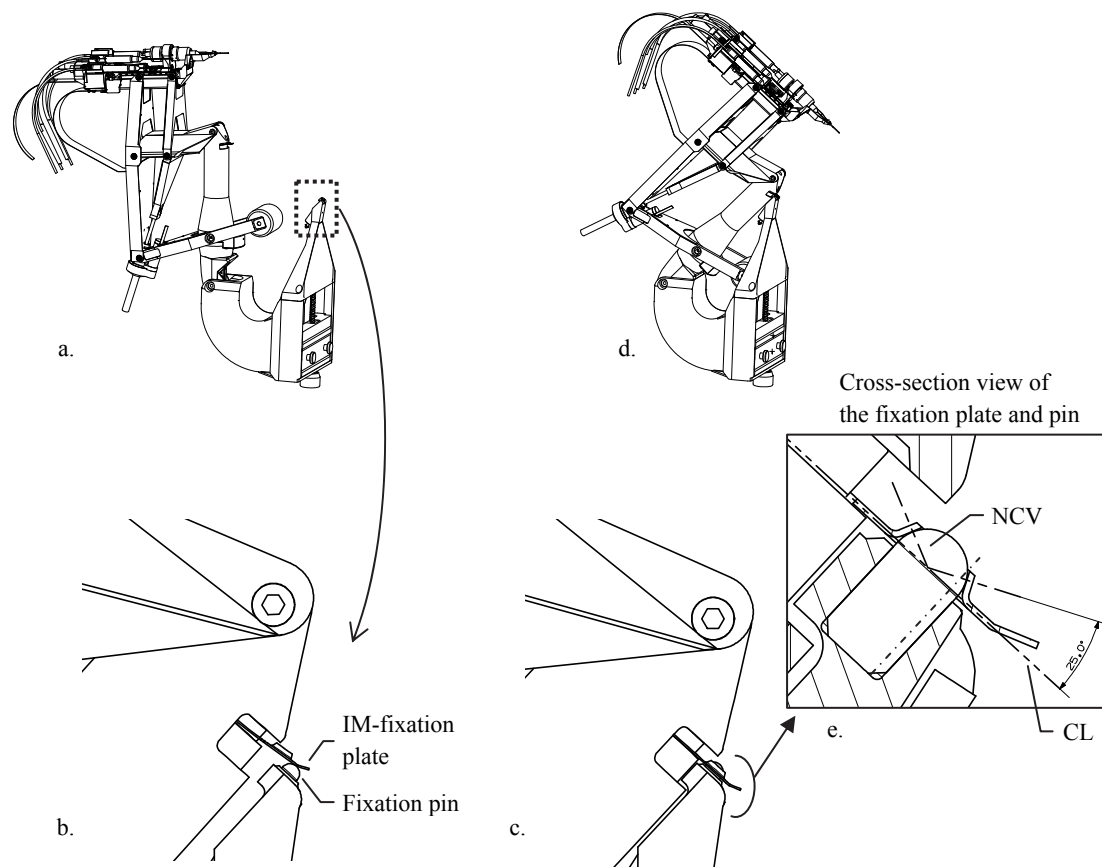


Figure 3.13/ Instrument manipulator release mechanism. The instrument manipulator is pushed downwards in surgical position (a-d), by which the IM-fixation plate locks over the fixation pin (b, c). Forces acting on the IM-fixation plate are transferred as in-plane forces to the fixation pin (e).

The fixation hole in the manipulator fixation plate has a tapered flange of 25° , which makes contact with the rounded tip of the manipulator fixation pin. The hole diameter and flange angle at the fixation plate and the pin diameter are chosen such, that the normal contact vector (NCV) intersects at the centerline (CL) of the plate (Figure 3.13-e). This way forces acting on the fixation plate are transferred as in-plane forces to the fixation pin.

In case of an emergency, a solenoid actuator pushes the fixation plate off the fixation pin, allowing the torsion springs to bring the instrument manipulator back up, to the initial position. The instrument manipulator can thus be removed from the eye in a second.

Fixation

For installation of the Z-arms the pull rods are hooked in the two slots at the side of the X-stage (Figure 3.14). One rod slides into a rounded slot, the other slot has a flattened bottom for a statically defined placement. The pull rods have a sliding fitment inside the connection part. Extended contact surfaces define accurate vertical placement.

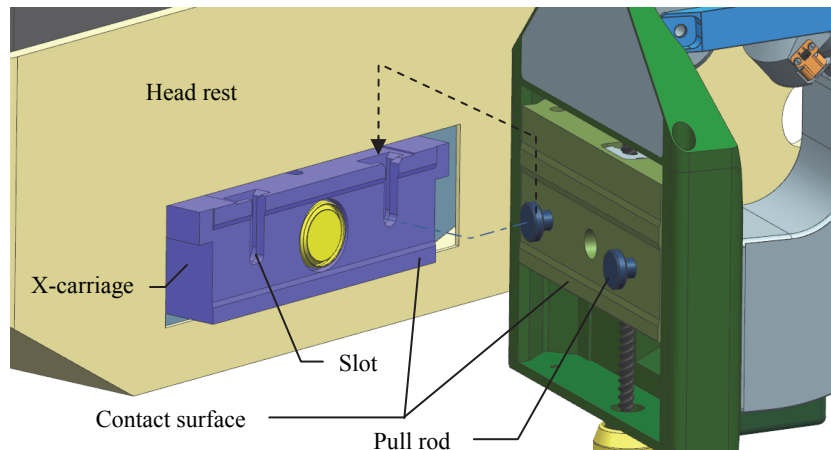


Figure 3.14/ Installation of the short Z-arm.

The fixation mechanism of the short Z-arm has two functions: (i) to fixate the short Z-arm to the X-stage and (ii) to lock the Z adjustment. This is arranged in three situations (Figure 3.15):

- a) to install the short Z-arm,
- b) to adjust the Z degree of freedom, the short Z-arm is fixated to the X-stage,
- c) where the short Z-arm is completely locked up.

In Figure 3.15 a horizontal cross-sectional view indicates the short Z-arm fixation mechanism in the three stages. An eccentric shaft ($e = 0.4 \text{ mm}$) is controlled by a handle at the bottom of the short Z-arm. The eccentric axis is suspended by roller bearings to the carriage. The crossbar is suspended by a roller bearing to the eccentric axis.

In situation a) the eccentric shaft pushes the crossbar inwards (to the left in Figure 3.15, left image), by which at both ends it pushes the pull rods outwards, allowing the short Z-arm to be placed (or removed). At each side two Belleville springs between the crossbar and the connection part push the eccentric axis to an end stop which is 10° beyond the most inwards point. Hereby an equilibrium position is created. The force loop is inside short Z-arm and is from the eccentric axis, via the crossbar, Belleville springs and connection part transferred back via the Z-roller bearings to the carriage (also indicated in Figure 3.15, left image). No force is transferred via the pull rods or X-stage.

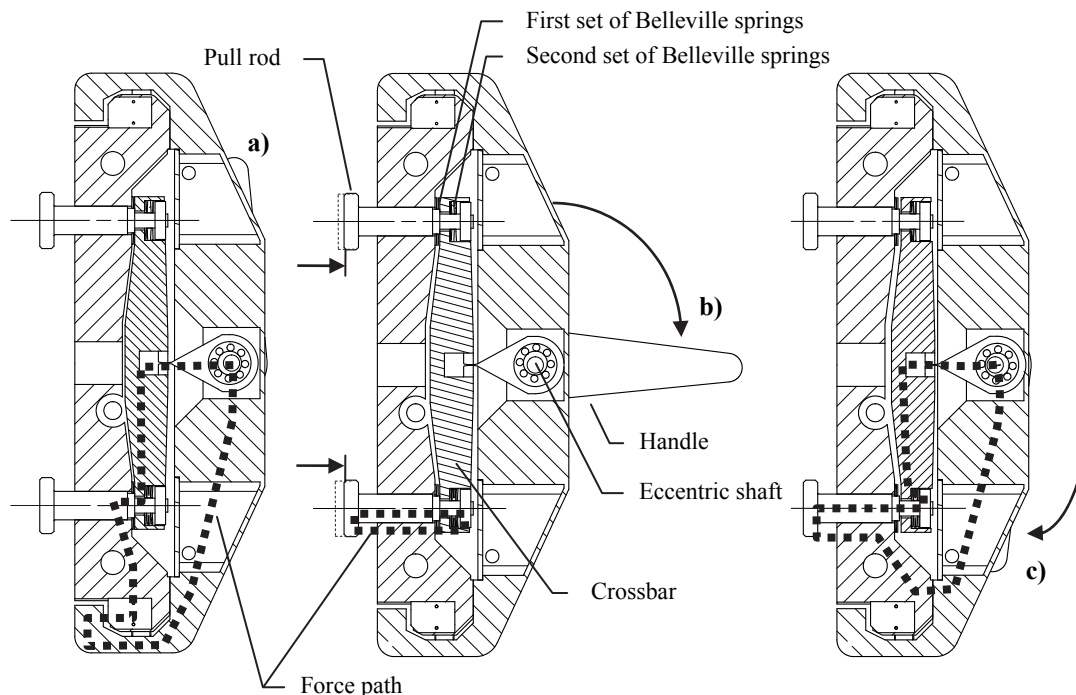


Figure 3.15/ Horizontal cross-section of the Z-low arm, at the central height of the Z-low fixation mechanism. a) indicates an opened mechanism, b) indicates a local closed mechanism by which the Z-arm is fixated and Z-DoF not, c) indicates both Z-arm and Z-DoF fixated.

In the transition from situation a) to b) the handle and subsequently the eccentric shaft is rotated 100° , where a second equilibrium position is found (Figure 3.15 middle image). The Belleville springs between the crossbar and the connection part push the crossbar outwards (in Figure 3.15 to the right), subsequently pulling the pull rods inward via a second set of Belleville springs. The pull rods force the connection part to the X-stage by 70 N. The second set of Belleville springs are not further deflected due to their pre-load force of 140 N. The force loop (Figure 3.15 middle image) is locally through the pull rod, the crossbar, connection part and X-drive, forcing the connection part to the X-stage. In a similar fashion to X-Y clamp, the roller bearing in the crossbar slides over the eccentric shaft, when the short Z-arm is adjusted in Z direction.

In the transition from situation b) to c) the handles are rotated another 100° , by which the crossbar is pulled just over the most outwards position of the eccentric axis. There it is forced to an end stop, similar to position a). Because the position of the pull rods are fixed, the crossbar deflects the second pair of Belleville springs against the end piece of the pull rods. As a result the X-stage connection part and carriage are clamped to each other by 370 N. Force is transferred from the eccentric axis to the carriage and via the sliding surfaces to the connection part and toward X-drive (Figure 3.15, right image). Similar to the X-drive, the sliding surfaces are used for fixation, by which a stiff fixation is realized without dislocating the remote center of motion.

To go from equilibrium situation b) to situation a) or c), the user must overcome a torque, to pull the crossbar through one of the sets Belleville springs. Vice versa, the

user must gently counter this torque applied by the handle. The maximum torque to actuate the Z-fixation handle depends on the angle of the eccentric shaft and the stiffness and deflection of the second set of Belleville springs. The highest calculated actuation torque is in the transition from situation a) to b) and is 90 Nmm, which is 4.5 N at 50 mm of the handle.

3.2.3 Tall Z-arm

Unlike the short Z-arm, for the tall Z-arm a closed tubular guidance can be used. Where the short Z-arm carriage encapsulates the connection part in a U-shape, the Z-high carriage can be executed as a rectangular tube. The guidance is performed inside that tube. The rectangular shape forms a slender but stiff design.

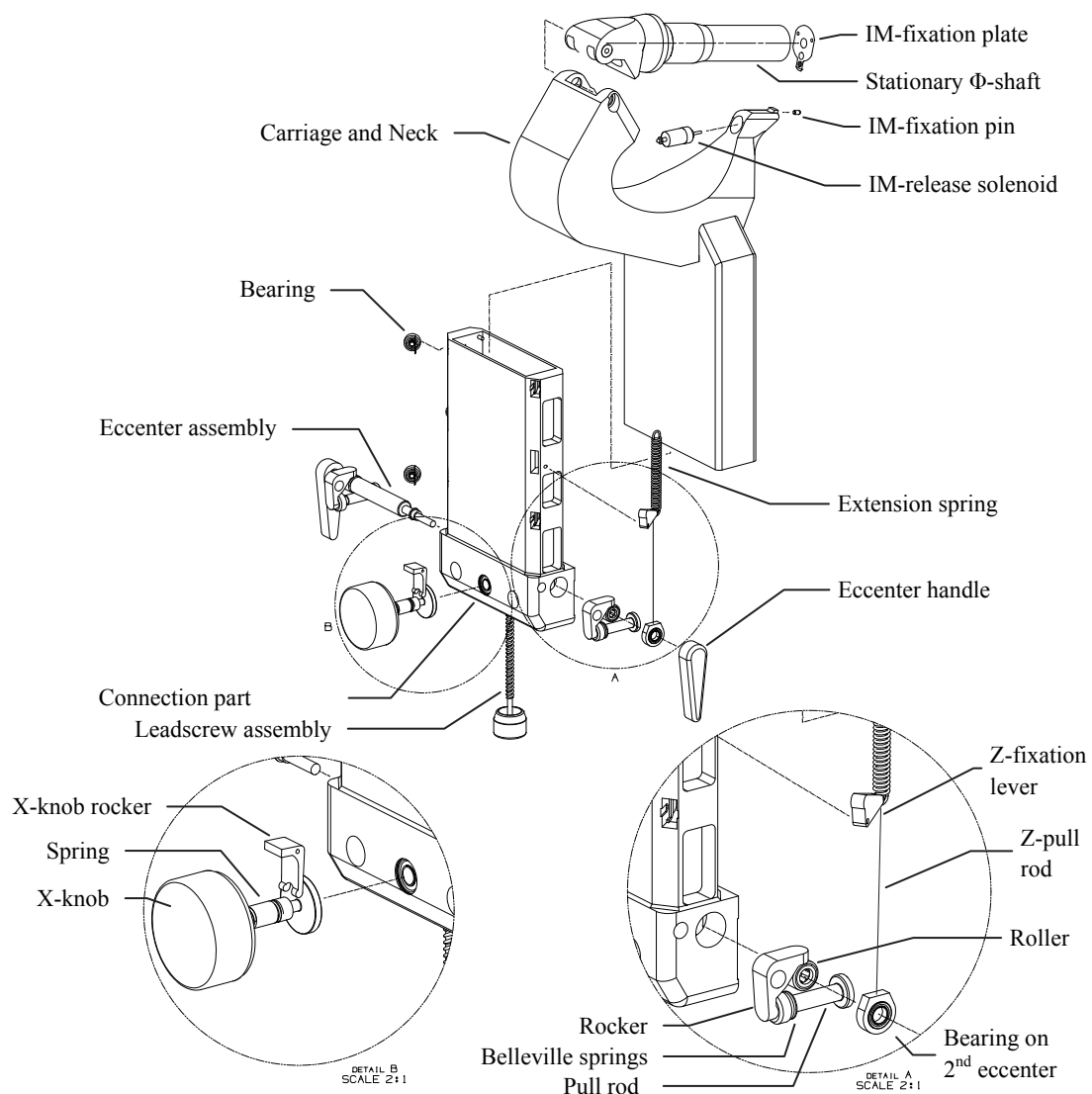


Figure 3.16/ Partially exploded view of the Z-high arm.

Figure 3.16 shows a partially exploded view of the tall Z-arm, some parts are used in numbers and shown in exploded view once. The stationary Φ -shaft, the instrument manipulator release mechanism and the leadscrew assembly are similar to the short Z-

arm. Moreover, they are suspended to the neck and carriage of the tall Z-arm in a similar fashion. The carriage is in Z-direction suspended by springs for weight compensation (not shown in Figure 3.17).

The lower part of the connection part forms a solid base and a stiff connection to the X-stage. The upper part of the connection part is for guidance of the carriage. The edges of the upper part are chamfered and at one side, form the sliding guidance for the carriage (exaggerated illustrated in Figure 3.17). At the opposing chamfered edges four spring wire suspended bearings ($F_{bZ} = 10 \text{ N}$) ensure the sliding surfaces to maintain contact. The inner corners of the carriage are equally chamfered, realized by wire electrical discharge machining (EDM).

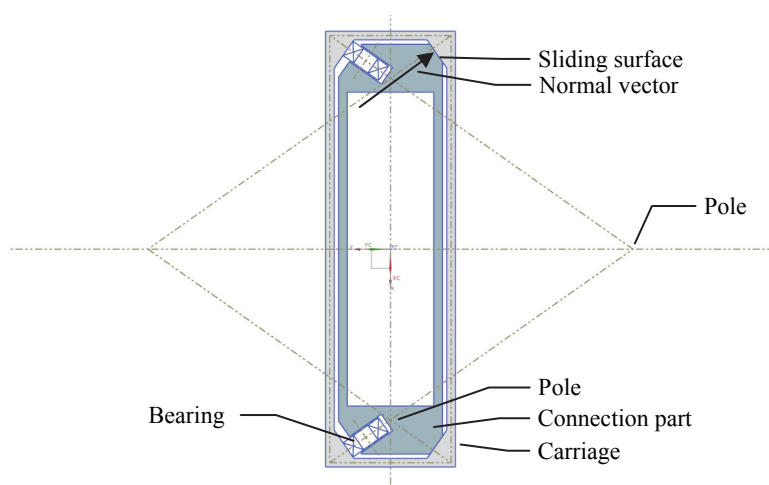


Figure 3.17 /Cross-section illustration of the guidance of the Z-high carriage.

The normal vectors of the contact surfaces as well as the radial vectors of the bearings intersect the centerlines of the carriage's walls. This results in forces or torques applied to the carriage, to be transferred as in-plane forces in the carriage's walls, so as to prevent bending the carriage's walls. For high stiffness torque transfer in Θ -direction, poles of the normal contact vectors are positioned wide apart at the mirror lines of the connection part (Figure 3.17). In Z-direction the contact length is maximized to at least 100 mm, creating a stiff transfer of forces in X and Y direction as well as torques applied in Ψ and Φ direction.

The carriage is fixated to the connection part by two Z-fixation levers. The levers are on both sides positioned in between the guide bearings at the connection part. They apply a force to the roller surfaces of the carriage, consequently increasing the friction/contact force at the opposing sliding surfaces. Force to tumble the levers is applied by tension springs (also shown in Figure 3.19) hooked at the end of the horizontal side of the lever and to a pin near upper end of the connection part. Per lever the spring force is 50 N, with a leverage of $i = 0.5$ the force applied to the roller surface is $F_{Z\text{lever}} = 100 \text{ N}$. With the coefficient of friction of anodized aluminium ($\mu_{\text{ano}} = 0.3$), the total fixation force becomes $F_{\text{fixZ}} = \mu_{\text{ano}}(4F_{Z\text{lever}} + 4F_{bZ}) = 132 \text{ N}$. The levers are released by pulling the horizontal-end downwards, via the pull rod and the associated bearing by the eccentric shaft.

Fixation

For exchangeability the installation of the tall Z-arm is identical to the installation of short Z-arm (like in Figure 3.14). Like the short arm, fixation is obtained from an eccentric shaft ($e = 0.5 \text{ mm}$) located inside the bottom of the connection part. It is extended on both sides, with on each end a handle. This allows easy installation for right as well as left handed people. It makes no difference which hand holds the tall Z-arm and which controls the handle. The handles control (i) the fixation of the tall Z-arm to the X-stage, (ii) the fixation of the Z-DoF and (iii) the positioning the X-knob to the X-drive (for X-adjustment). The eccentric shaft has three stationary positions, in a similar fashion as the short Z-arm:

- handles downwards; to install the tall Z-arm,
- handles horizontally; to manipulate of the Z and X-DoF, at which the tall Z-arm is fixated to the X-stage,
- handles upwards; where the tall Z-arm is completely locked up.

In situation a) the eccentricity is upwards by which the rockers push the pull rods outwards, allowing the tall Z-arm to be placed (or removed). Belleville springs try to push the pull rods back inwards, subsequently the tumbler downwards onto the eccentric shaft. Because the eccentric axis is 10° over the most upwards point, it is pushed to an end stop creating a stationary position. In a similar fashion, at the middle of the eccentric shaft, the X-knob rocker pulls the connector of the X-knob inwards. On the same eccentric shaft a second eccentricity, with a phase shift of $+80^\circ$, releases the tension of the Z-pull rods by which the Z-fixation lever locks the Z-adjustment for safe fixation.

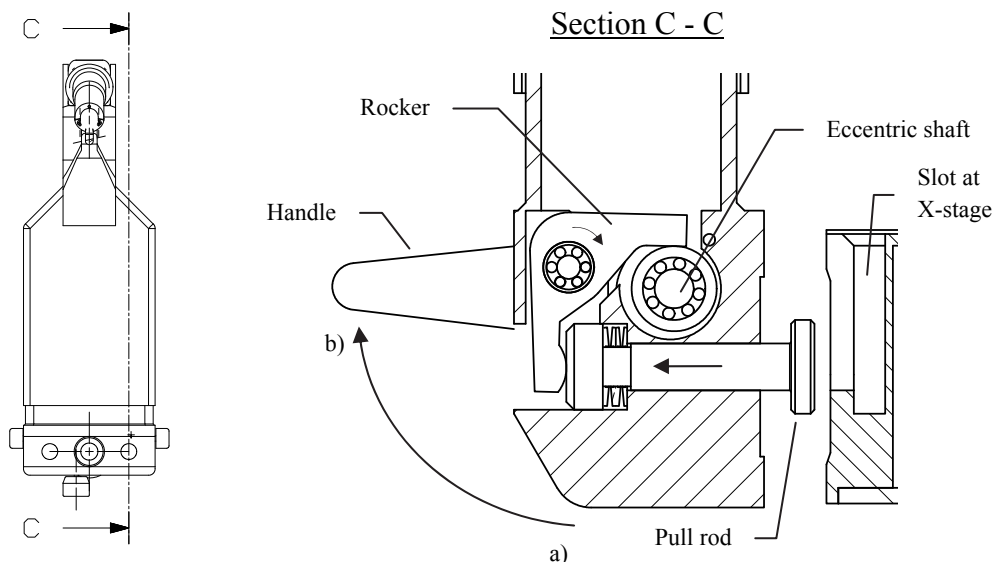


Figure 3.18/ Fixation of the tall Z-arm to the X-stage with the pull rod in a slot of the X-stage.

In the transition from situation a) to b) the handles are rotated 100° upwards to the horizontal position, where a second equilibrium position is found (Figure 3.18). The eccentricity is lowered, by which the rockers allow the Belleville springs to push the

pull rods inwards (indicated with arrows in Figure 3.18). Consequently, the pull rods in their respective slots on the X-stage, force the tall Z-arm to the X-stage ($F_{\text{fix}} = 350 \text{ N}$). Simultaneously, the X-knob rocker on the middle of the eccentric shaft, allows a spring to push the X-knob inwards (and the X-knob connection part outwards) to make a connection with the X-drive (Figure 3.20). The second eccentricity pulls the Z-fixation lever downwards, unlocking the Z-DoF to be positioned. The second equilibrium position is found by the second eccentricity. It is 10° before the most downwards position, by which the tension springs of the Z-fixation levers apply a torque in negative direction with respect to the much higher torque applied by the rockers. I.e. in situation b) the handles are pulled downwards, towards the point where the pull rods make contact with the X-stage and fixate the tall Z-arm.

In the transition from situation b) to c) the handles are rotated another 100° to the most upward position. Action is only applied by the second eccentricity, which in horizontal position releases the tension of the Z-pull rod and bearing, subsequently the Z-fixation lever is again forced to the carriage where it is relocked.

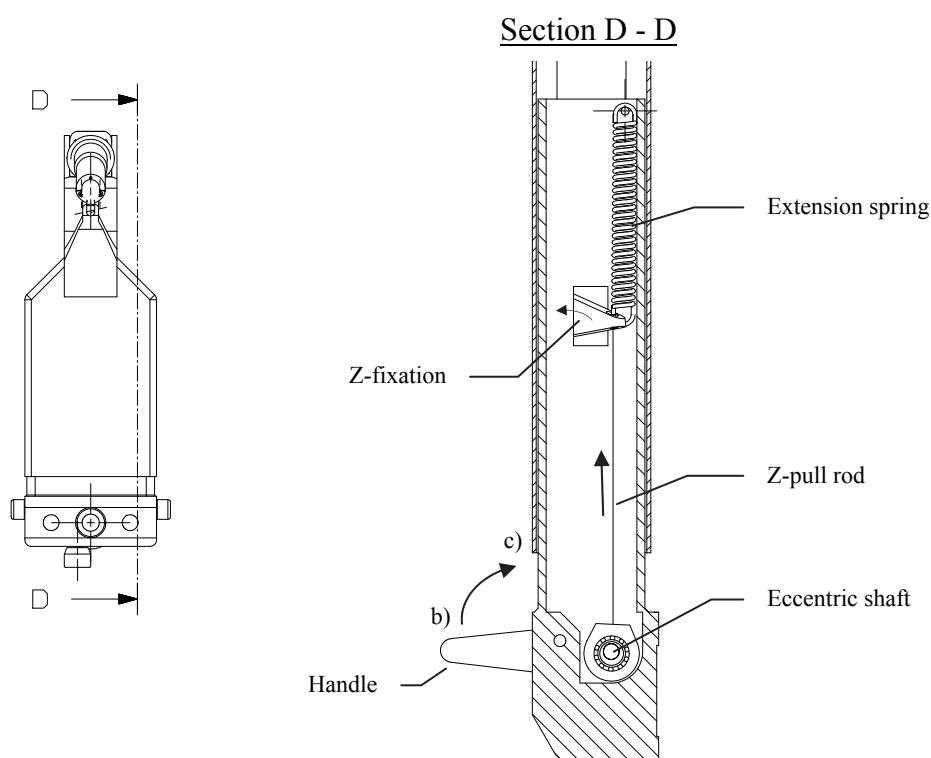


Figure 3.19/ Fixation of the Z-adjustment. In the transition from situation b) to c), the Z-fixation lever locks the Z-degree of freedom.

In case of unlocking the tall Z-arm, in the transition of situation b) to a), the highest calculated torque must be overcome. Torque is applied by the friction of the X-knob rocker and the torque that is generated by the force of all rockers on the eccentricity. A torque of 300 Nmm at a handle length of 50 mm results in a 6 N actuation force. This is very light and in comparison, this equals the maximum torque to tighten an M2 bolt.

X-knob positioning

In the transition from situation a) to b) the X-knob is connected to the X-drive. The connection is made by forcing the conical shape of the X-knob connector to a ring with a rounded edge at the X-screw connector (Figure 3.20). The X-knob is only suspended by a bearing on the knob side, which allows minor radial movement at the connecting side. Furthermore at the X-screw connector a membrane like shape between the contact surface and the rigid X-screw, allows minor angular misalignment. For easy decoupling, a hinge-like shape is placed in the membrane shape by which the connection surface prefers to go inwards to be released from the connector.

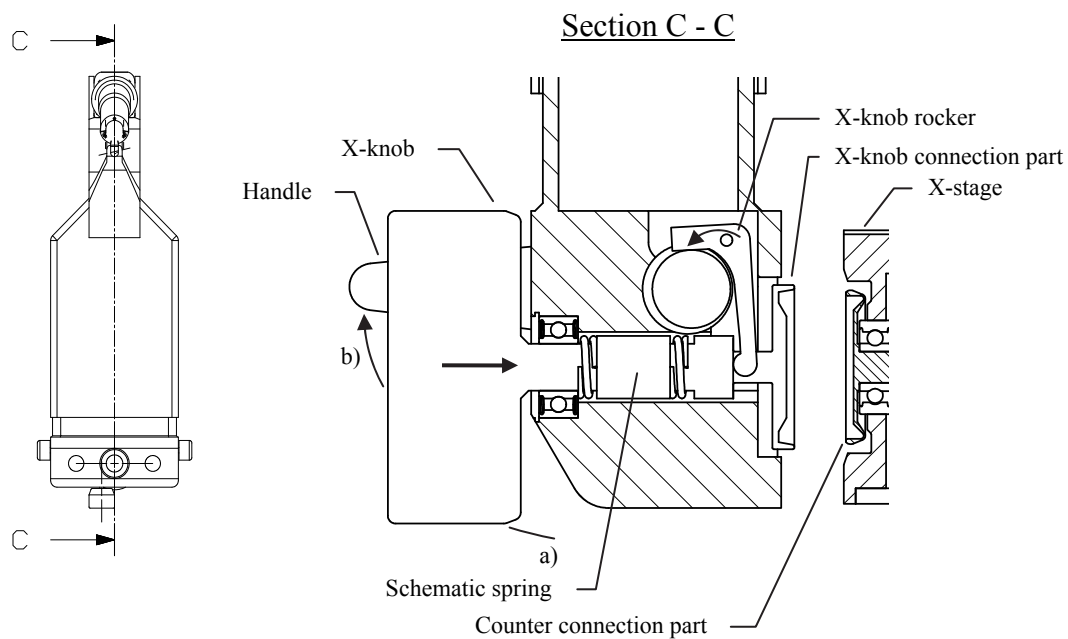


Figure 3.20/ Positioning of the X-knob. The connection part connects with the counter connection part on the X-stage.

The connection is similar to a tapered interface fit and the transferred torque is calculated as such. With the conical shape of $\alpha = 20^\circ$ and the axial preload force $F_s = 20$ N, the radial normal force becomes:

$$F_n = \frac{F_s}{\sin\left(\frac{\alpha}{2}\right) + \mu_{ano} \cos\left(\frac{\alpha}{2}\right)} = 32 \text{ N} \quad (3.3)$$

Here, the coefficient of friction is considered to be $\mu_{ano} = 0.3$. The torque that can be transferred is:

$$T_{X_{\max}} = F_n r \mu_{ano} = 96 \text{ Nmm} \quad (3.4)$$

In which $r = 10$ mm, the outer radius of the connection surface. With $T_{X_{\max}} = 96$ Nmm, a safety factor of about 7.2 is realized over the calculated torque to manipulate the X-stage ($T_X = 13.3$ Nmm, Section 3.2.1).

3.2.4 Stiffness and eigenfrequencies

The Z-arm stiffness

The overall stiffness and eigenfrequencies of the pre surgical adjustment system are determined by finite element software. The stiffness is calculated by determining the deflection under influence of the force or torque applied by the instrument manipulator in its respective degree of freedom. In the finite element model, forces and torques are applied as they would act on the shaft of the harmonic drive and the additional supporting bearing on the stationary Φ -shaft (Figure 4.17). In addition, stiffness in relation to external forces (X, Y) is calculated as well, where the force is considered to be applied at the location of the cannula (trocar). Each Z-arm is analyzed independently. Since the loads acting on the Z-arms are directly introduced to the head rest via the X-carriage, four surfaces on the sliding surfaces of the X-carriage are used to constrain the model. The displacement to calculate the stiffness is measured at the tip of a thin rod, which is extruded from the stationary Ψ -shaft. Its tip represents the location of the cannula (or remote center of motion). Stiffness in Θ -direction not analyzed, because that torque will have little effect on the setup since it is about 2% of the torque applied in Φ and Ψ direction.

Figure 3.21 represents the finite element analysis of the tall Z-arm stiffness in Z direction. The applied force ($F_z = 10$ N), considered at the instrument, reacts as a torque to the Z-arm. A deflection of $f_z = 16$ μm is measured, which results in a stiffness of $c_z = 625$ N/mm. In a similar fashion the stiffness is determined for the short Z-arm. In Table 3.2, the stiffness for both Z-arms is summarized.

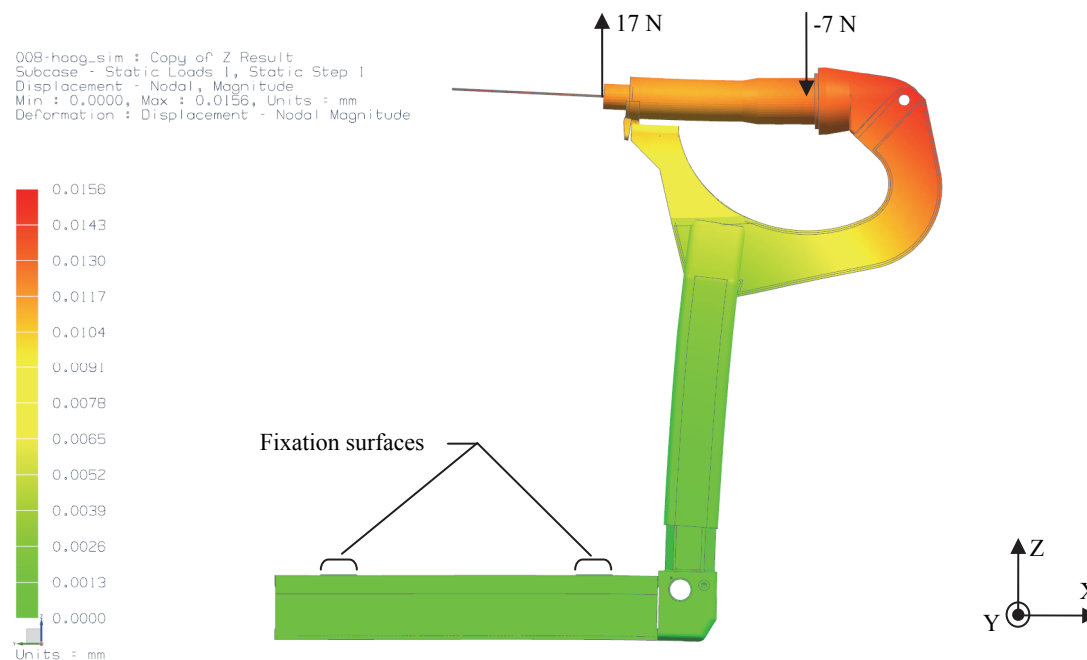


Figure 3.21/ Deflection of the tall Z-arm by a Z-force at the instrument. The deflection is measured at the tip of the thin rod.

Table 3.2/ Stiffness of the short and tall Z-arm.

	Tall Z-arm			Short Z-arm		
	Deflection	Load	Stiffness	Deflection	Load	Stiffness
X	29 μm	10 N	345 N/mm	7.8 μm	10 N	1280 N/mm
Y	30 μm	10 N	330 N/mm	11 μm	10 N	910 N/mm
Z	16 μm	10 N	625 N/mm	8.0 μm	10 N	1250 N/mm
Φ	$550 \cdot 10^{-6}$ rad	100 Nmm	$1.80 \cdot 10^6$ Nmm/rad	$150 \cdot 10^{-6}$ rad	100 Nmm	$660 \cdot 10^3$ Nmm/rad
Ψ	$7.40 \cdot 10^{-6}$ rad	100 Nmm	$13.5 \cdot 10^6$ Nmm/rad	$1.35 \cdot 10^{-6}$ rad	100 Nmm	$73.5 \cdot 10^6$ Nmm/rad
Θ	Not analyzed					

The Z-arm eigenfrequencies

In a similar fashion to the stiffness analysis, the eigenfrequencies are determined. A mass of 1 kg, representing the instrument manipulator, is attached to the stationary Φ -shaft. The first eigenfrequency (Figure 3.22) is found at $\omega_{t1}=86$ Hz; a sideways motion over the Y-axis. This satisfies performance requirement RP4.

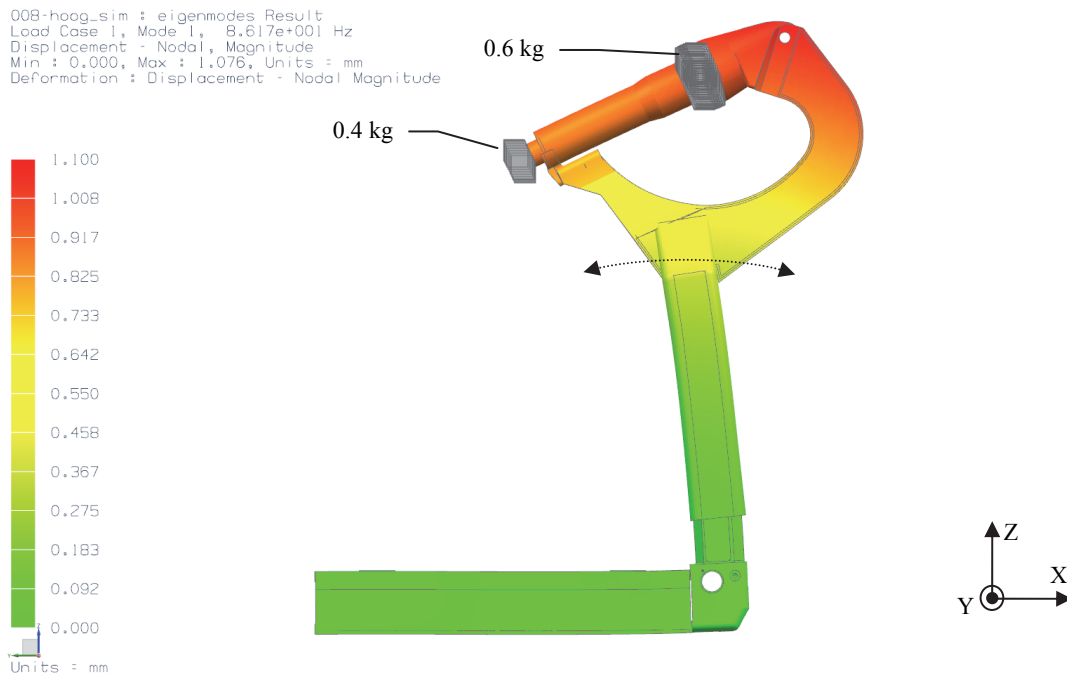


Figure 3.22/ First eigenfrequency of the tall Z-arm: a sideways motion over the Y-axis.

The second eigenfrequency is found at $\omega_{t2}=152$ Hz, which is a back and forth motion over the X-axis. The third is a twisting motion over the longitudinal Z-axis of the carriage and is at $\omega_{t3}=217$ Hz. The short Z-arm shares the same motions for the first

three eigenfrequencies. In Table 3.3 the first three eigenfrequencies of both Z-arms are summarized.

Table 3.3/ Summary of the first three eigenfrequencies

	Tall Z-arm	Short Z-arm	
ω_1	86 Hz	183 Hz	Sideway motion over the Y-axis
ω_2	152 Hz	287 Hz	Back and forth motion over the X-axis
ω_3	217 Hz	500 Hz	Twisting motion over the Z-axis

3.3 Instrument manipulator orientation

The instrument manipulator positions are optimized to reach most of the eye's inside volume. The most optimal reach should be obtained when both IMs are inserted in neutral positions aligned with the insertion point's normal vector. However, this implies both instrument manipulators to be positioned under an angle of 45° to the eye's normal vector of sight (like the left instrument manipulator in Figure 3.23).

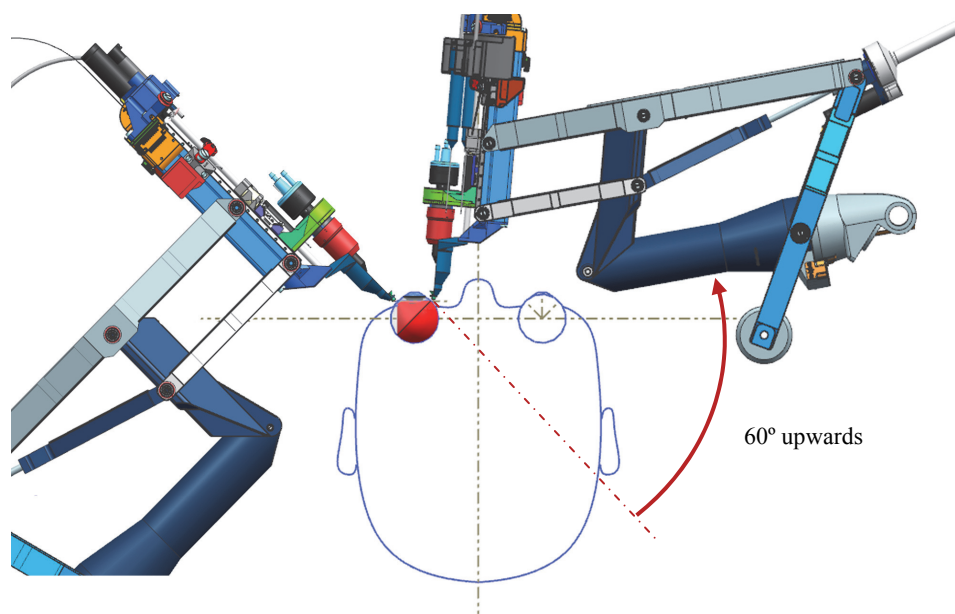


Figure 3.23/ Instrument manipulator tilted 60° upwards to make room for the patients head. The red cone inside the eye represents the reach of the left instrument manipulator.

For the eye to be kept in conventional orientation, one instrument manipulator can stand aside the patient's head. At the opposing side, the instrument manipulator's reach of motion is drastically reduced, as it would intersect with the patient's nose. The nose side instrument manipulator must be rotated 60° upwards (Ψ -direction) to leave enough room for safe operation. This leaves a 30° reach of motion to operate (indicated in Figure 3.24, right image).

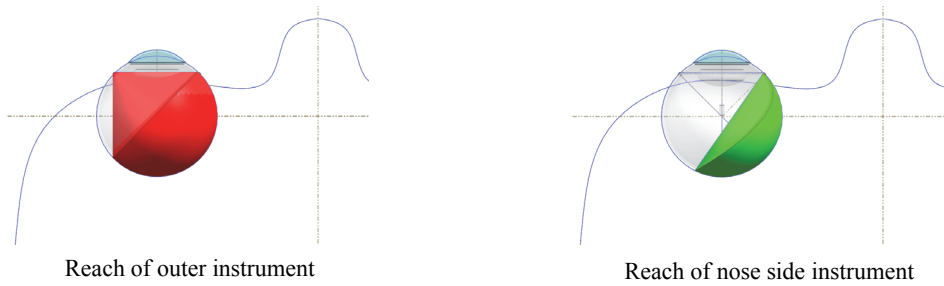


Figure 3.24/ Reduce in reach of motion for the nose side instrument.

To optimize the reach of motion, the eye is rotated 25° to 30° towards the side of the head and fixated in that position. The angle of rotation can average the reach of both instruments. The instrument manipulators are positioned in opposing direction in the transversal plane, by which the angle between the instruments in neutral instrument manipulator positions is set to 35° (Figure 3.25). As a result the total reachable part of the eye is maximized. The major part of the vitreous humour and the complete rear side 170° of the retina can be reached (also seen in Figure 3.25). Without the constraint of a maximum cannula rotation of 45° , the reach will be larger than 180° . Fixation of the eye can be performed by e.g. grabbing both cannulas by the instrument manipulators or by placing a vacuum cup on the eye which can be locked to the instrument manipulators.

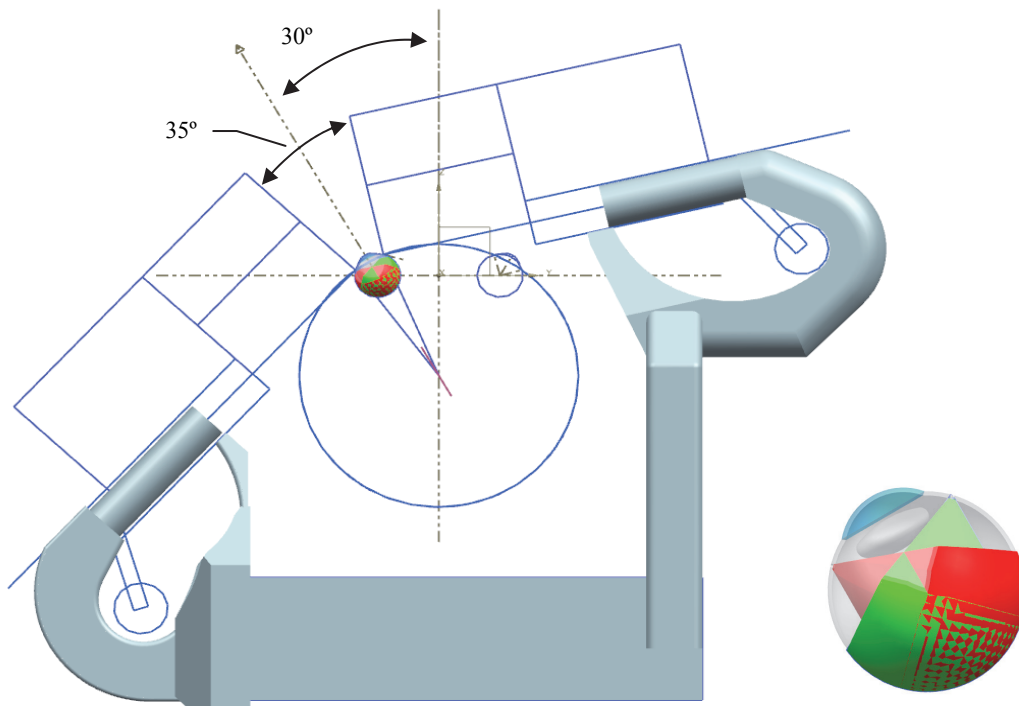


Figure 3.25/ Schematic representation of the instrument manipulator layout in optimized orientation and the combined reach in the eye.

In this chapter the design of the passive pre-surgical adjustment setup is described. In the next chapter the instrument manipulator that handles the instrument will be discussed.

Instrument manipulator

Two instrument manipulators are realized. Each instrument manipulator has four degrees of freedom, which are used to position the instrument. A fifth degree of freedom is used to actuate the instrument. The instrument is manipulated about the access point to the eye. Instruments can be changed automatically via an onboard instrument change system. The design and realization of the instrument manipulator is discussed in this chapter.

4.1 Requirements of the instrument manipulator

The most important mechanical part for robotic surgery is the instrument manipulator. The instrument manipulator takes over the tasks of the surgeons hand by handling the instrument (or surgical tool). Although it is desired to have as much functionality as a surgeon's hand, the design requirements are set as in Chapter 2. Briefly summarized, the requirements for the instrument manipulator are:

- four degree of freedom minimally invasive instrument manipulation (RP3), with the scleral opening being constrained passively (RS1), with:
 - $\Phi, \Psi = \pm 45^\circ$,
 - $Z = 30 \text{ mm}$,
 - $\Theta > 360^\circ$,
 - accuracy of $< 10 \mu\text{m}$,
 - a gravity balanced instrument manipulator (RS2),
 - backdrivable degrees of freedom (RS3),
 - high instrument manipulator stiffness ($>100 \text{ N/mm}$, RS4),
 - parts that wear, must be made of biocompatible materials (RS5),
 - a possibility to change instruments rapidly (RV2),
 - easy to setup and a short preparation time (RV4),
-

- a possibility for automated cannula (or trocar) placement (RP2),
- suitable for surgery via microscope and endoscope (RV11),
- a bandwidth of > 60 Hz (RP4),
- a force/torque sensor as close as possible to the instrument (RP5),
- a force measuring accuracy of 1 mN over ± 2 N at tip of the instrument (RP6).

4.2 Concepts of manipulating Φ and ψ

With requirement (RS1), it is chosen to constrain the pivoting point passively, where the instrument enters the eye (Figure 1.5). This is realized by a design, which defines that point kinematically by use of a remote center of motion (RCM). In such a design, all degrees of freedom intersect at this RCM (degrees of freedom as Figure 1.5). A serial linked design is most suitable. Here, the degrees of freedom are grouped in a manipulator for the axial Z-translation plus the Θ -rotation about the Z-axis and a manipulator for the lateral Φ and Ψ rotations. To the Φ - Ψ manipulator, the Z- Θ manipulator is attached. First concepts to manipulate Φ and Ψ are discussed followed by concepts to manipulate Z and Θ .

4.2.1 Double rotor mechanism

The kinematic design in Figure 4.1 is called the double-rotor mechanism. The double rotor mechanism has two rotors and practically three axes. Via axis 1 the primary rotor is mounted to the pre-surgical adjustment system. Axis 2 is orientated at an angle of 22.5° to axis 1 and connects the secondary rotor to the primary one. The third axis represents the centerline of the instrument and is orientated at an angle of 22.5° with respect to axis 2. Every angle within $-45^\circ < \Phi, \Psi < 45^\circ$ can be realized, by varying the primary and secondary rotor in 360° .

Although axes 1 and 3 can be concentric in neutral positions, rotating the system about axis 1 is not meant to actuate the Θ degree of freedom. To manipulate Φ or Ψ , both rotors need to be actuated and are directly depending on one another. This implies a coordinated control of the actuation. The major advantage of this concept is its slender and simple design and the low number of moving parts. However, wiring the system is difficult and hoses for e.g. vitrectomy could get tangled up and squeezed off. Changing an instrument can be difficult because the primary rotor may be obstructing the exchange i.e. not all orientations may be suitable for changing instruments.

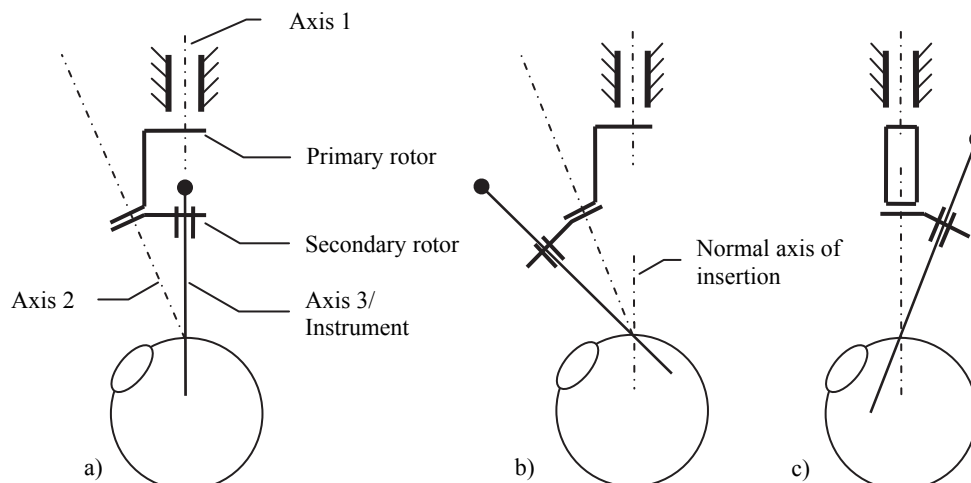


Figure 4.1/ A schematical representation of the double rotor mechanism in a) neutral, b) extreme and c) arbitrary position.

4.2.2 Curvature rail mechanisms

In Figure 4.2, three remote center of motion mechanisms are shown based on curvature rail units. System a) rotates a curvature rail in 360° on which a slide unit guides the instrument between $0^\circ < \alpha < 45^\circ$. The rail can make fast and awkward movements at small angle variations, when the instrument is near the rail's rotation axis (near singularity), which is in the center and most used operation area.

System c) is similar to system a), but the slide unit makes a total $-45^\circ < \Psi < 45^\circ$ and the rail's rotation axis $-45^\circ < \Phi < 45^\circ$. The instrument can still become singular with the Φ -axis, but this point is moved to one far end of its reach. Fast system movements are still present, when the instrument is manipulated near the Φ axis. Although executed with two curvature ball rails, The University of Tokyo [83] uses such a RCM layout.

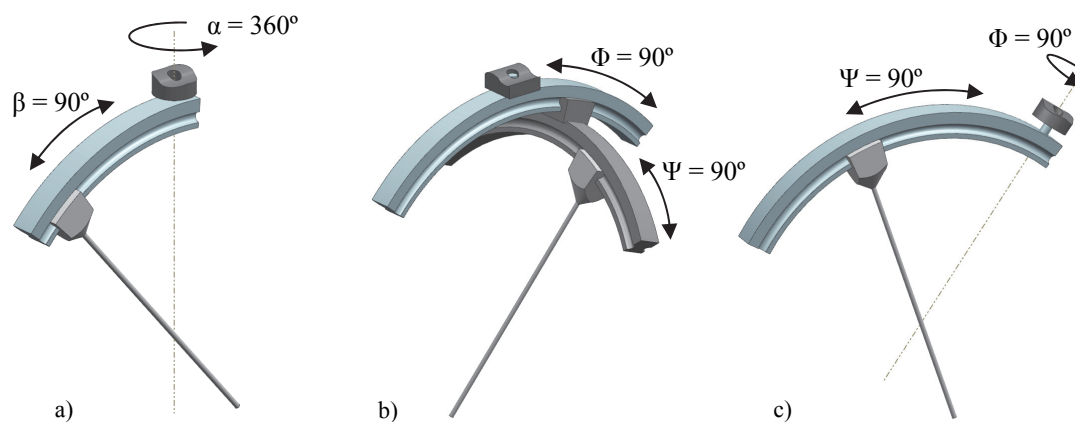


Figure 4.2/ Curvature rail remote center of motion mechanisms.

In system b) two curvature rails are used. The first is rigidly mounted to the pre-

surgical adjustment system. The second segment is rigidly mounted to the slide unit of the first segment and is guided along in Φ . The instrument is mounted to the slide unit of the second segment by which a total stroke can be reached of $-45^\circ < \Phi, \Psi < 45^\circ$.

None of these systems are chosen for reasons of practicality. Access to the instrument might be obstructed by the permanent overhead presence of the curvature rails. The rails will obstruct peripheral equipment and the view of the microscope or the microscope body. Furthermore, during surgery, these systems might make unexpected movements for unaware operating room assistants.

4.2.3 Parallelogram mechanism

Figure 4.3 shows a planar wire model of the parallelogram mechanism. By connecting two parallelograms in the way shown, the instrument movement at the secondary parallelogram (SP) is copied from the primary parallelogram (PP). The PP is mounted via linkage A_0-B_0 to the pre-surgical adjustment system. The upper linkage is shared by both parallelograms. The lower linkage (E-D) of the SP is connected via a hinge to the left vertical linkage (B-B) of the PP. Typically by actuating the PP the upper linkage remains horizontal, while both vertical linkages rotate in Ψ .

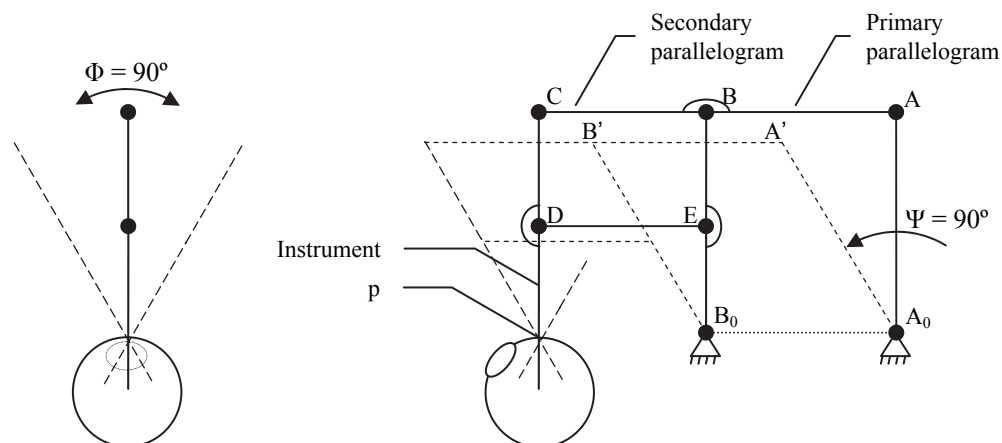


Figure 4.3/ Parallelogram mechanism.

Considering the left linkage (C-D-p) of the SD to be the centerline of instrument, the Ψ rotation of the instrument about point p is realized. By rotating the complete parallelogram mechanism sideways over linkage A_0-B_0 , the Φ rotation is realized and its pivot point p is defined as the remote center of motion.

The major advantage of the parallelogram mechanism is the possibility to create a slender design near the instrument, whilst maintaining good lateral stiffness on the instrument axis. Like in a circle sector centered on the eye, the further away from the eye the more room for the mechanical design. This allows freedom of movement with respect to the anatomical shape of the head, accessibility of the instrument and peripheral equipment. Wires to and hoses for the instrument can easily be guided away over the mechanism. Actuation of Φ and Ψ is possible via multiple single-input-

single-output control, like: to and from the dedicated master [33]. The parallelogram mechanism concept is chosen for manipulation of the Φ and Ψ degrees of freedom. This remote center of motion type mechanism is also described by van den Bedem [7][8] for the manipulation of MIS endoscopic instruments.

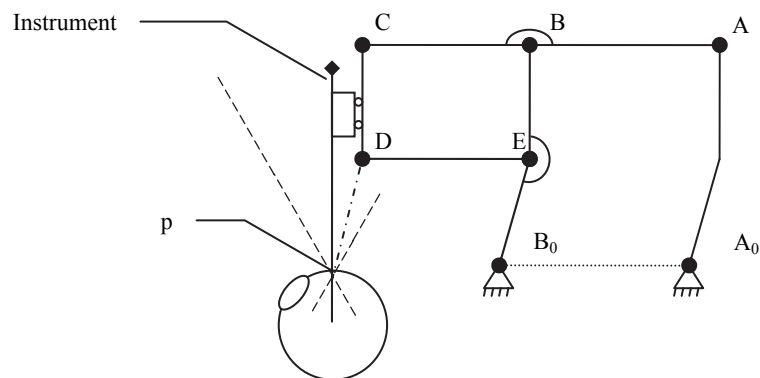


Figure 4.4/ Parallelogram mechanism with hinges offset.

The location of the hinges C and D do not necessary need to intersect the Z axis as the case in Figure 4.3, as long as the relative location of C and D is copied to the PP. Figure 4.4 shows a planar wire model of a parallelogram mechanism, where hinges at the instrument axis (C, D) and corresponding hinges at the PP (B,E and A) have an equal offset to the back. Because hinges C and D are offset backward, it leaves room for further mechanics e.g. the Θ -Z manipulator.

4.2.4 Concepts to manipulate θ and Z

Manipulating Θ and Z is done after Φ and Ψ , otherwise it would imply a shift of the remote center of motion. Variation in concept refers to the order of manipulation Θ and Z. The most obvious choice is a serial structure where Z is manipulated first, the Θ degree of freedom is taken along in Z direction. A Θ -manipulator can be lighter and more compact and therefore easier to manipulate in Z-direction than the other way around.

Concepts for Z-manipulation with flexure mechanics, like a double parallelogram and quasi-linear ways are considered, however are not suitable because of their limited straight reach in combination with the large mechanical volume. The relatively large reach for the Θ and Z DoF, values concepts with an unlimited reach more suitable. For the Z-DoF this refers to the use of rollers over a track rail, a low friction guidance or commercially available ball-circulating linear ways. These concepts are more or less equally suitable. For a concept based on a low friction guidance, actuation torque can be limited and wear can be well controlled by choosing the right materials (e.g. low friction plastics resistant to wear and FDA/CE approved.) in combination with the right pre-load. With high actuator stiffness, hysteresis can be minimized which results

in an acceptable positioning accuracy. The low friction guidance concept is not chosen for guidance of the Z-DoF. For Z-actuation a concept with similar aspects based on a commercially available leadscrew is realized. The use of rollers on a rail appeared to take up the most construction volume, and was therefore not applied. To minimize production cost and for easy replacement in case of failure, a concept based on a commercially available ball-circulating linear way was chosen for Z-guidance. To accommodate the Θ -DoF, a conventional ball bearing is perfectly suitable.

4.3 Design characteristics of the instrument manipulator

Figure 4.5 shows the resulting design of the instrument manipulator. It is designed for high stiffness, low mass and low inertia and high accuracy positioning. The manipulator has a serial layout, by which the manipulated degrees of freedom (DoF) are grouped into a Z- Θ and a Φ - Ψ manipulator.

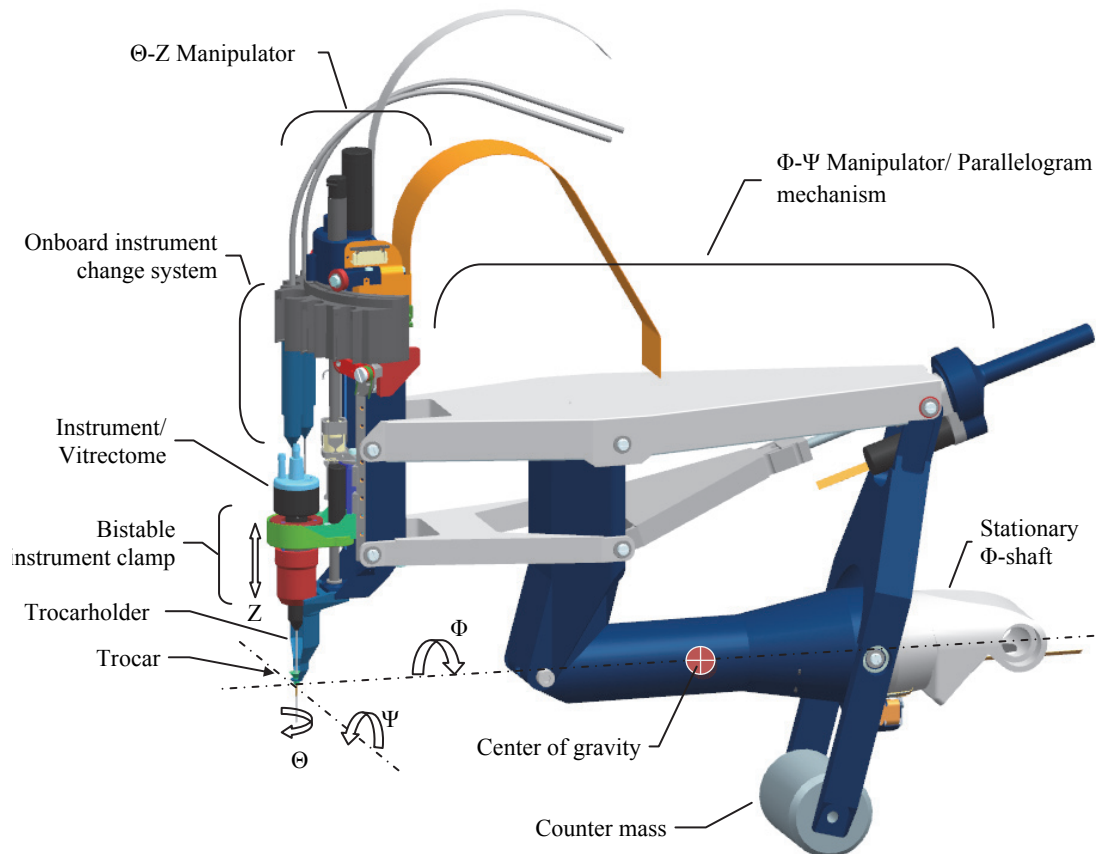


Figure 4.5/ The instrument manipulator.

Beside technical and performance properties, which will be discussed further on, the instrument manipulator has several practical design properties, which are discussed first.

Physical characteristics

The instrument manipulator is about 270 mm in length, 65 mm wide and from the Φ -axis to the top of the Θ -Z manipulator 175 mm in height. Most of the instrument manipulator's mass is actuated in Φ and Ψ direction, therefore a counter mass is added, by which the center of gravity is brought to the Φ -axis (indicated in Figure 4.5, only slightly depending on Φ angle and the position of the Z-DoF). The instrument manipulator weighs about 830 g, of which 480 g is contributed by the counter mass.

For overall safety, all DoF are backdrivable (RS3), whereby the surgeon or surgical assistant is able to overrule the actuator. Using the counter mass the instrument manipulator is balanced (RS2), resulting in additional intrinsic safety. Regardless of the orientation, the instrument manipulator will not drift away in case of system failure (e.g. power loss). Additionally, the actuation torque is drastically reduced, even with the increase of the inertia (Section 4.5).

Accessibility

The instrument manipulator is designed in such a way, that all the mechanics are placed towards one side, away from the instrument and eye. Here, a slender front-end of the manipulator is the key. Except for the clamp enclosing the instrument, no mechanics are placed in front or aside of the instrument. This is beneficial for accessibility to the eye in several ways, like:

- view onto the eye,
- accessibility to the eye for the surgeon or assistant,
- room for multiple instrument manipulators,
- accessibility for peripheral surgical instrumentation, e.g. infusion,
- minimizing obstruction of the light envelope of the microscope.

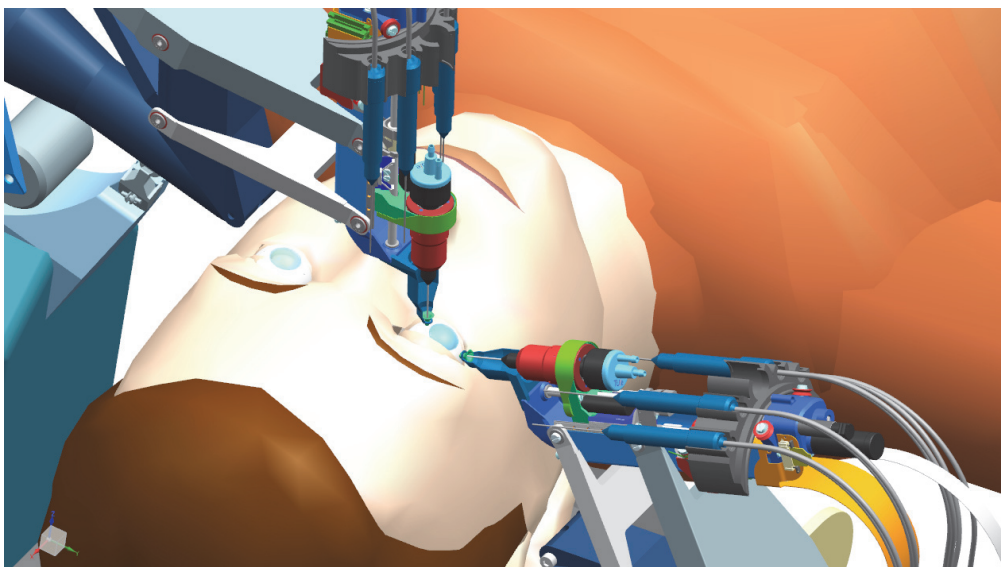


Figure 4.6/ The slender instrument manipulator design leaves room around the eye for e.g. the use of a microscope or peripheral equipment.

At bimanual surgery, the instrument tips are always pointing towards each other, as they operate in the same region. Since movements are inverted by the entry point to the eye, outside the eye, the instruments axes and consequently, the instrument manipulators are orientated away from each other. This also contributes to the accessibility to the eye and leaves room for the light envelope of the microscope (Figure 4.6).

Automated actions

Although the instrument manipulator is mostly controlled by the surgeon, some simple tasks can be performed by the instrument manipulator automatically. For instance:

- the first instrument can be a one step stiletto/trocar assembly [22]. When the trocar is placed by the instrument manipulator, it can literally define the entry point to the eye at the remote center of motion,
- at vitrectomy a large part of the vitreous humour may automatically be removed, e.g. up to 1 mm near the retina,
- a detached retina can be reattached to the eyeball by laser photocoagulation. By defining a certain area, by e.g. manually setting the boundaries, the instrument manipulator can coagulate a certain pattern e.g. honeycomb or rectangular, reattaching the retina,
- instruments can be changed automatically. Where the surgeon can position the instrument's tip at a safe location, wherefrom the automated action can retrieve the instrument and exactly reposition the next, for the surgeon to take over control.

Additional to the latter, the trocar is held by a trocarholder (Figure 4.5), which is connected to the instrument manipulator. The trocar is manipulated along in Ψ and Φ direction, by which the cannula is always optimally aligned with the instrument axis. With the trocar aligned, the instrument manipulator can always find the trocar's access point, when introducing an instrument to the eye. This is crucial for (automatically) changing instruments. Moreover, by holding the trocar aligned, the least forces and torques are applied to the instrument by the trocar. Which is beneficial for surgical force/torque measurement and improves positioning as the friction is reduced by avoiding normal forces on the cannula wall.

Onboard changing system

In manually performed eye surgery, changing an instrument is time consuming. Changing instruments implies certain steps, first the instrument to be changed must be withdrawn from the eye and the following tool must be chosen. To re-enter the eye often a part of the microscope must be rotated away from the scene, to create a view of the superficial outer part of the eye. By using trocars the entry points are well defined, however, hard to access, because the tip of the instrument must accurately be

positioned within the access area with a diameter of typically 0.5 mm. Then, the part of the microscope that was turned away is repositioned and the microscope focused to the point of operation. Most of the time, the instrument in the other hand is also withdrawn from the eye, for safety or to swap instruments from right to left or vice versa. To add additional advantages over manual surgery, each instrument manipulator is equipped with an onboard automated instrument change system [50][52]. Up to five instruments are available in a container, from which an instrument can be taken with the Z-stage. In only seconds an instrument can be changed at a single command i.e. all steps are automated by selecting the next instrument.

Although having the container adds weight and increased inertia, it has numerous advantages over an external changing ability:

- instruments can be changed in each possible instrument manipulator orientation as the container maintains its position relative to the active position in the working area, allowing no further movements than the Z-DoF to exchange the instrument,
- instruments in the clamp, and container are always aligned with the trocar, beneficial for an easy exchange and reintroduction of the next instrument to the eye. Contrary to an external container, where the instrument manipulator somehow has to dock and get perfectly aligned to make an exchange, subsequently has to perfectly realign with the trocar to reintroduce the next instrument,
- maintaining the instrument manipulator's remote center of motion at the eye's entry point ensures it to be positioned. Contrary to the uncertainty when the instrument manipulator is flipped away to the external changer,
- having the changing ability as close as possible to the operating instrument, allows the shortest time to change,
- it allows a compact solution, with the least amount of (moving) parts. Where an external changer is over headed, standing aside or behind the instrument manipulator and takes more volume and parts to realize the exchange.

Haptic properties

To measure forces and torques applied to the instrument, the most accurate commercially available 6 DoF force/torque sensor is chosen (ATI AI Nano17 [6]). This sensor has mN and Nmm force measuring abilities over $-12 < F < 12$ N and $-120 < T < 120$ Nmm. For the most direct force measurement, mounting the sensor coaxial with and directly to the instrument is desired (RP5). As a result forces and torques will be introduced with the least conversion. However, it is placed onto the Θ -module, parallel to the instrument, since it is chosen to change instruments axially (top loaded instruments).

4.4 Θ -Z manipulator

Besides manipulating Θ and Z, the Θ -Z manipulator is designed to change instruments. Instruments are changed axially, therefore the Θ -drive, like the force/torque sensor is placed parallel to the instrument. The onboard instrument change system only consists of the bistable instrument clamp, the Z-stroke and instrument container. To change instruments, the only additional DoF is to index the container to offer the desired instrument to the Z-drive. In the following, the Θ -Z manipulator will be discussed in detail.

4.4.1 Θ -module

The Θ -module mainly consists of the bistable instrument clamp, the Θ -motor and the Θ -Z interface. Figure 4.8 shows both an assembled and an exploded view of the bistable clamp and the Θ -module. Via the force/torque sensor and the Z-carrier the Θ -module is mounted to the Z-manipulator (Figure 4.8 and Figure 4.10).

To actuate Θ , the smallest motor available with an encoder is used, a Maxon EC6 with a 64 counts per turn encoder [49]. The motor efficiency is poor, but the torque output is sufficient. Resistance torque in Θ -direction is applied by the Θ -bearing, the friction of the instrument with trocar squeezed by the sclera, viscous resistance of the vitreous humour and torque applied during tissue manipulation. The total calculated torque to overcome is $T_{\Theta r} = 0.176$ Nmm (Appendix B). The torque that can be applied by the motor is $T_{\Theta} = T_{nom}\eta_{\Theta} / i_{\Theta} = 0.46$ Nmm (RP6). Herein, $i_{\Theta} = Z_1/Z_2$ the gear ratio and the gear efficiency assumed to be $\eta_{\Theta} = 90$ %. Functional tests in practice show a free run torque of $T_{\Theta f} = 0.072$ Nmm. The Θ resolution at the instrument is $\Delta\Theta = 0.715^{\circ}$ (RP3), which is sufficient for axial instruments. Instruments with a bent tip of 4 mm would have a resolution of 0.05 mm at the tip. This might not be sufficient, but announced encoder developments should solve this problem. A hall sensor mounted to the Θ -Z interface (Figure 4.8, Θ -module) and a magnet glued to the push-ring (Figure 4.8-Bistable clamp), functions as a Θ -indexation, as well as a sensor for instrument change verification (Section 4.4.4).

The bistable clamp including instrument is $m_{\Theta} = 23.6$ g in weight. With an inertia of $J_{\Theta} = 50 \cdot 10^{-9}$ kgm² relative to the motor shaft, plus the torque acting on the instrument during surgery an angular acceleration of 3240 rad/s² can be realized. This indicates that the torque due to inertia is inferior to the torque applied during surgery.

The flex foil conductor (FFC) of the motor and the hall sensor is led away over the Z-carrier, to a second FFC, which is guide towards the control electronics. (Figure 4.8- Θ -module).

The bistable instrument clamp is suspended to the Θ -Z interface, by a custom made angular contact ball bearing. The bearing's outer and inner ball raceways are machined into resp. the Θ -Z interface and the base-ring of the clamp (raceways are

indicated on the base-ring in Figure 4.8). The contact angle is 45° and the ball diameter is 0.7 mm. For the most accurate raceways a radius of 0.4 mm is chosen, where it equals the radius of the cutting tool of the turning lathe. For installation of the bearing, the base-ring is divided in two. These parts are adjusted in axial length to eliminate free play. Two bearing versions are compared: one with 13 caged balls (Figure 4.7) and one with 72 uncaged balls per raceway. Endurance tests show no difference in friction torque ($T_{\Theta f} = 0.072 \text{ Nmm}$). Contrary to the uncaged version, the caged version showed signs of wear resulting in free play. Bearing calculations are made and presented in Appendix B. The clamp and Θ -Z interface are made of stainless steel AISI 420, which is commonly used for surgical equipment. Moreover, AISI 420 allows being hardened, where the clamp and bearing parts were hardened to 52 HRC to resist wear.



Figure 4.7/ Caged balls in a micro stereo lithographed cage, for the benefit of the Θ -bearing.

The bistable clamp is fitted with a gearwheel ($Z_2 = 59$), driven by a pinion ($Z_1 = 30$) at the Θ -motor. To mount the Θ -motor to the Θ -Z interface, it is glued to a cup (Figure 4.8-C). During installation, the cup has the ability to shift in radial direction towards the centerline of the instrument/bistable clamp. Subsequently, the pinion can be pushed into the gearwheel, by which any backlash is minimized. For a smooth run, the bistable clamp is turned several times, by which any irregularities of the gear- and pinion push the pinion/motor outwards. Then the cup is clamped to the Θ -Z interface by the fixation fork. The residual free play in the Θ -drive is not noticeable because it is a fraction of the Θ accuracy.

4.4.2 Bistable instrument clamp

The instrument is held by the bistable instrument clamp. The clamping function is based on a collet style clamp, where the instrument is rigidly clamped as close as possible to the surgical shaft. Clamping close to the shaft benefits stiffness, as the clamp is much stiffer than the instrument handle body.

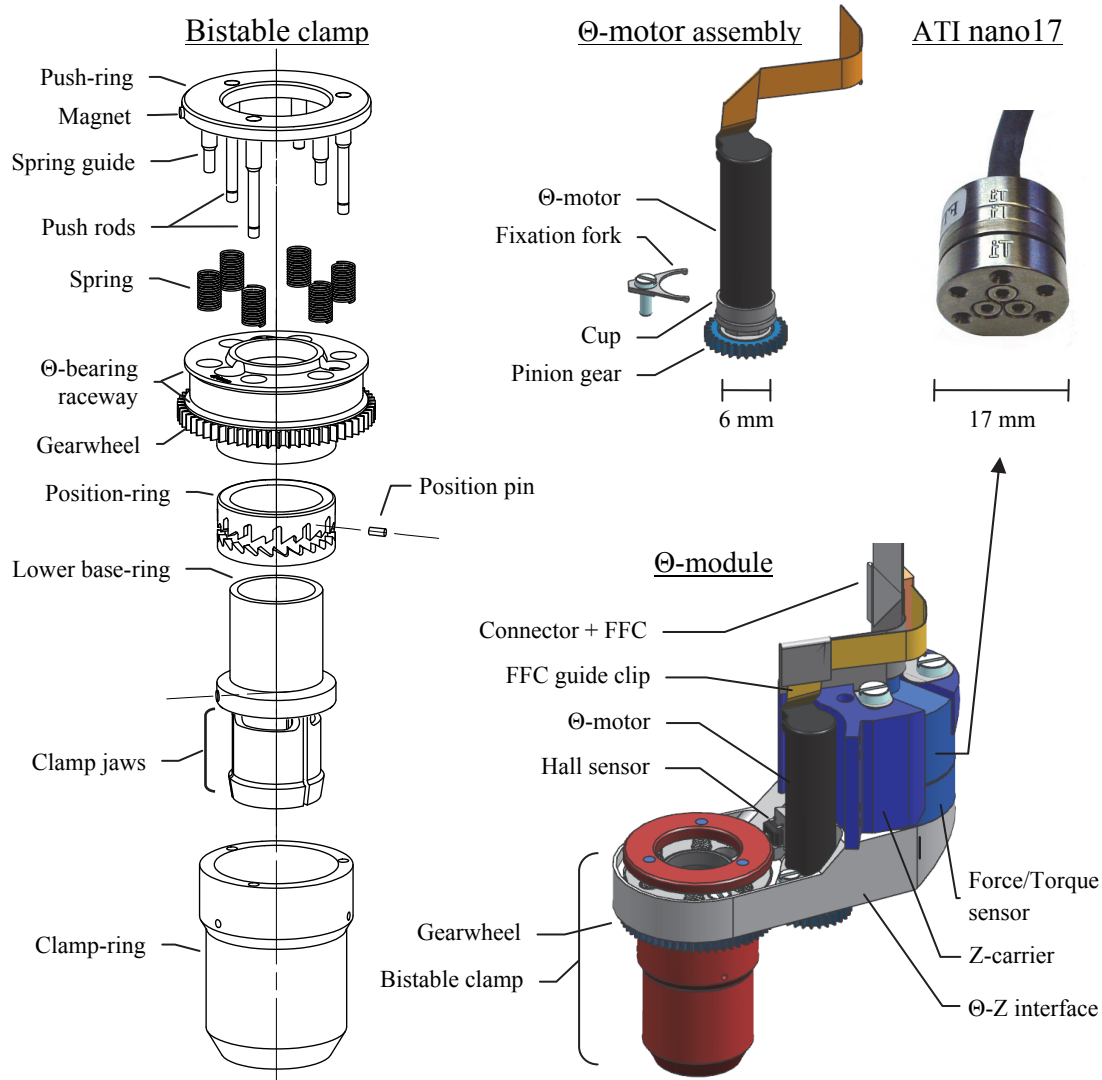


Figure 4.8/ The bistable clamp in exploded view on the left, the Θ -module on the right below. On top in the middle; the Θ -motor is clamped to the Θ -Z interface by the fixation fork. To measure forces, the smallest commercially available force/torque sensor is uses (upper right corner).

Clamping is realized by pulling the outer clamp-ring upwards, by which three clamp-jaws on the inner lower base-ring, are pushed radially inwards, via a cone shape (collet style). The outer clamp-ring is held by (three) push rods connected to a push-ring. Multiple springs push the push-ring and thereby pull the clamp-ring upwards with respect to the upper base-ring, to generate the clamping force. By pushing the push-ring downwards the clamp is opened. The bistable ability of the bistable clamp is realized by the position-ring. The position-ring is axially enclosed by the base-rings, leaving only one DoF free to rotate about its cylindrical axis. The position-ring is applied with a pattern onto the outer face of the cylindrical shape, in which three pins (one shown in Figure 4.8), mounted to the outer clamp-ring, are radially positioned. The pattern is as such, that an up and downwards movement of the outer clamp-ring rotates the position-ring with respect to the base-ring via the three pins in the pattern.

With each up and down movement, the pins drop into a high or a low notch, leaving the clamp in an opened or clamped position.

For safety, the clamping force is determined to an axial break loose force of 2 N, where it is considered the highest force applied during surgery (Section 2.2). By the relatively long cylindrical connection face and the property to centre the collet style clamp, the instrument is fixated in an accurately aligned manner. To define the Θ -orientation of the instrument with respect to the bistable clamp, an axial groove on the cylindrical surface of the instrument (Figure 4.9) encloses a pin extended inwards from the lower base-ring.

Modified instruments

Conventional instruments (Figure 2.5) are used with only minor modifications to make the handle-body fit for mechanical, collet style clamping into the instrument manipulator. Their manufacturer can be the supplier of today's disposable manual instruments, without changing much of their production methods. Instruments with an additional degree of freedom, like scissors or forceps need an additional modification to actuate this degree of freedom. The actuation can be pneumatic, by which their design can be similar to a vitrectome. Figure 4.9 shows a realized instrument, a vitrectome (like Figure 2.5), with the handle body modified.



Figure 4.9/ Realized modified instrument: a vitrectome.

4.4.3 Z manipulation

The Z-DoF is used for manipulation of the Θ -module with the surgical instrument, as well as for changing the instrument. Therefore, a somewhat larger Z-stroke is desired to change instruments, over the stroke required for high accuracy positioning for surgery within the eye itself. Figure 4.10 shows the Z-manipulator.

Z-Guidance

To guide the Θ -module in Z-direction, chosen is to use miniature linear guide ways, IKO LWL1Y [58]. These are the smallest commercially available ball-circulating

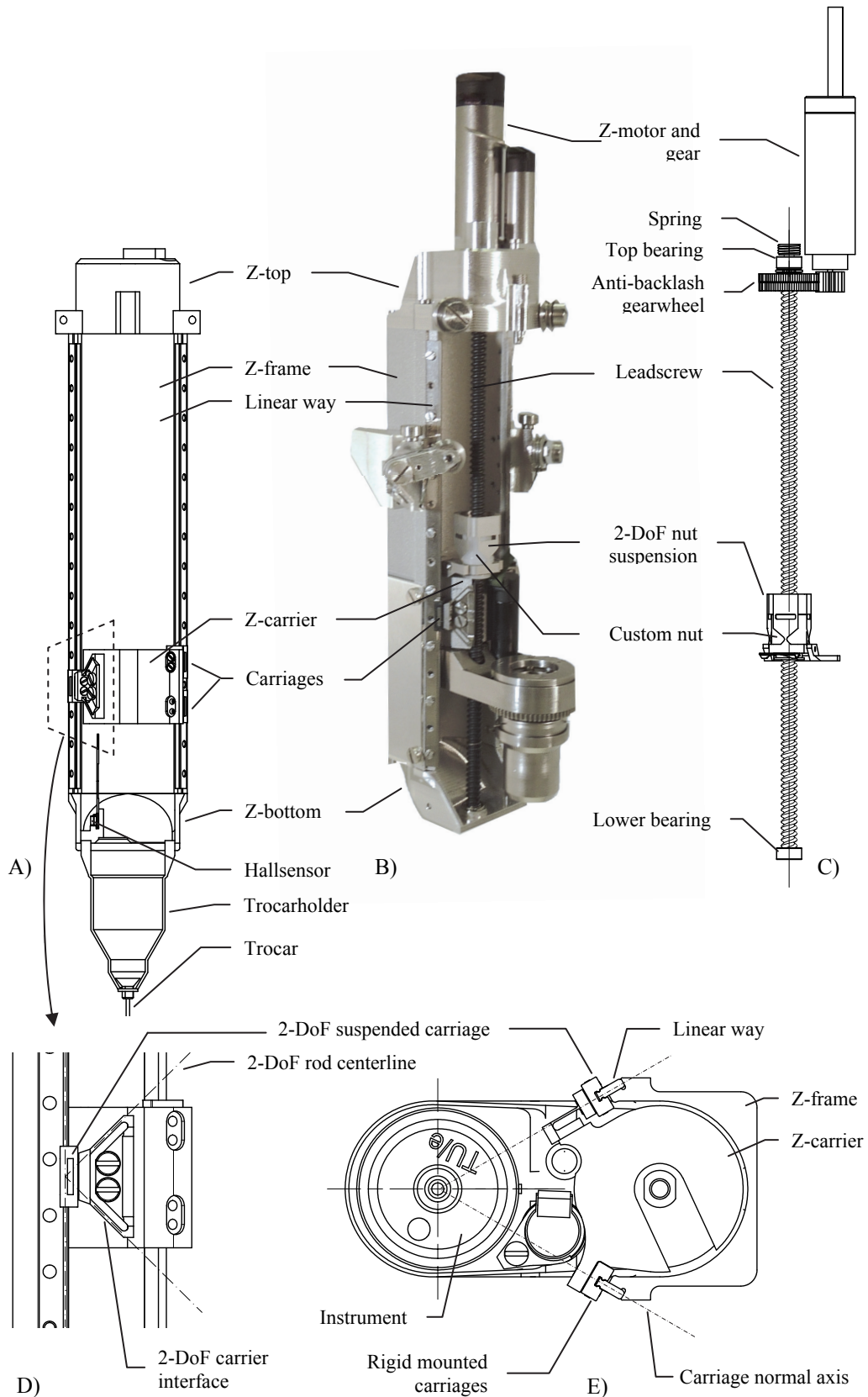


Figure 4.10/ Center top: realized Θ -Z manipulator (B) with: to the left, the Z-guidance (A) and to the right the Z-drive (C). On the lower left in isolated view, the 2-DoF suspended carriage (D) and the lower right, the carriage orientation (E).

linear ways, where the track width is 1 mm and the carriages upper surface is 4x6 mm. The LWLIY is capable of resisting relatively high forces ($C_0 = 113 \text{ N}$), but are relatively vulnerable for torques applied ($T_0 = 0.06 \text{ Nm}$). Therefore, to suspend the Θ -module three carriages on two linear ways are used. The carriages are orientated as such that forces are introduced as normal forces, by which the normal vectors of the carriers intersect the longitudinal axis of the instrument (Figure 4.10-E). The linear ways are mounted to the Z-frame (Figure 4.10-A, B, E). Two carriages on the single linear way are mounted rigidly to the Z-carrier (Figure 4.10-E). Their mounting surface is assumed to be perfectly aligned, because the Z-carrier contour is created in a single step by wire electrical discharge machining (EDM). For any misalignment, the opposing carriage is suspended to the Z-carrier in two degrees of freedom (Figure 4.10-D), the DoF normal to the carriage and the Z-DoF to take the carriage along in Z-direction. This is realized by an interface of two struts in V-arrangement, where from the normal axis of the struts intersect at the centerline of the raceway (Figure 4.10-D). This way the least force/moment due to strut stiffness is introduced to the carriage when the carriage is misaligned. The carriages have a slightly hollow mounting surface, which is flattened when mounted. This eliminates any free play as the carriage raceways come inwards (the u-shaped sides of the carriage), closing the balls towards the raceway of the linear way.

Finite element calculations of the 2-DoF carrier suspension and the respective linear way overload calculations are presented in Appendix C.

Actuation of Z

For actuation of the Z-DoF a miniature ballscrew was considered [78]. The advantages of a ballscrew are the smooth run, high axial stiffness and the ability for high positioning accuracy. The major disadvantages are the idling torque of 3 Nmm and the fact that miniature ball screws aren't play free. Two nuts pushed apart by a spring can solve the play problem, but demands more construction height and it will not benefit the costs. As an alternative, a leadscrew is about 1/20 of the price of a miniature ballscrew. A TFE coated LNTB3 (3.2 mm) leadscrew [65] is chosen to actuate Z. The respective anti-backlash nut is dismissed, it appeared to have an undesired angular misalignment, due to the two relatively short parts pushed apart by a spring. As springs are compressed, their axial core leaves the center line, as all windings tilt under torsion and the outer windings are prevented from doing so by the faces against which they are held [70]. The resulting moment causes the misalignment. Moreover, the short parts do not benefit stiffness, because just a small contact surface of the plastic nut is addressed. Therefore, a larger custom made nut is used. The nut is made of POM, an FDA approved plastic, which is highly resistant to wear, has a high impact strength and a relatively low coefficient of friction ($\mu_{\text{pom}} = 0.1-0.2$). The nut is made by use of a modified leadscrew (Figure 4.11-A).

In four steps the custom nut is manufactured from a bar stick. First, the outer contour is machined and a central hole is bored. Secondly, the thread is pre-cut. Then, a modified leadscrew is used to cut the exact right thread shape. The modified leadscrew is turned to a taper at the end, after which a radial cut is grinded in to create a cutting edge. The other end of the modified leadscrew (not shown in Figure 4.11-A) is roughened by sandblasting. The nut thread surface is smoothed over the roughened leadscrew. A perfect enclosed fit is ensured, because while cutting, the plastic is partially plastically, as well as elastically deformed due to material properties. The custom nut measured friction torque is $T_{\text{nut},f} = 0.02 \text{ Nmm}$. Because the thread over the complete nut length is used the highest stiffness is realized.

The leadscrew is suspended by two bearings to the Z-bottom and the Z-top (Figure 4.10-C). The upper bearing is pre-loaded by a spring (20 N) to eliminate free play. The nut is suspended to the Z-carrier via a 2-DoF elastic cardanic suspension, stiff in only Z-direction and Θ direction. By two sets of incut leaf springs placed perpendicular to each other with a rigid body in between (Figure 4.11-B, C), two translations and two rotations are left compliant. This allows the nut to follow along the spindle. Each set of parallel placed leaf springs leaves the translation normal to the leaf spring surface and the rotation about that normal axis compliant (illustrated by a simplified version of the elastic cardan in Figure 4.11-C). Figure 4.11-B shows the actual 2-DoF nut suspension, with the second set of leaf springs downwards. This brings the leaf springs' hinges all to the same Z-height, by which a pivoting point is created near the centre of the nut. The nut is easily fixated to the elastic cardan by a clip by which the nut is fixated on friction inside the elastic cardan (Figure 4.11-B).

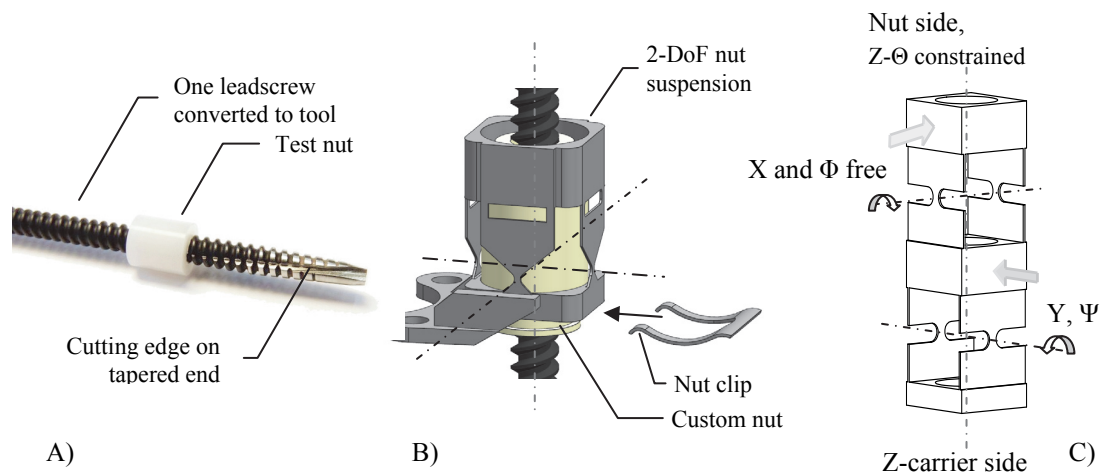


Figure 4.11/ Custom leadscrew nut and the 2-DoF nut suspension; A) the modified screw for nut realization, B) the nut and 2-DoF elastic cardanic suspension, C) simplified representation of the 2-DoF elastic cardanic suspension.

The highest surgical force is about 2 N when a stiletto penetrates the eye for trocar placement at the start of surgery [63], thereafter the average force during surgery is 300 mN [30]. The highest force for the Z-drive to overcome is 10 N, compressing the springs under the push-ring while changing an instrument (Section 4.4.4). With a lead

of $p = 1.22$ mm and the efficiency of $\eta_z = 61$ %, the torque to drive the screw is $T_{Z_{\text{surg}}} = 0.095$ Nmm and $T_{Z_{\text{max}}} = 3.18$ Nmm. For actuator stiffness a direct driven leadscrew, by a Maxon EC10 motor [49] would be a perfect solution. Its nominal and stall torque are respectively $T_{\text{nom}} = 1.83$ Nmm and $T_{\text{stall}} = 19.3$ Nmm. Equipped with highest resolution encoder possible (256 counts per turn), it would result in a positioning resolution of $\Delta Z = 1,2$ μm . It is desired to have (sub) μm positioning resolution (RP3). Therefore, an anti-backlash gearing is applied ($Z_1 = 17$ and $Z_2 = 38$), by which the positioning resolution becomes $\Delta Z = 0,52$ μm . First functional tests show a no-load torque of $T_z = 0,055$ Nmm to set the Z-DoF in motion. The lead of $p = 1.22$ mm is chosen for its backdrivability, which theoretically is $p/D_{\text{out}} \geq 1/3$ [63] and confirmed in practice. Near the lower end of the Z-stroke a hall sensor is placed, which, by use of a magnet placed on the Θ -module, provides a homing signal.

The mass manipulated in Z-direction is $m_z = 56$ g. The total inertia of the mass and inertia of the Z-drive relative to the motor shaft is $J_z = 18 \cdot 10^{-9}$ kgm^2 . The calculated maximum acceleration is 3460 mm/s^2 . The theoretical time to exit the eye (from maximum insertion, $Z = 25$ mm) is $t_{z\text{-exit}} = 0.12$ sec, for a constant acceleration. Then, the exit speed becomes $v_{z\text{-exit}} = 415$ mm/s. This is much faster than (RP3) and provides the possibility of rapid removal in case of emergency. However it is not certain what the reaction of the patient's eye would be to the instrument speed. This should be examined in clinical experiments.

4.4.4 Onboard instrument change system

To change instruments, the bistable instrument clamp, the Z-manipulator and the instrument container form the onboard instrument change system [50][52]. The basic design parameters of the onboard instrument change system are:

- easy and fast pre-surgical preparation,
- easy instrument replacement when alternative instruments are desired, which aren't present in the container,
- possibility to change instruments manually,
- simple and hence low mass mechanical design, e.g. passively clamping instruments in the container, the least amount of additional degrees of freedom (only indexing),
- simple and low cost disposable container design.

To match the design parameters, the instrument container is designed as a single injection moldable product and to be molded from ultra-high-molecular-weight polyethylene (UHMWPE). The material is chosen for its biomedical compatibilities and the low coefficient of friction. The container is packaged completely sterile, with a set of instruments for a specific intervention installed in it. The container has capability up to five instruments (Figure 4.12). The instruments are each passively held by two leaf springs, pushing the instrument to a cylindrical surface. Towards the

inside the leaf springs have a rounded stop-rim, which along with the friction force, prevent the instrument from slipping out of the holder pocket. To change an instrument, it is crucial for the instrument to be in contact with the rim i.e. in the lowest position. If not, the instrument will not be inserted completely into the bistable instrument clamp. Instruments in the container, which are not in use, are pushed against these rims by a spring.

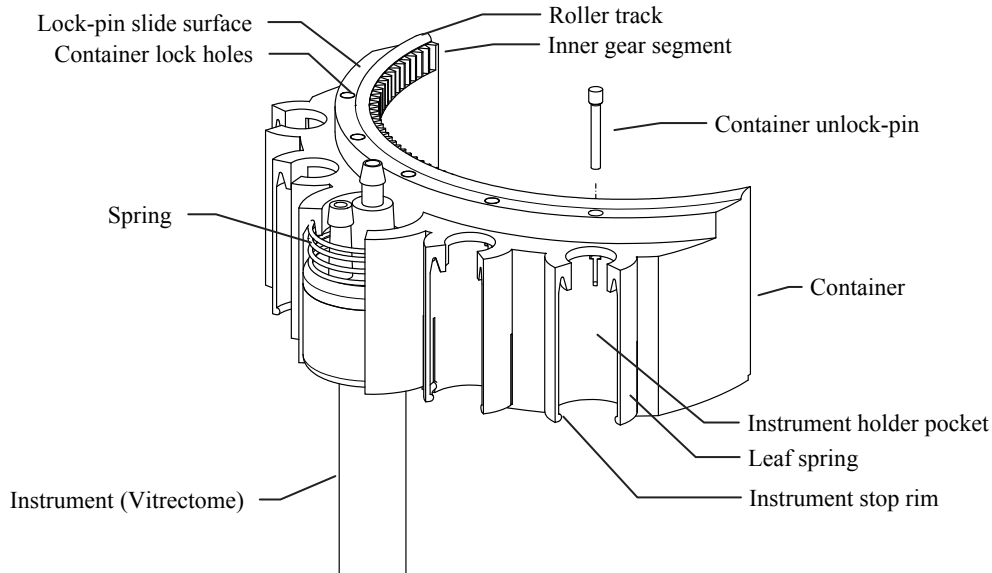


Figure 4.12/ The instrument container, with a vitrectome installed.

When other instruments are needed suddenly, which are not present in the container, or to replace a malfunctioning instrument, they can easily be replaced from the container. Simply by pulling the instrument downwards out of the holder pocket and introducing the next vice versa, an instrument can be replaced. Because most instruments will have a wire or hose attached (Figure 2.5) (e.g. a vitrectome, laser probe or illumination probe), the holder pockets are left open at the front. The spring pushing the instrument to the rim, is part of the instrument assembly and removed with it.

The container has an outward segmented shape, with a cylindrical shape on the inside away from the instrument holders. On the top and bottom edge, rounded roller tracks are situated (Figure 4.12). Over these roller tracks, the container is suspended in four V-rollers to the Θ -Z manipulator (Figure 4.13). The top rollers are mounded rigidly to the Z-top. The lower rollers are each placed on a lever, which forces the container to the top rollers by a torsion spring. Via a cable, each lever is connected to a release handle, located at the side of the Z-frame. By squeezing both handles inwards simultaneously, with thumb and index finger of the same hand, the levers swivel downwards (Figure 4.14) allowing a fast and easy container exchange.

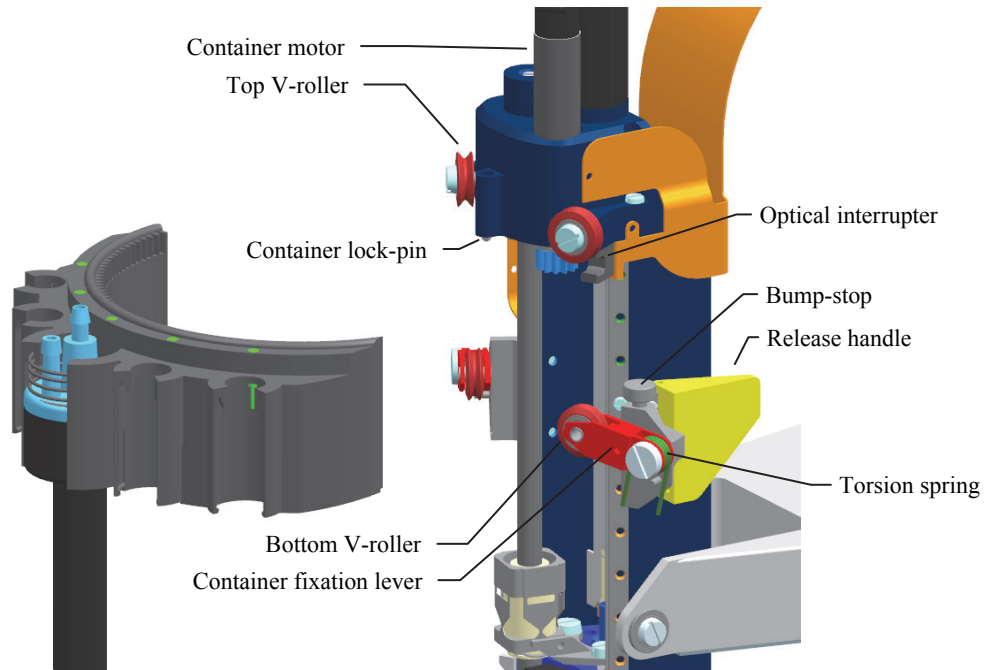


Figure 4.13/ The onboard instrument change system.

The container is installed by placing the upper roller tracks onto the upper V-rollers (Figure 4.14 (1)), before the lower tracks are inserted. Installation is simplified by two bump-stops to which the container may be bumped (Figure 4.14 (2)). After letting go of the release handles the container will align automatically to the instrument manipulator (Figure 4.14 (3)).

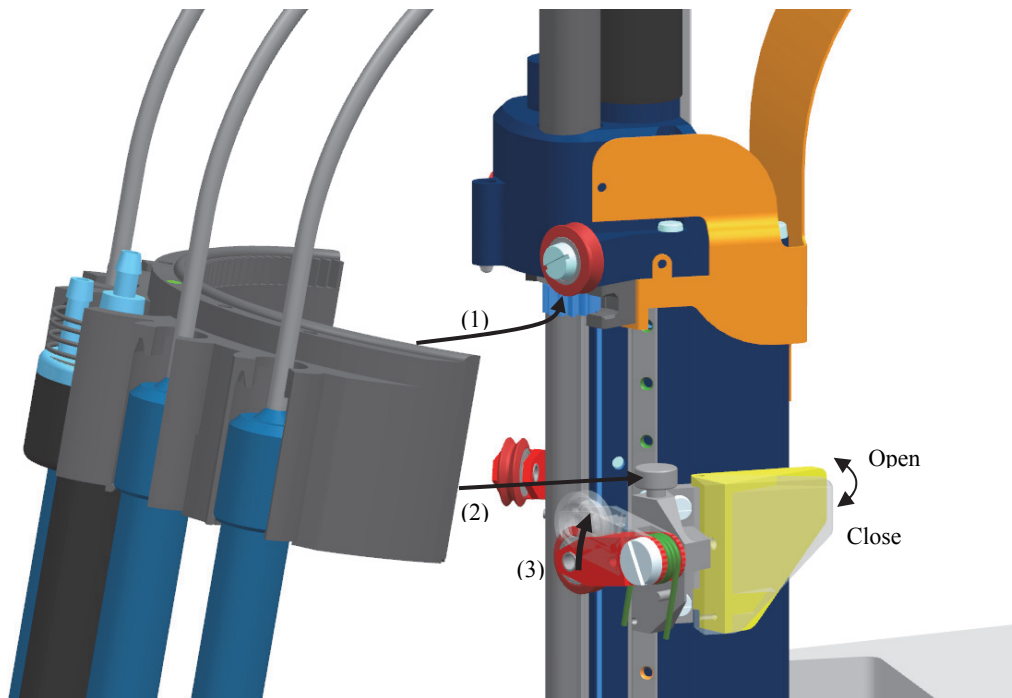


Figure 4.14/ Installation of the instrument container. First, the container is placed into the upper V-rollers. Then, rotated inward against the bump-stops, where after the fixation levers can swivel upward by releasing the release handles.

On the container at the upper side of the cylindrical shape, a segment of a ring gear is situated (Figure 4.12). A Maxon EC6 motor with planetary gearbox, mounted to the Z-top, drives the container in a circular index motion, by which an instrument is selected. The container is unlocked, when all instruments are in their respective holder pockets. If an instrument is taken from the holder pocket, the respective unlock-pin (Figure 4.12) drops, which leaves a hole on the lock-pin slide surface. This allows the lock-pin (Figure 4.13), located at the Z-top, to drop into that hole, subsequently locking the motion of the container. When the instrument is placed back into the holder, it pushes the unlock-pin back up, by which the unlock-pin's upper surface forms an even surface with the lock-pin slide surface. Now, the lock-pin is able to slide freely over the lock-pin slide surface, subsequently the container is free to rotate. Two optical interrupters at the Z-frame are used as end-switches (Figure 4.13), where a pin extended inward (not shown in Figure 4.12) at each end of the ring gear provide the interruption of the light path.

Procedure of instrument change

In Figure 4.15 the procedure of instrument change is illustrated. When a tool change is desired, the tool is withdrawn from the eye by an upwards Z movement (Figure 4.15-a,b). By the Z movement the instrument is returned to the instrument container (Figure 4.15-b, c.1). Simultaneously, the bistable instrument clamp is opened with the Z movement, by pushing the push-ring against the lower surface of the container (Figure 4.15-c.2). After opening, the bistable clamp stays open by its bistable nature, where the clamping force of the instrument container is higher than the remaining friction force in the bistable clamp (Figure 4.15-c.3). The bistable clamp can be lowered by the Z-s, leaving the instrument in the instrument holder (Figure 4.15-c.3). The next instrument can be selected by indexing the container (Figure 4.15-d). Next, the bistable clamp can make the upwards Z movement, to take the next instrument from the container (Figure 4.15-e). The bistable clamp is automatically closed, as it is yet another time pushed against the instrument container while taking the new instrument. Now, the clamping force in the clamp is higher than the clamping force of the container, which on a downwards Z movement (Figure 4.15-f) results in taking the instrument from the container. The instrument manipulator is ready to proceed with the newly introduced instrument in the surgical procedure.

The relation between the forces applied by the clamp, the holder and the spring over the instrument is relevant for changing instruments and further presented in Appendix C.2.

On the Θ -module a Θ indexation hall-sensor is placed (Section 4.4.1), which is also used as a change safety sensor. The magnet on the push ring (Figure 4.8) is positioned in front of the hall-sensor to change an instrument. When the clamp has been opened, the push ring and magnet do not come completely back up, which is detected by the hall sensor. If the signal is equal to that before changing instruments, the clamp has

not been set to opened position. A simple retry of opening might solve the problem, if not the system gives an error.

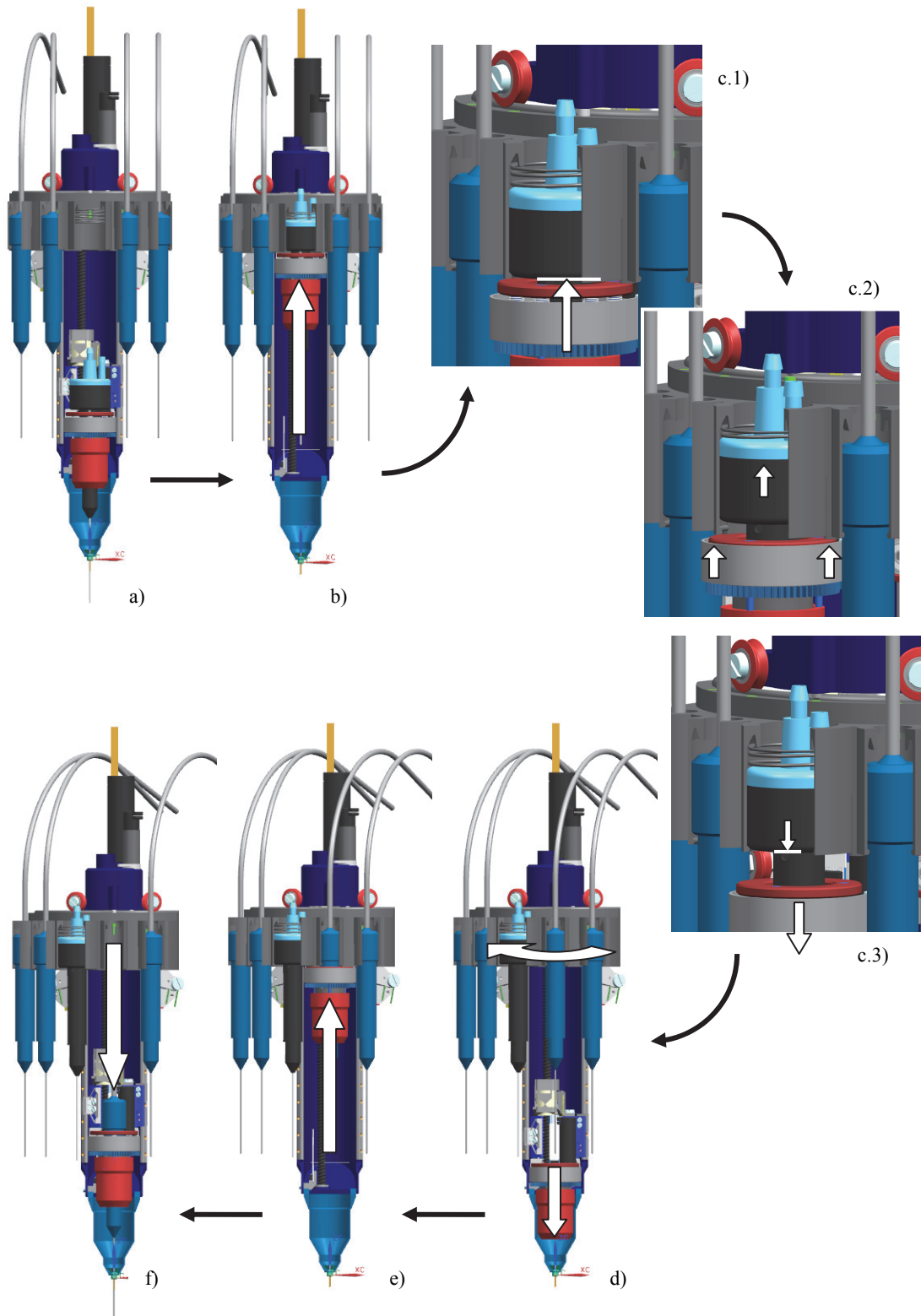


Figure 4.15/ Procedure of instrument change. By an up and downward Z-motion, the instrument is changed (indicated by the arrows).

4.5 Manipulating Φ

Like the Θ -Z manipulator, the Φ - Ψ part has a serial order (see Figure 4.16). From the stationary Φ -shaft, Φ is manipulated first. Onto the Φ degree of freedom, the parallelogram mechanism to manipulate in Ψ direction is mounted. The Θ -Z manipulator in turn is serial mounted to the parallelogram mechanism.

Where the design of the instrument manipulator is set for high stiffness and low mass, this certainly applies to the parallelogram mechanism. Because the respective parts are manipulated in both Φ - Ψ direction and some parts have a relative large distance from either the Φ or Ψ -axis, the inertia must be minimized. This is doubly rewarded as the counter mass shrinks at the same time. High stiffness benefits the position accuracy and helps to minimize hysteresis. To realize the lowest mass with the highest stiffness, the parts are designed as hollow box shaped bodies. Figure 4.16 shows the instrument manipulator, where the parts are indicated with additional weight information. The junctions corresponding to Figure 4.3 are indicated as well.

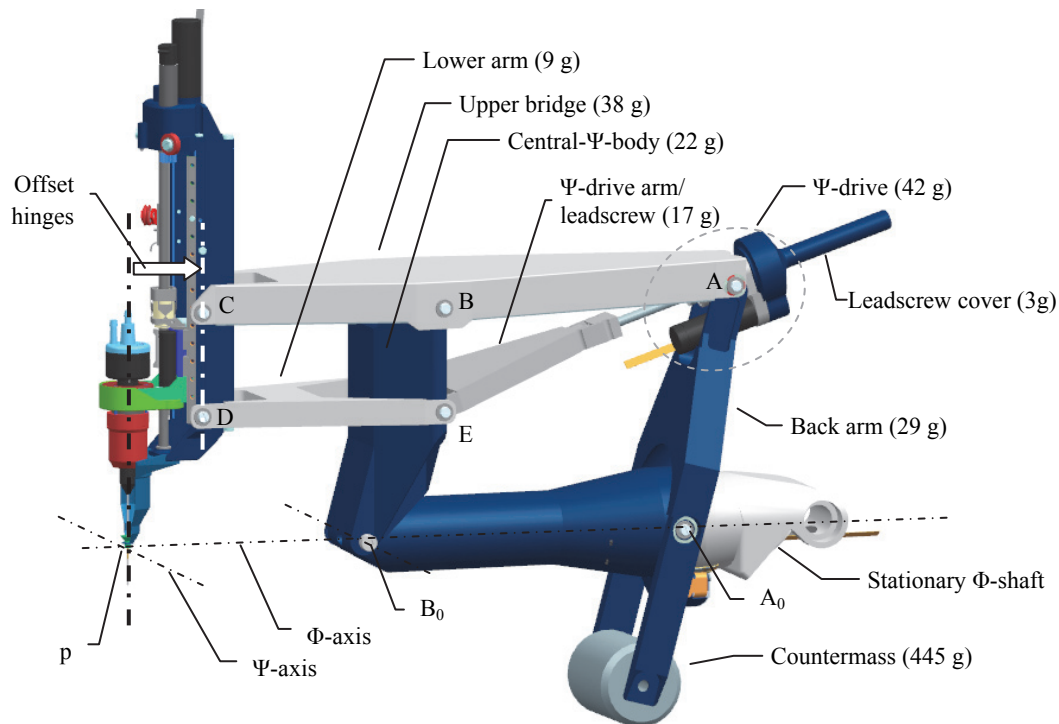


Figure 4.16/ Light weight parallelogram mechanism.

For the parallelogram mechanism in Figure 4.16, the junction layout with hinges offset is used (already indicated in Section 4.2.3 and Figure 4.4). Here, junctions C and D are set 21.5 mm backward with respect to the instrument axis and the remote center of motion at point p (Figure 4.16). Consequently, junction B, E and A have the same offset backward with respect to B_0 and A_0 . Now, at the front of the instrument manipulator, there is room for the Θ -Z manipulator and for stored instruments to pass when indexing the container.

4.5.1 Φ -drive

The Φ -drive consists of a central- Φ -body, a supporting bearing and an actuator (Figure 4.17). As an actuator, a PMA-5-80 Harmonic drive/motor combination [32], with a 512 counts per turn (cpt) encoder was chosen. The benefits of a commercially available, factory assembled product, with μm positioning ability (at 25 mm) are chosen over a custom made gearbox/motor. The harmonic drive is located inside the stationary Φ -shaft. On the closed end of the central- Φ -body, it is directly mounted to the shaft of the harmonic drive. On the open end, the central- Φ -body is suspended on a pre-loaded bearing to the stationary Φ -shaft.

The central- Φ -body has a cylindrical shape for torsional stiffness, torque applied at the closed-end (B_0 in Figure 4.16) as well as to the open-end (A_0 in Figure 4.16) is led stiffly into the actuator.

With a harmonic gear ratio of $i_{\text{HD}} = 80$ and the encoder resolution of 512 cpt, the angular resolution becomes $\Delta\Phi = 3.835 \cdot 10^{-5}$ rad, resulting in $\Delta\Phi = 0.96 \mu\text{m}$ at the tip of the instrument (at 25 mm from the trocar, RP3). With the maximal output torque of the harmonic drive ($T_{\Phi} = 350 \text{ Nmm}$), an angular acceleration of $86.6 \cdot 10^3 \text{ rad/s}^2$ can be realized. The harmonic drive appeared backdrivable in practice (RS3).

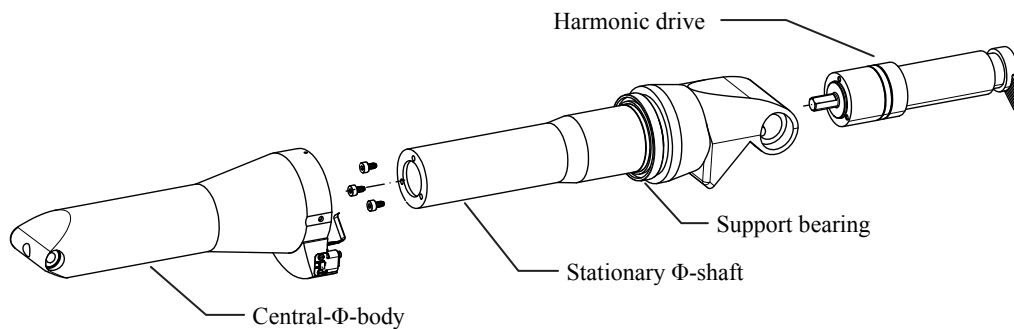


Figure 4.17/ Exploded view of the Φ -drive.

4.5.2 Ψ manipulation

Besides guiding the Θ -Z manipulator in Ψ direction, each part in the parallelogram mechanism has a specific task in transferring force from the actuator, stiffly to the instrument and stationary- Φ -shaft.

The central- Ψ -body is considered to transfer force to the rigid closed-end of the central- Φ -body, where it is directly led into the stationary- Φ -shaft via a relatively large bearing inside the harmonic drive [32]. The central- Ψ -body is designed as a thin-walled rectangular tube, combined with triangular shaped tubes on the sides (Figure 4.18). The walls centerlines of the triangular shaped tubes intersect the poles of the bearings at axes B and E, wherewith load is introduced as in-plane force to the central- Ψ -body.

Load from the Θ -Z manipulator is transferred to the central- Φ -body via the upper-bridge and the lower arm. Both parts are designed as hollow box-shaped bodies (Figure 4.18), where the upper bridge has a higher profile and additional ribs. This is due to the additional function of supporting the Θ -Z manipulator in Z-direction, where a force in Z is transferred stiffly to the central- Ψ -body and the moment from that force is held by the back arm. It was chosen to support the Θ -Z manipulator in Z-direction with the upper bridge instead of the lower arm. As the upper bridge can be extended to the back arm without being intersected, like the lower arm or the central- Φ -body would be.

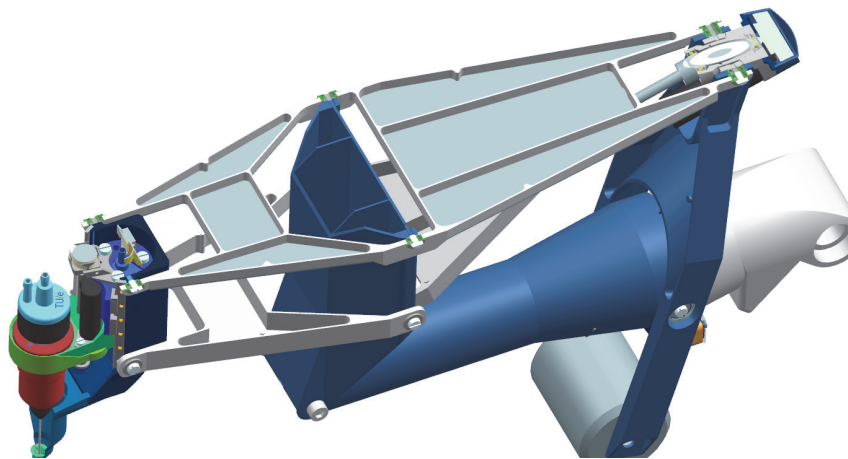


Figure 4.18/ Opened-up hollow shaped bodies of the parallelogram mechanism.

The location in height and the length of D-E of the lower arm is determined as such to leave room for the patient's nose. During surgery, the Θ -module operates in the lower 30 mm of the Z-DoF. To transfer load directly into the parallelogram mechanism, the distance between the upper bridge and lower arm is set just under and over this typical Z-reach.

Initially the back arm only functioned to support of the upper bridge in Z-direction and therefore, should only be stiff in supporting direction. However, with the introduction of the counter mass, a stiff back arm is require to e.g. increase the eigenfrequency of the back arm with the counter mass attached.

Per axis A/E (Figure 4.16, A_0 , B_0 , A-E) two bearings are used. The bearings at the left side are rigidly mounted. The opposing bearings are preloaded (5 N) by wave springs, positioned between the flange and the part. The springs are custom made from shims ($D \times d \times t = 8 \times 5 \times 2$). The bearings in axis A_0 and B_0 are slightly larger and are preloaded with 10 N.

Ψ Drive

With the experience gained by the realization of a cost efficient, simple, though highly efficient and accurate Z-drive, it was chosen to create a leadscrew Ψ -drive in a similar

fashion. The Ψ -drive is positioned between axis A and E (Figure 4.16), creating a stiff triangular framework (see Figure 4.20). Forces introduced by the upper bridge and lower arm are directly substituted by the Ψ -drive. The Ψ -drive is shown in Figure 4.19.

Contrary to the Z-drive, at the Ψ -drive, the leadscrew nut is actuated and the leadscrew is stationary. The screw is rigidly mounted to the Ψ -drive arm, which is suspended to the central- Ψ -body at the E-axis. Like the Z-drive, the custom leadscrew nut is made of POM. To avoid the nut from extending in time by creep, subsequently introducing axial play, the nut is glued in a stainless steel bushing before suspending it by bearings. Onto the leadscrew nut bushing, the inner bearing raceways are separated by a second bushing (not shown in Figure 4.19) and enclosed via the anti-backlash gearwheel ($Z_2 = 70$) by a nut. The latter is screwed onto the threaded end of the leadscrew nut bushing. The bearing at the gearwheel side, is rigidly mounted in the motor/bearing housing, the opposing bearing is mounted in a harmonic bushing. The length of the bushing between the bearings determines the deflection and as such the pre-load by the harmonic bushing, which is set to 30 N. A Maxon EC10 motor with a pre-mounted pinion gear ($Z_1 = 17$), is mounted to the motor/bearing housing.

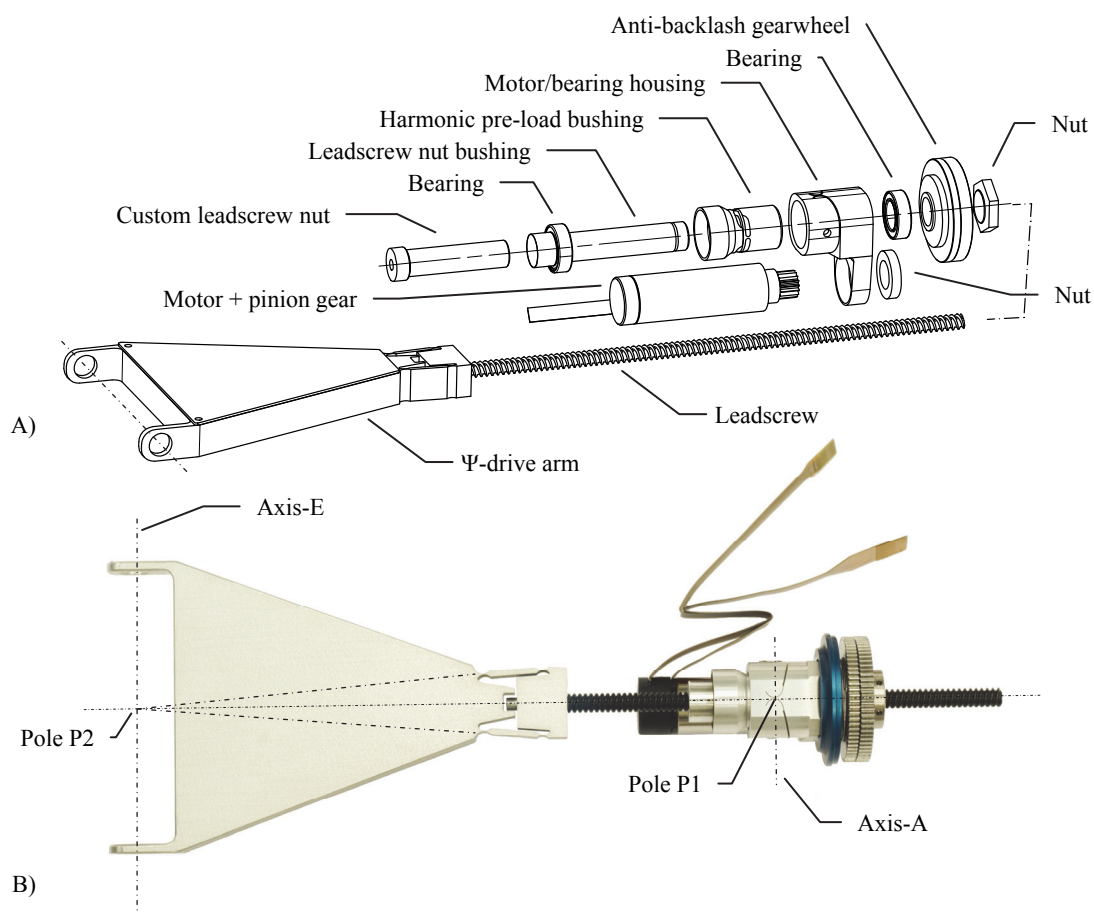


Figure 4.19/ The Ψ -drive in A) exploded view and B) realized Z-drive, indicated with centerlines.

The Ψ -drive is suspended in two degrees of freedom (DoF), where only the axial direction and the rotation about the leadscrew are desired to be stiff. Two DoFs are released by the rotation about axes A and E. Two poles (P1 and P2, indicated in Figure 4.19) allow a shift and rotation sideways, releasing another two DoFs.

Two system points are generated by positioning poles P1 and P2 at the intersection of the leadscrew axis and respectively Axes A and E (Figure 4.19). Pole P1 is realized by a hinge in the motor/bearing housing, between the part where the nut and motor are mounted to and the suspending to axis-A. Pole P2 is realized by two leaf springs from the part where the leadscrew is mounted to, to the part that is suspended by bearings at axis-E. The leaf springs point towards pole P2, by which the part where the leadscrew is mounted to rotates about pole P2 when e.g. it is forced sideways.

The leaf springs allow a leadscrew misalignment of 0.2 mm to either side, which corresponds with rotation of 0.13° . To align properly, P1 should allow an equal rotation. However the maximum rotation of P1 is set as 1° , where it corresponds with closing the 0.15 mm slit at the entry point of the wire electrical discharge machining (wire EDM) cut. A 0.15 mm slit allows a 0.10 mm wire to make perfectly defined cut, when leaving the cut where it has entered. Finite element analyses of the Φ -drive's elastic elements are detailed in Appendix D.

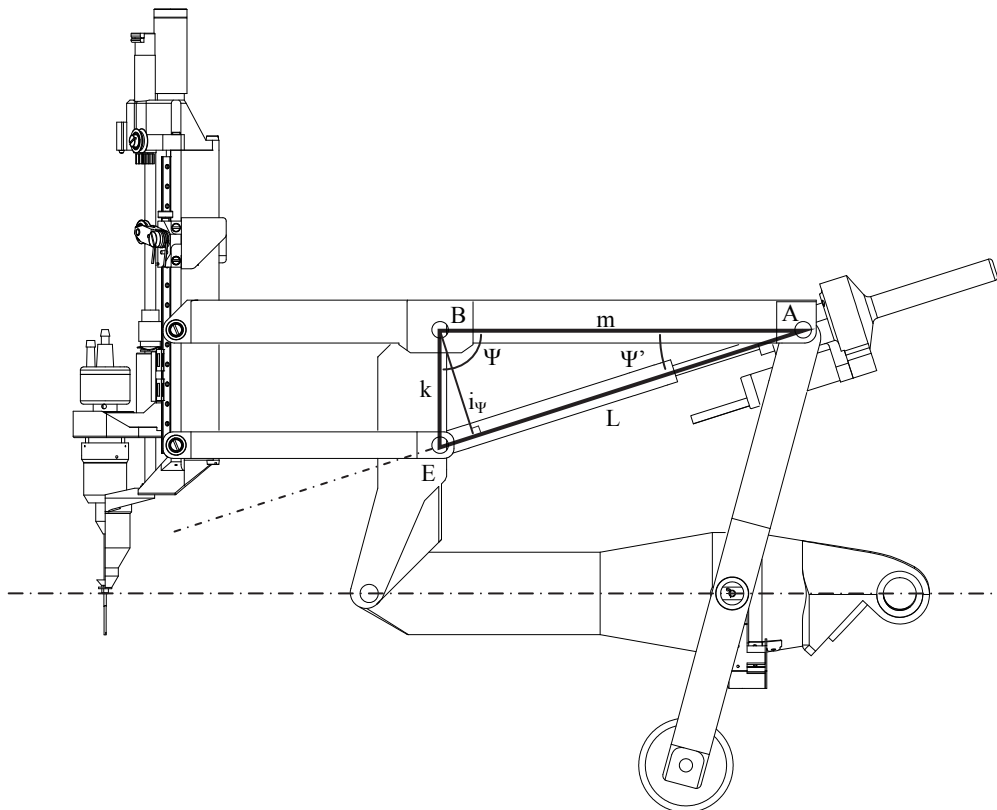


Figure 4.20/ Ψ actuator geometry.

In Figure 4.20, the geometry of the parallelogram mechanism with the Ψ -drive is shown. Point A, B and E relate to their respective axis (Figure 4.3, Figure 4.16). Line

L indicates the length of the spindle drive. By alternating the length of L, angle Ψ varies. With the rule of cosine the length of L can be calculated:

$$L^2 = k^2 + m^2 - 2km \cos(\Psi) \tag{4.1}$$

The torque that can be applied is the force of the actuator times distance between axis B and L, perpendicular to L. This is indicated by line i_Ψ . With length m and the angle Ψ' , which is also determined by the rule of cosine, length i_Ψ is calculated:

$$i_\Psi = m \sin(\Psi') \tag{4.2}$$

Since i_Ψ is not constant over the reach of the Ψ DoF, it becomes the Ψ -ratio between the linear Ψ -drive motion and the angular motion of the Ψ DoF. In the first graph in Figure 4.21, the ratio i_Ψ is illustrated. In Figure 4.21, $\Psi = 0^\circ$ is the neutral position of the instrument manipulator (like in Figure 4.20), is the positive angle Ψ a motion forward and the negative angle Ψ is a motion backwards.

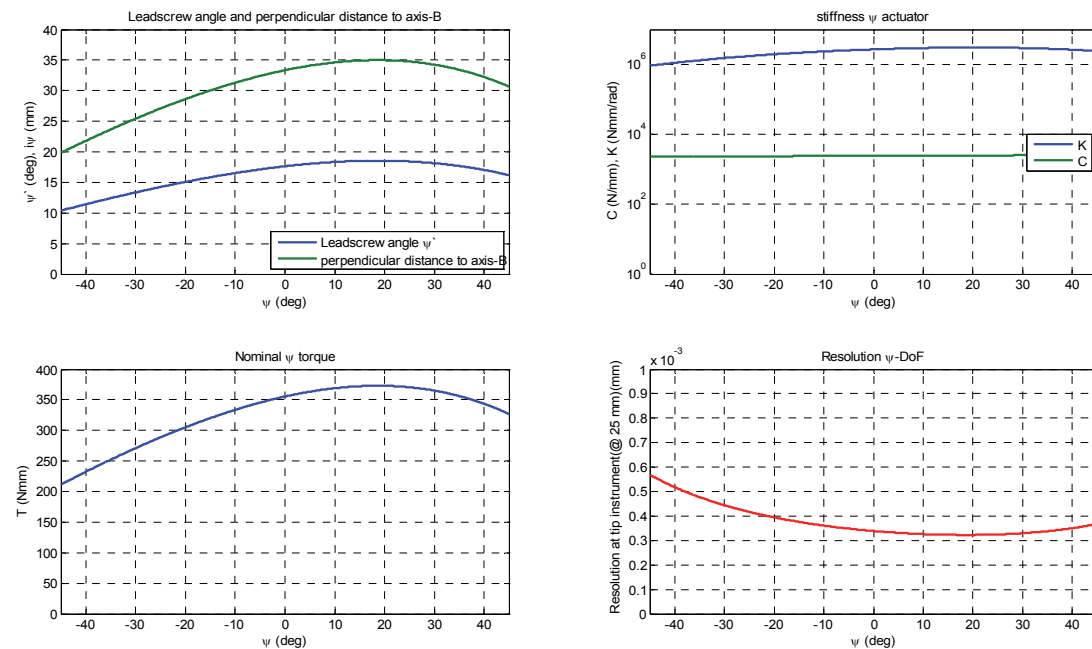


Figure 4.21/ Graphs of the Ψ -drive.

The second graph in Figure 4.21 shows the mechanical stiffness of the actuator, with c (N/mm) the stiffness of the Ψ -drive and k (Nmm/rad) the stiffness of the Ψ -drive in Ψ -direction. The stiffness is determined by the stiffness of the Ψ -drive A-arm, the nut-housing, bearing and the stiffness of the leadscrew. The leadscrew length is designed as 0 mm, when L is the shortest i.e. the Φ -drive arm touches the leadscrew nut. Depending on the length, the stiffness of the leadscrew part is $c_{\text{screw}} = EA/L_{\text{screw}}$, where E is the young's modulus (GPa) and A (mm^2) the cross-section of the screw.

In the third graph the nominal torque output in Ψ -direction is illustrated, which is calculated by ratio i_Ψ times the force output of the Ψ -drive:

$$T_{\Psi} = i_{\Psi} T_{nom} \frac{\eta_{screw} \eta_{gear}}{i_{screw} i_{gear}} \quad (4.3)$$

In which $T_{nom} = 1.18$ Nmm is the nominal torque of the motor, $i_{gear} = Z_1 / Z_2 = 17/70$ the gear-ratio from motor to nut, are $\eta_{screw} = 0.7$ % and $\eta_{gear} = 0.9$ % respectively the efficiency of the leadscrew and gear and is $i_{screw} = p/2\pi$ the ratio of the screw, with $p = 1.905$ mm the lead of the screw.

The fourth graph shows the resolution of the actuator in Ψ -direction in mm at the tip of the instrument (at $Z = 25$ mm). On average, the resolution is less than $0.5 \mu\text{m}$, it is calculated by:

$$\Delta\Psi = \frac{i_{gear} p}{4 * 256} i_{\Psi} Z \quad (4.4)$$

In which $4*256$ the evaluation of the encoder count and Z the instrumental distance from the trocar to the tip of the instrument.

To provide Φ and Ψ homing signals, two hall sensors are placed onto the central- Φ -body (Figure 4.22). Their magnets are placed respectively on the stationary Φ -shaft and the backarm. The hall sensors are soldered onto a custom flexible printed circuit (flex-PC).

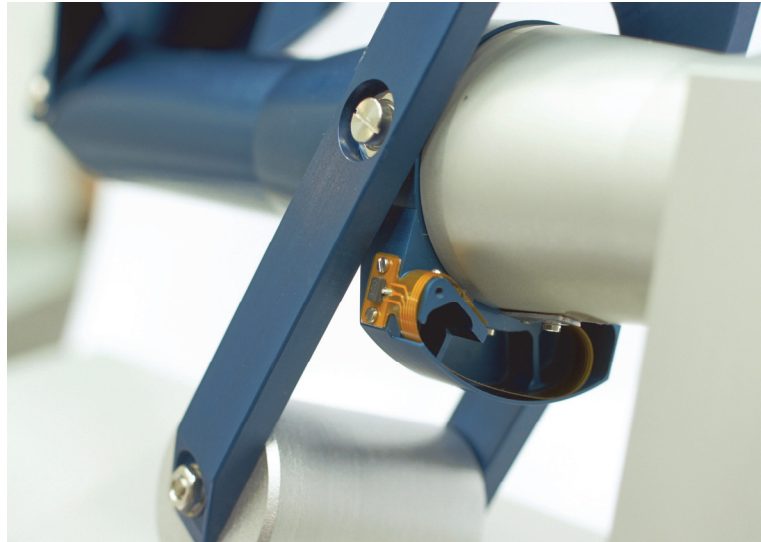


Figure 4.22/ Rear-side view from below of the instrument manipulator, with Hall sensors on a flexible-PC for Ψ and Φ indexation.

From the central- Φ -body, the flex-PC has to cross over the Φ degree of freedom, to reach the control unit. This is safely realized by rolling it over the cylindrical shape of the stationary Φ -shaft and a cylindrical shape concentric to the stationary Φ -shaft. A bending radius of 5 mm is chosen, where it is specified as the radius where a conductor thickness of $17 \mu\text{m}$ will not fatigue and give failure [90].

4.6 Instrument manipulator stiffness and eigenfrequencies

Each part is individually optimized for high stiffness and strength in finite element software. Likewise, the overall stiffness of the instrument manipulator is analyzed as an assembled model. While preparing the model for the finite element analysis, the challenge was to simulate junctions (A₀ to E, Figure 4.16). Here, the bearings are simulated with 1D elements applied like radial spokes from one edge to the associated other edge (Figure 4.23). One set of in plane (exactly radial) 1D elements provide a large radial stiffness, but a much lower tangential and axial stiffness (with respect to the bearing it represents). To add the desired axial stiffness a second set of more axially orientated 1D elements are added, by which, with the in-plane elements, triangles are created, thus stiff in radial and axial direction. Although, there is a minor parasitic tangential stiffness, it has very little effect in simulating bearings and provides a representative solution. The bearing simulation effect can be seen Figure 4.24, where the lower arm is rotated only and is not bent, thus not transferring moment. The upper bridge is bent, transferring the moment applied by the load on the Z-stage.

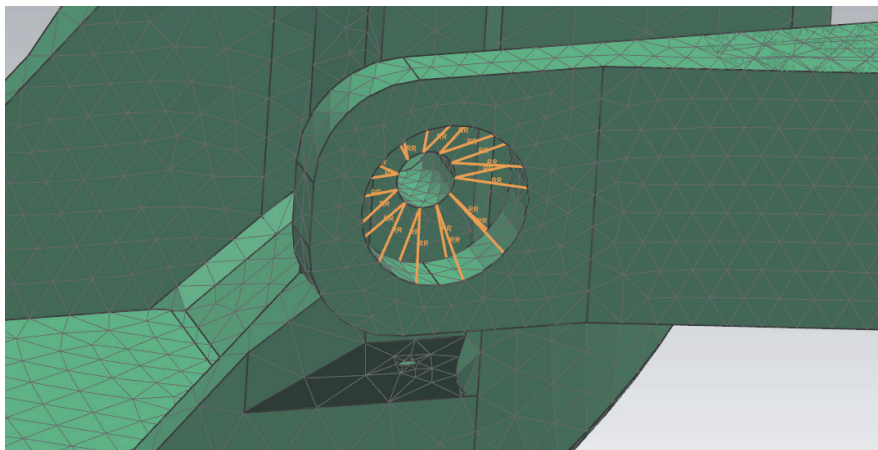


Figure 4.23/ 1D elements simulating bearings like spokes.

To suspend the model it is constrained like it would be to the stationary Ψ -shaft. At the location of the supporting Φ bearing (see Figure 4.17), the model is constrained by a pinned constraint. This constraint leaves only the rotational degree of freedom about the Φ -axis open. A fixed constraint is placed at a bar, connected to the central- Φ -body at the inside, which represents the shaft of the harmonic drive. Loads are applied like the respective actuator would. However, in the finite element model loads in Φ and Ψ direction are applied as counter forces in X and Y direction, while the actuators are considered fixed. These loads are applied at the Z-frame, between junctions C and D (Figure 4.16) at a height of 62.5 mm from axes Φ and Ψ . Stiffness in Θ -direction is not analyzed, because the associated torque will have little effect on the instrument manipulator since it is less than 2% of torque applied in Φ and Ψ direction.

Instrument manipulator stiffness analysis

Figure 4.24 shows the result of the Z-stiffness analysis. A load of 10 N is applied to the bottom of the Z-frame (see Figure 4.24). As a result, the finite element software determines the deflection as $f_Z = 45 \mu\text{m}$, which brings the stiffness to $c_{IM-Z} = 220 \text{ N/mm}$. A parasitic Ψ -movement of $\Psi = 88 \mu\text{rad}$ backwards appears, caused by a resulting force (in Z-direction) applied to junction B, which results in a Ψ -moment about junction B_0 .

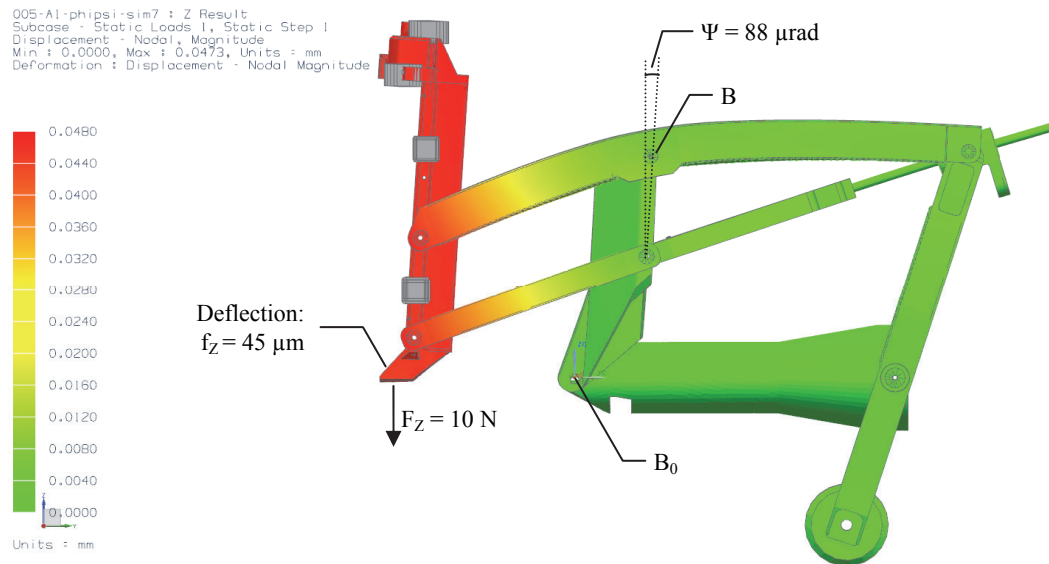


Figure 4.24/ Finite element analysis of the Z-stiffness. A deflection of $f_Z = 45 \mu\text{m}$ and a rotation of $\Psi = 88 \mu\text{rad}$ is caused by a force of $F_Z = 10 \text{ N}$ at the Z-frame.

During surgery, average loads are about $F_{\text{surg}} = 300 \text{ mN}$ [30][63], by which the predicted Z-deflection will be $f_Z = 1.4 \mu\text{m}$ (RP3), and will be hardly noticeable by the surgeon. Figure 4.24 clearly shows that the Z-stiffness mainly depends on the stiffness of the upper bridge.

Further stiffness analysis in Φ and Ψ direction is shown in Appendix D. In Φ -direction, a load of $F_Y = 10 \text{ N}$ (at 62.5 mm from the Φ -axis) represents a torque of $T_\Phi = 625 \text{ Nmm}$. As a result, the manipulator rotates $\Phi = 740 \cdot 10^{-6} \text{ rad}$, resulting in a torsional stiffness of $k_\Phi = 840 \cdot 10^3 \text{ Nmm/rad}$. Additionally, by the load applied in Y direction, the instrument axis shifts $f_Y = 40 \mu\text{m}$, wherewith the lateral Y-stiffness can be determined as $c_Y = 250 \text{ Nmm}$.

When during surgery a load is applied at the tip of the instrument, the tip position inaccuracy due to k_Φ and c_Y is $f_Y = 1.6 \mu\text{m}$. This will appear when e.g. an Epiretinal membrane is peeled from the retina. This inaccuracy will not be noticeable by the surgeon, since the stiffness of the instrument is much lower. The instrument stiffness is approximately $c_{\text{instr.},X,Y} = 0.2 \text{ N/mm}$, which (in that case) will result in a deflection of $f_{\text{instr.},Y} = 1.45 \text{ mm}$.

The weakest link in the Φ -stiffness analysis appears to be the torsional stiffness of the shaft of the harmonic drive. This was noticed by the Φ -rotation of the complete instrument manipulator. The Y-stiffness mainly depends on the torsional stiffness of the central- Ψ -body, where the Y-load results in a Θ -rotation.

Similar to the latter analysis, is the analysis in Ψ -direction (Appendix D). Where a similar load is applied in X-direction and as a result a Ψ -rotation and a deflection in X-direction can be determined. Here, a Ψ -rotation of $\Psi = 150 \cdot 10^{-6}$ rad results in a stiffness of $k_{\Psi} = 4.20 \cdot 10^6$ Nmm/rad. The X-deflection is 20 μm , wherewith the X-stiffness becomes: $c_X = 500$ N/mm. In the table below, the instrument manipulator stiffness is summarized.

Table 4.1/ Summary of the instrument manipulator stiffness.

	Deflection	Load	Stiffness
X	20 μm	10 N	500 N/mm
Y	40 μm	10 N	250 N/mm
Z	45 μm	10 N	220 N/mm
Φ	$740 \cdot 10^{-6}$ rad	625 Nmm	$0.84 \cdot 10^6$ Nmm/rad
Ψ	$150 \cdot 10^{-6}$ rad	625 Nmm	$4.20 \cdot 10^6$ Nmm/rad
Θ	Not analysed		

Instrument manipulator eigenfrequency analysis

In addition to the stiffness analysis, an estimation of the eigenfrequencies is made. In Figure 4.25 the lowest four eigenfrequencies of the instrument manipulator are illustrated. Here, the instrument manipulator is constrained similarly. Additional mass is applied to the Z-frame at: the Θ -module location during surgery (56 g), the height of the instrument container (40 g) and at the Z-frame top representing e.g. motors (30 g). The lowest eigenfrequency is found at $\omega_{IM1} = 78$ Hz, which is an Φ -movement mainly by twisting the shaft of the harmonic drive (upper left image in Figure 4.25). This allows a bandwidth of at least 60 Hz to match the bandwidth of the haptic interface at the master side, as proposed in [33] (RP4).

The second eigenfrequency is found at $\omega_{IM2} = 122$ Hz and is the Ψ -movement resulting from a pendulum motion of the counter mass (upper right image in Figure 4.25). The third eigenfrequency is a twist about the central- Ψ -body at $\omega_{IM3} = 150$ Hz (lower left image in Figure 4.25). The fourth is at $\omega_{IM4} = 191$ Hz, which relates to bending the upper bridge by a Z-movement of the Θ -Z manipulator (lower right image in Figure 4.25). The first four eigenfrequencies are summarized in the table below. The manipulator stiffness satisfies RS4.

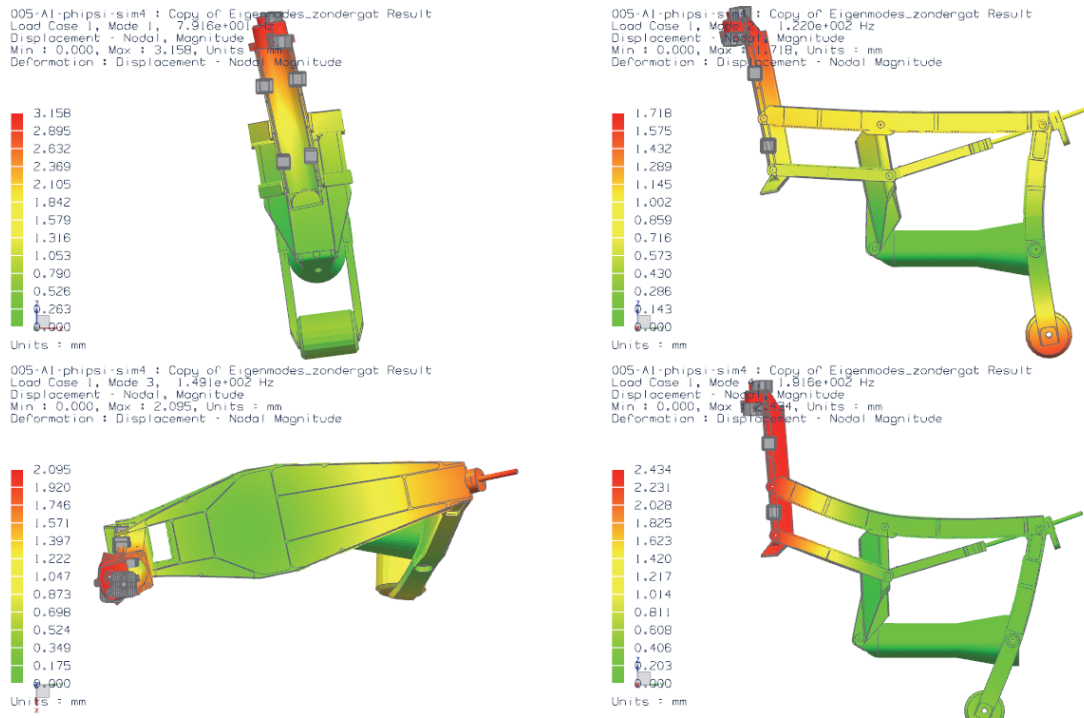


Figure 4.25/ The first four eigenfrequencies of the instrument manipulator.

Table 4.2/ Summary of the first four instrument manipulator eigenfrequencies.

Eigenfrequency		Mode
ω_1	78 Hz	Swing sideways over the harmonic drive's shaft
ω_2	122 Hz	Back and forth pendulum motion of the counter mass
ω_3	150 Hz	Twist about the longitudinal (Z) axis of the central- Ψ -body
ω_4	191 Hz	Bending of the upper bridge in Z-direction.

4.7 Wiring and electronics of the instrument manipulator.

Special attention is paid to the instrument manipulators electrical wiring routing. Since there are electrical devices (e.g. motors and sensors) manipulated in various degrees of freedom, their cables add additional resistance. Moreover, by frequently bending the cable, fatigue and subsequently a wire break must be avoided.

For communication of the control data, it is chosen to use EtherCAT. This way, global control is executed in a so called EtherCAT-master computer and data is send in digital packages to each EtherCAT-slave module. There, the EtherCAT protocol determines which data package is meant for that particular EtherCAT-slave, other data packages will be passed through to the next EtherCAT-slave. At an EtherCAT-slave the data is converted to the input for the actuators, wherewith actuator control is decentralized and power amplification can be performed locally. Vice versa, sensor

and encoder data is send similarly from the EtherCAT-slave to the EtherCAT-master. One single master module can have multiple slave modules (Figure 4.27). A slave module can be the control of e.g. one haptic interface, a single sensor or a Z- Θ manipulator. Figure 4.26 shows the instrument manipulator with the realized EtherCAT module and electric routing.

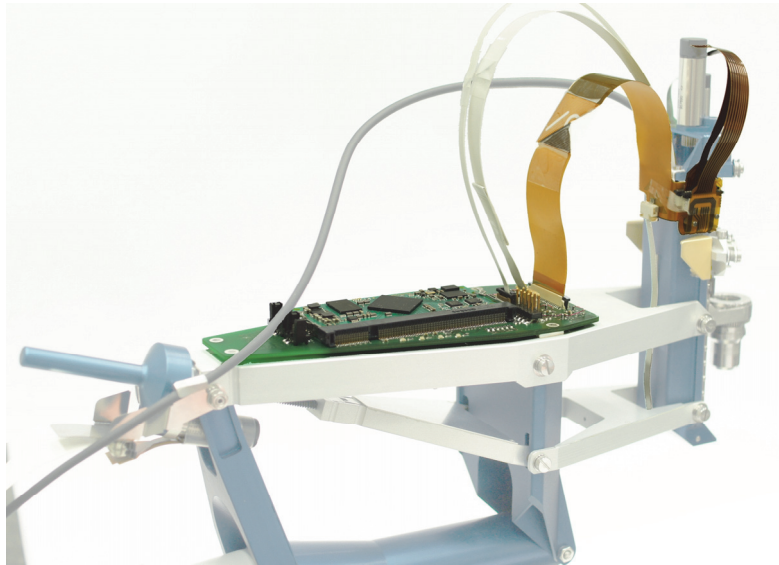


Figure 4.26/ EtherCAT module to control the Z- Θ manipulator, placed on top of the upper bridge.

Decentralized control by EtherCAT has several advantages over centralized control. First, the local actuator control and signal processing, avoids analog signals to be conducted over longer distances with potential signal loss as a result. Secondly, to supply an EtherCAT-slave, just four signals are required; + and – for power supply and two for EtherCAT data. Additionally, redundant power and data connections can be made for safety. For example the Z- Θ manipulator has 59 conductors in total. By use of EtherCAT, motor amplifiers and signal processors are placed locally on top of the upper bridge. This way the 59 signals only cross over from the Z- Θ manipulator to the upper bridge via flex foil conductors (FFCs). Here, the FFCs bend in their low stiffness direction, introducing the least parasitic resistance. Then, from the upper bridge to the stationary Z-arm only four signals have to cross over to the stationary passive support system.

A third major advantage is the data loop and compatibility of EtherCAT-slaves. EtherCAT-slaves can be linked in a loop, wherewith the last EtherCAT-slave is linked back to the master (Figure 4.27). Packages of data can be transferred in both directions, by which the data always will arrive at the EtherCAT-slave, even in case a cable is unplugged. Furthermore, a module can be unplugged and exchanged, without disabling other modules still in function.

Most conductors used are FFCs (flex foil conductors) or flex-PCs (flexible printed circuits). For the stationary electronics on the Z-frame, a custom flex-PC is used (left picture in Figure 4.28). Soldered onto it are the optical interrupters (instrument change

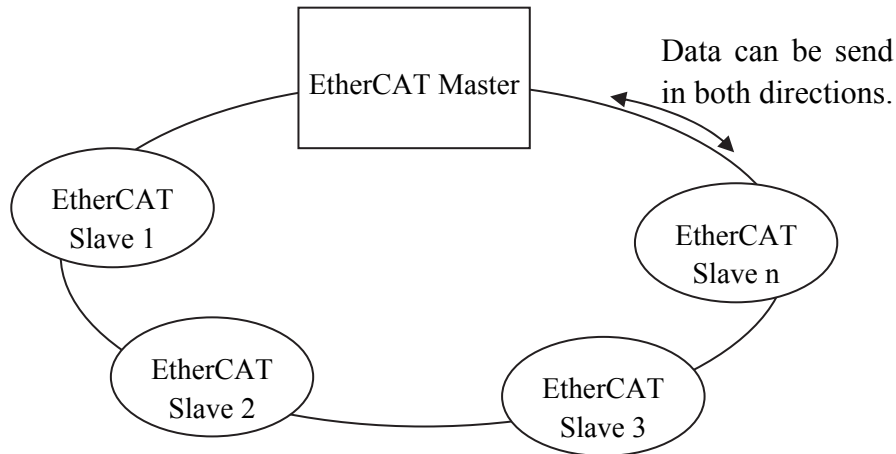


Figure 4.27/ EtherCAT loop, data can be send in both directions.

system) and the connectors of the: Z-motor and encoder, container motor and the hall sensor at the bottom of the Z-frame. This flex-PC end is folded around and fixed to the Z-frame (Figure 4.26) for pull relief. To connect to the Z- Θ EtherCAT module, the tail of 150 mm allows for a large bending radius, whereby it suffers the least from stress and fatigue, as well as it has the least stiffness. In a similar fashion, the FFCs of the hall sensor on the Θ -module and the Θ -motor are directed to the Z- Θ EtherCAT module. They are separated from the flex-PC (Figure 4.26), because their length, extended from the Z- Θ -manipulator, depends on the Z-height of the Θ -module. The force/torque sensor is calibrated with its cable included. Therefore, its cable is directed over the instrument manipulator to the stationary Z-arm and to its amplifier near the EtherCAT-master.

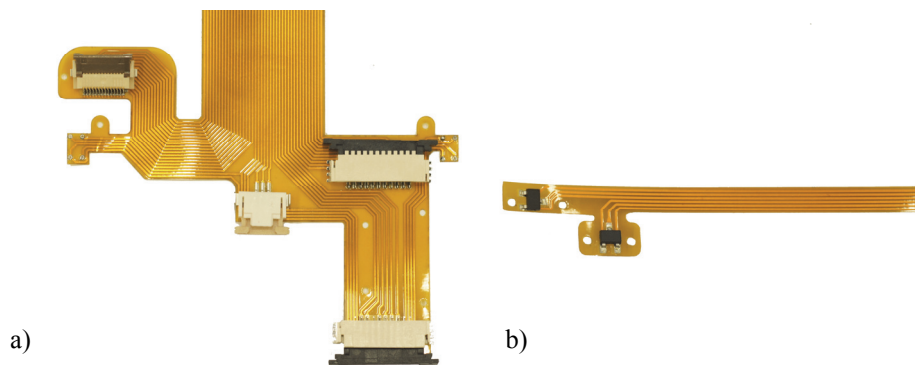


Figure 4.28/ Flexible printed circuits: a) for the stationary electronics on the Z-manipulator and b) for the hall sensors to Φ - Ψ indexation.

The FFCs of the Ψ -motor are directed to the back of the instrument manipulator. There, they are connected to a second set of FFCs, which is locally fixated to the instrument manipulator for pull relief. From there, it bends with a large radius to the Φ - Ψ EtherCAT module inside neck body of the Z-arm (Figure 4.29). In a similar fashion, the cable from the EtherCAT module on the upper bridge is directed to the Φ - Ψ EtherCAT module. The cable of the harmonic drive and the Φ / Ψ hall sensor flex-PC directly go to the Φ - Ψ EtherCAT module from inside the stationary Φ -shaft. From

the Φ - Ψ EtherCAT module, a connection is made to other EtherCAT-slaves and the EtherCAT-master (like Figure 4.27), by which each instrument manipulator becomes modular.

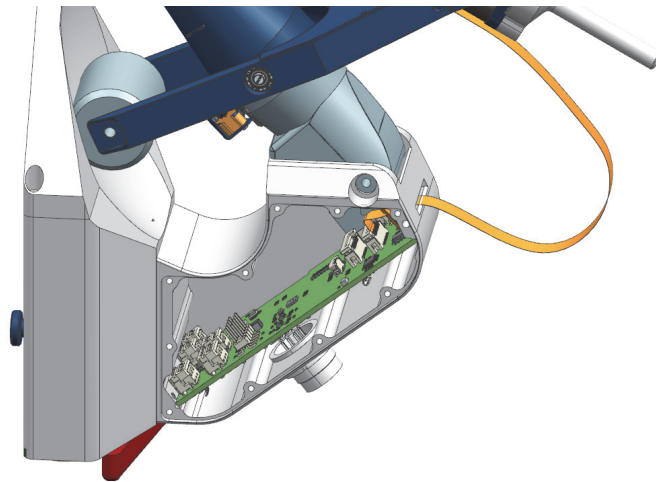


Figure 4.29/ EtherCAT module to control the Φ and Ψ manipulation placed inside the Z-arm.

4.8 Realized manipulator

The instrument manipulator as discussed in the previous sections is realized. Figure 4.30 shows the instrument manipulator realized in endurance setup. First functional tests are performed, which indicate low actuation torque and high accurate positioning ($< 10 \mu\text{m}$).

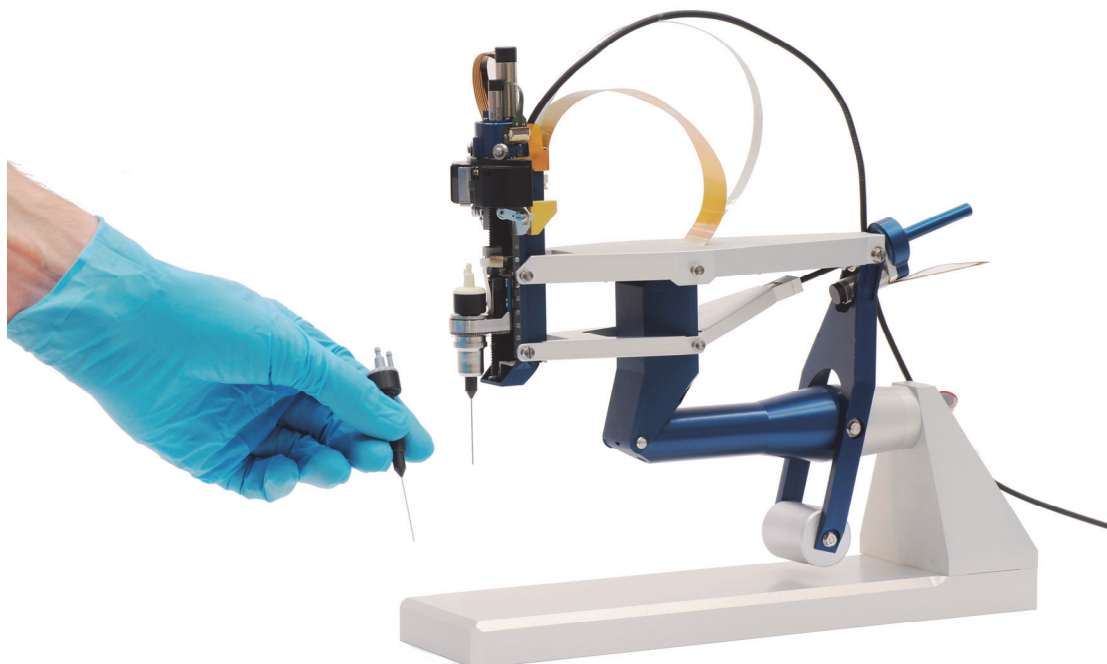


Figure 4.30/ Endurance setup/display stand of the instrument manipulator.

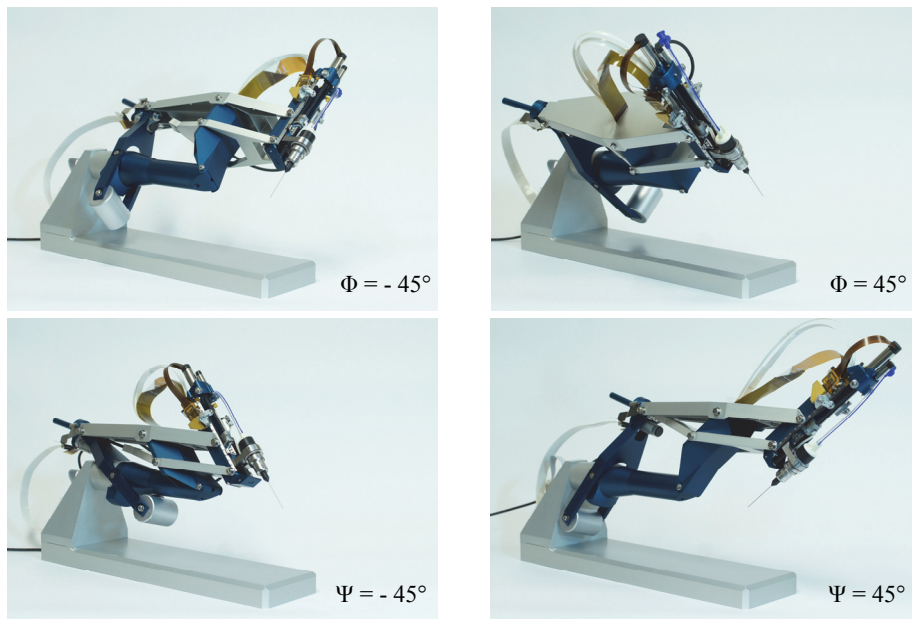


Figure 4.32/ Four extreme positions of the parallelogram mechanism

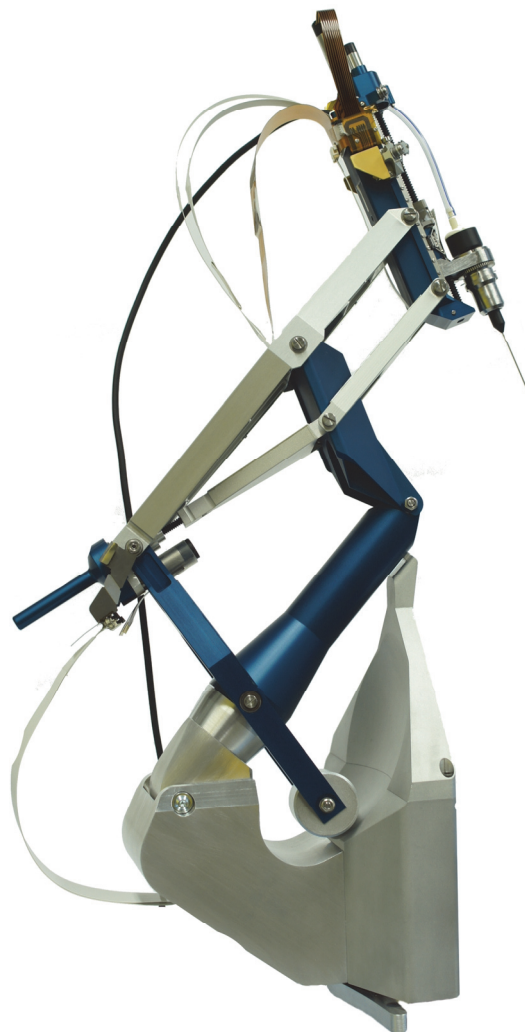


Figure 4.32/ The instrument manipulator on the short Z-arm.

Patient fixation, sterilization and safety.

In this chapter some further safety considerations, the view on sterilization and additional fixation of the patient is discussed.

5.1 Additional safety considerations

In the previous chapters various safety measures with respect to the mechanical design are already discussed. In this section other additional safety aspects are discussed which do not directly relate to the mechanical design or which are not applied yet.

Redundant control loop in EtherCAT

The local control on the EtherCAT modules is executed via a field-programmable gate array (FPGA). The FPGA used has sufficient capacity to: apply redundant control loops, do system monitoring, do system heartbeat evaluation and execute various safety strategies in case of an emergency.

Emergency buttons

Each person involved in the operating room should be able initiate an emergency procedure. Not only the surgeon, but also the surgical assistant in case the surgeon becomes unwell. Each side of the robotic system should have an emergency button. These buttons might require a certain action, in order not to start the emergency procedure unintentionally. The action might involve flipping up a cover first, or pushing two buttons simultaneously.

Safe zone

The eye can be divided in different safety zones. Each zone should have different restrictions, e.g. maximum instrument velocity. The safest zone can be the vitreous cavity up to 2 mm from the retina. The zone near the retina requires more restricted movements.

Patient monitoring

During surgery, the patient's condition is monitored, e.g., heart rate and blood pressure. Additional monitoring devices can be used, to sense hazardous activity or motion, where the robotic system anticipates the resulting action and sets by an appropriate action in motion. Additional sensors might imply accelerometers to measure patient movements, sensors that sense muscle activity or brain activity. Reactions of the robot can vary from moving the instrument to a safe position e.g. moving the tip to the center of the eye, to a total retrieval of the instrument and manipulator.

Hard cover

Kazanides [40] points out a major difference in safety between industrial and medical robots. In an industrial setting, safety systems typically involve gates/cages, pressure-sensitive mats, and flashing lights. These are devices designed to keep people out of the robot's workspace or to shut down the system if a person comes too close. In the operating room, it is rarely possible to keep the robot away from people. This is especially true in surgical applications, where the robot is directly interacting with the patient's body and is often working alongside the surgical staff.

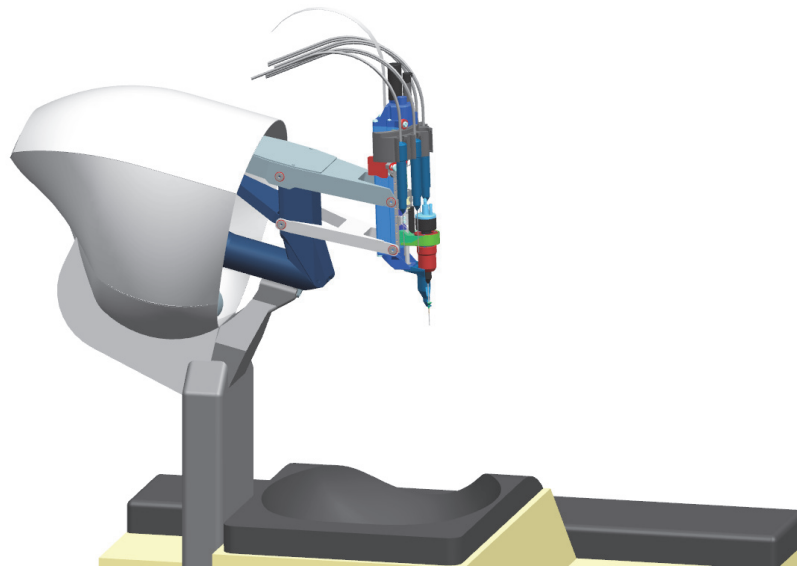


Figure 5.1/ A caged instrument manipulator on the tall Z-arm. The hard cover prevents from accidental interaction between the surgical staff and the manipulator.

With respect to this statement, the robotic system discussed in this thesis cannot be kept away from the patient. However, the instrument manipulators and their

supporting arms are compact and have a relatively small volume of motion, which allows them to be shielded from the surgical staff. The supporting arms can be fitted with a cage, in the form of a hard cover, which surrounds the working volume of the instrument manipulator (Figure 5.1).

5.2 Sterility

Sterility is another safety aspect of a surgical system. With respect to the system as discussed in this thesis, it can be divided in parts that do make contact and those that do not make contact with the surgical area.

The parts that do make contact must be sterile and include: the cannulas, the instruments and the trocarholder. They are all anticipated to be supplied sterile and are disposable.

The parts that do not make contact to the surgical area, does not necessarily need to be sterile. Here, a separation that prevents contamination is sufficient. This separation should be bi-directional: the surgical area must be protected from particles and debris potentially generated by the robotic non sterile portion (including dust) of the instrument manipulator. Vice versa, the manipulator must be protected from surgical loose matter and fluids. A cover, in the form of a sterile sack, around the instrument manipulator and the rest of the robotic slave can separate them from the sterile surgical area.

5.3 Patient fixation

Safety measures can prevent the system from doing harm to the patient, but unintentionally, the patient can cause harm to himself. This is due the use of local anesthetics, the patient is conscious. Possible harmful patient actions and their respective movements are:

- a cough; the patient will shake a little,
- a sneeze; can cause a tensed shiver,
- a shiver of cold,
- sedation of a patient due to the local anesthetics: the patient slides/rotates slowly sideways,
- waking up from sedation; might cause a startle,
- intensive breathing; moves the head,
- moving because of an itch,
- a movement of panic.

The latter has a high risk value and requires a completely fixed head. Preliminary research is performed on fixating the patient's eye and head.

5.3.1 Eye fixation

The eye is constrained compliant inside the eye socket. It has some freedom of movement in the order of about 2 to 4 mm. This allows the eye to be fixed to the instrument manipulators and having a safety margin for the head to move. Of course, the head must be kept within this margin. Fixating the eye to the instrument manipulators is beneficial not only for safety, but it also contributes to a short eye-instrument force loop. This is also used by manual surgery.

Suction ring

A scleral suction ring can be used to fixate the eye. The suction ring is placed onto the sclera (not touching the cornea) and by vacuum (40-100 mmHg) the ring is fixated to the eye. This is also used at Lasik² and Lasek² procedures. By these procedures, the eye is fixated to accurately correct refractive inaccuracies of the cornea by use of a laser. The suction ring can only be used for a short period of time, as it can cause (post) surgical complications e.g. a scleral hemorrhage.

Fixation by cannulas

The cannulas are held by the instrument manipulators. This way the instrument manipulators can fixate the eye at the cannula location. Two instrument manipulators fixate the eye over the line between the two cannulas. The only degree of freedom not fixated by the line is the rotation over it, which is obstructed by the eye socket.

A combination of the suction ring and fixation by cannulas can be made. The suction ring can be used to position the eye sideways (paragraph 3.3), by which the cannulas run through both the suction ring and the sclera. Then, the vacuum is only applied while placing the cannulas.

5.3.2 Head fixation

The possible movements of the patients head can be restricted in different gradations, these are:

- 1 Degree of freedom (DoF); a flat surface head rest that only supports the head,
- 3 DoF; a cup style comfortable head rest (Figure 5.2). The head is not able to move, but can rotate (although not easily),
- 6 DoF; a comfortable head rest, with neck and side support. The cup style head rest is extended to the lateral side of the head, restricting the head from rolling sideways and backwards. In addition, a safety strap over the forehead can be use to constrain the head completely.

² Laser-assisted in situ keratomileusis and Laser epithelial keratomileusis



Figure 5.2/ A comfortable cup style head rest.

Probably, the latter must be applied to rule out all risks and to satisfy the safety regulations. Methods used in radio therapy are a solution. Figure 5.3 shows such a fixation method by which the head is constrained within 2 mm [60]. Here, the head rests on a comfortable support cushion (3 DoF) and is fixed to the table by a thermoplastic mask.

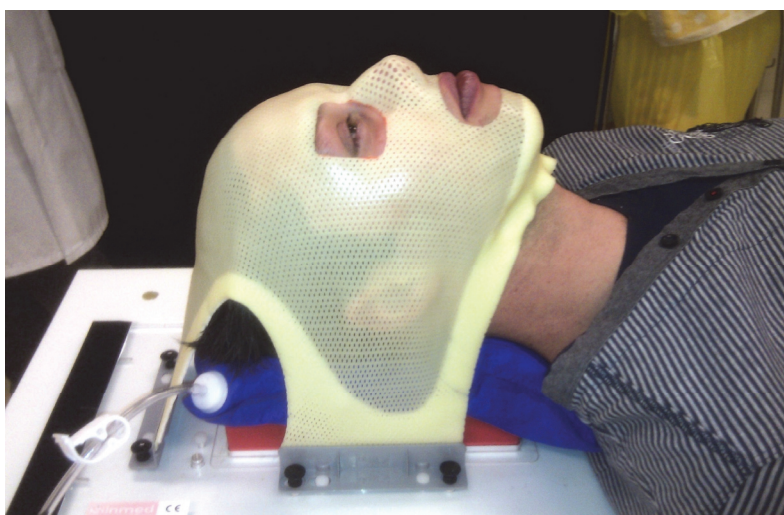


Figure 5.3/Author tests fixation method. For radiotherapy, a mask is used to constrain the patients head within 2 mm.

Molding a mask takes only 5 minutes. First, the flat mask is brought to a temperature of 65° C in a bath of water. Before molding the mask, it is dried by a towel. While drying, the outer layer cools to a point that does not cause burns, but leaves the core at a temperature to remain flexible. Then the mask is shaped around the head by laying it over the patient's face and stretching the sides towards the table. In the next two minutes, the mask cools down and goes from a flexible to a solid state. During this time, the mask is pressed firmly to the more rigid parts of the head, like the nasal bone. In the last few minutes, the mask cools to body temperature and shrinks a little due to its coefficient of expansion thermal, creating a tighter fit. After molding, holes can be cut as desired, for e.g. the nose, mouth or eyes.

If the mask is not shaped correctly, the mask can be re-molded. When reheated, the mask transforms back to a flat surface.

An alternative method can be a comfortable 6 DoF head rest, where the patient's head is held in by use of a fixation strap.

When a mask or fixation strap is used, it should be attached to the head rest via a quick release mechanism. The release mechanism must allow manual and electronic control. This way, sensors sensing an emergency, as well as the surgical staff or the patient using an emergency switch can set an emergency release procedure in motion.

The emergency procedure should proceed as follows. In three steps the patient can be released. First, within a second the instrument is retrieved from the eye. Then, the instrument manipulator release mechanism unlocks the manipulator, by which a torsion spring rotates it upwards. In the third step the mask is released, where after the patient can be assisted.

The emergency procedure above is executable in less than 3 seconds, by the robotic slave system described in this thesis.

Conclusions and recommendations

In this chapter, the main conclusions are summarized and recommendations for future work are discussed.

6.1 Conclusions

This thesis describes the design and realization of a dedicated robotic slave system, as a part of a haptic master-slave system to perform vitreo-retinal eye surgery. The system can assist in tasks like: vitrectomy, membrane peeling, repair of retinal detachment and retinal vein cannulation.

The slave system mainly consists of:

- two instrument manipulators that perform the actual surgery by handling the surgical instruments,
- a passive support system, on which the instrument manipulators are mounted and which allows pre-surgical adjustments to position the instrument manipulators over the eye.

The passive support system is mounted to the top end side of the surgical table. The head rest is part of the passive support system. The passive support system can be adjusted in: lateral direction $X = 25$ mm, longitudinal direction $Y = 30$ mm and in height $Z = 30$ mm. By use of additional support cushions, the adjustments cover the major range of the human anatomical diversity. The passive support system consists of an X and Y stage, located inside the head rest and two instrument manipulator support arms: the tall Z-arm and short Z-arm. The short Z-arm supports the instrument manipulator on the side of the eye under surgery, alongside the patients head. The tall Z-arm supports the opposing instrument manipulator, which reaches over the patient's nose. The instrument manipulators and their support arms approach the eye laterally. The support arms switch side to operate the left or the right eye.

The slave system features the following aspects.

- Compactness; the system does not extend much from surgical table, it allows current operating room arrangements and leaves legroom underneath the head rest for the surgeon.
- Low weight; the total weight is about 8 kg in which both support arm modules are 1.9 kg. Low weight contributes to easy installation and high eigenfrequencies, which result in highly accurate motion.
- Easy to install; the support arms are easily attached to the X-stage at the head rest and easily fixated by a handle on an eccentric shaft.
- Easy to adjust; positioning screws allow straight forward instrument manipulator positioning in: X, Y and separately for each support arm Z.
- High stiffness; the passive support system has a stiffness of $> 300\text{N/mm}$, the lowest eigenfrequency is 78 Hz.
- Play free; free play is equally transferred to inaccuracy.
- Low friction; low friction contributes to a more precise instrument manipulation.

Vitreo-retinal surgery is performed not unlike minimally invasive surgery. Instruments are inserted via small openings, by which a pivoting point is created. This allows four degrees of freedom: two lateral rotations Φ and Ψ , an axial Z-stroke and the rotation about the Z-axis Θ . Procedures like vitrectomy, epiretinal membrane peeling or repairing detached retina require a reach of: $\Phi = \pm 45^\circ$, $-35 < \Psi < 45^\circ$, $Z = 32\text{ mm}$ and $\Theta > 360^\circ$. The instrument manipulator satisfies these requirements, covered by an accuracy of $10\ \mu\text{m}$ at the tip of the instrument. The reach is optimized by rotating the eye 25° to 30° outward and fixating it there.

The instrument manipulator defines kinematically the pivoting point at the entry point to the eye. This is realized by a remote center of motion mechanism, based on a parallelogram mechanism. The Ψ -rotation is realized by the back and forth parallelogram movement, and by rotating the complete parallelogram mechanism sideways, the Φ -rotation is realized. The instrument is fixated in a bistable instrument clamp, which is manipulated in Θ -direction by the Θ -module. The Θ -module is manipulated in Z-direction by the Z-stage. In turn, the Z-stage is mounted to the parallelogram mechanism.

Forces are measured to apply as force feedback on the haptic interfaces at the master side. A commercially available force/torque sensor is used and placed as close as possible to the instrument. It is placed next to the instrument, with only the Θ degree of freedom in between.

The instrument manipulator is equipped to perform complete interventions. Various instruments are used and changed by a fast onboard instrument change system. It carries up to five instruments. An instrument can be changed in every arbitrary instrument manipulator orientation. The instrument is changed immediately i.e. the

change does not require robot motion. Changing an instrument is performed by only the Z-movement and an indexation motion of the instrument container. The instrument container can easily be inserted, by pinching two levers by index finger and thumb.

It is to be expected that the master-slave system for vitreo-retinal eye surgery is beneficial for both the surgeon and the patient by allowing more precise surgery in a more ergonomic environment for the surgeon. The surgeon's skills will be enhanced, time of surgery will be reduced and their career will be extended, where currently hand tremor and backaches may force him to stop performing surgery early. The system discussed in this thesis, will lead to sustainable precision. The compact layout makes that the system easily fits in the current operating room arrangement. As with all new technologies, it is likely that it will lead to new surgical approaches which are not possible with manually performed surgery.

6.2 Recommendations

Although the realization of the slave robot has finished, remaining research is both necessary and relevant for future development of robot technology for medical applications, in particular eye surgery.

First, at the publishing date of this thesis, the slave system is not yet electronically tested, and also not yet coupled to the haptic interfaces of the master. The performance of the instrument manipulator must be validated, which can be performed separately from the master. Related experiments should include: positioning accuracy validation, force measurement validation in a controlled environment, determining its dynamic behavior/system identification and testing the procedure of changing instruments.

It is recommended to establish the software connection between the master part and slave part as quickly as possible. The usability and intuitive way of working of the master-slave system must be tested. Experiments must be performed to optimize the usability, by way of testing various motion scaling factors, the usefulness of force feedback and if so, the amount of force feedback amplification. Experiments with emphasis on dexterity may include tasks like: pointing on a piece of paper, tracking a curved line or simple pick and place tasks. For force feedback, they may include identifying different stiffnesses. More advanced experiments may include performing tasks like dissecting an egg's chorioallantoic membrane or cannulation of a chorioallantoic vein. The added value of the master-slave system must be evaluated, by comparing the results with manually performed tasks.

Next, more advanced experiments must be performed, which simulate vitreo-retinal surgery. These experiments can be performed on phantom eyes (for consistent reproducibility), porcine eyes and cadaveric eyes. To stand out from other

experimental systems, these experiments should focus on complete interventions, from placing cannulas, to vitrectomy and e.g. peeling a membrane. Therefore, the procedures to evaluate must include at least: vitrectomy, membrane peeling, repair of a detached retina and next retinal vein cannulation. A number of complete interventions should be examined in: surgical precision, quality of intervention and the time to accomplish the intervention. Again, these results must be compared to manually performed eye surgery.

Based on the experiments mentioned above and the slave system described in this thesis, it is recommended to design a second version of the slave system. This version should be designed for production and in accordance with CE regulations.

Other applications which relate to the high performance of the accomplished master-slave system should be explored. This exploration should encompass other purposes in medicine, mainly microsurgery, but also non-medicinal purposes, e.g. for tasks in hazardous environments.

Nomenclature

Symbol	Description	Unit
A	surface	mm ²
c	stiffness	N/mm
C	load rating	N
d	inner diameter	mm
D	outer diameter	mm
e	eccentricity	mm
E	module of elasticity	GPa
f	displacement	mm
F	force	N
i	transmission ratio	-
J	inertia	kgm ²
k	torsional stiffness	Nmm/rad
l	length	mm
m	mass	kg
n	number	-
p	lead	mm/turn
p	pressure	MPa
q	distance from corneal limbus to insertion point	mm
r	radius	mm
t	thickness	mm
T	torque	Nmm
v	velocity	m/s
X	position	mm
Y	position	mm
Z	position	mm

Greek	Description	Unit
α	contact angle	°
Θ	rotation about the Z-axis	° or rad
$\Delta\Theta$	displacement in Θ -rotation	° or rad
$\Delta\Phi$	displacement in Φ -rotation	° or rad
$\Delta\Psi$	displacement in Ψ -rotation	° or rad
ΔZ	displacement in Z-direction	mm
ε	strain	-
η	efficiency	-
μ	coefficient of friction	-
ν	Poisson ratio	-
σ	stress	MPa
Φ	rotation about the X-axis	° or rad
Ψ	rotation about the Y-axis	° or rad
ω	eigenfrequency	Hz or rad/s

Subscript	Description	Subscript	Description
0	static rating	N	normal
ano	anodized	nom	nominal
b	bearing	out	outer
c	contact	r	resistance
Cc	clamp closed	race	raceway
Co	clamp opened	scl	sclera
ecc	eccentric shaft	sp	spring
f	friction	t	tall
fix	fixated	tot	total
frh	friction in holder	vit.h.	vitreous humour
frl	friction by leafspring	vm	Von Mises
HD	harmonic drive	vis	viscosity
hr	holder rim	X	direction
IM	instrument manipulator	y	yield
Inst	instrument	Y	direction
l	leadscrew	Z	direction
max	maximal		

Abbreviation Meaning

1D	one dimensional
2D	two dimensional
3D	three dimensional
AISI	American Iron and Steel Institute

AMC	Academisch Medisch Centrum
CAD	computer-aided design
CAM	computer-aided manufacturing
CE	Conformité Européenne
CST	Control Systems Technology group
da Vinci®	surgical system for robotically assisted MIS, registered trademark of Intuitive Surgical, Inc.
DoF	degree of freedom
EDM	electrical discharge machining
EyeRHAS	eye robot for haptically assisted surgery
FDA	Food and Drug Administration
FEA	finite element analysis
FFC	flex foil conductor
Flex-PC	flexible printed circuit
FRF	frequency response function
ILM	internal limiting membrane
IM	instrument manipulator
JPL	Jet Propulsion Laboratory
KAIST	Korea Advanced Institute of Science and Technology
Lasek	laser-assisted sub-epithelial keratectomy
Lasik	laser-assisted in situ keratomileusis
MIS	minimally invasive surgery
NEN	Nederlandse norm
OR	operating room
OT	operating table
PCB	printed board circuit
PhD	doctor of philosophy
POM	polyoxymethylene
PPSU	polyfenylsulfon
RCM	remote center of motion
RMS	root mean square
RP	requirement performance
RS	requirement safety
RV	requirement added value
TFE	trifluorethyle
TU/e	Technische Universiteit Eindhoven
UHMWPE	ultra high molecular weight polyethylene
U.S.	United States
UvA	Universiteit van Amsterdam

Term	Meaning
anterior	Front part of the eye.
cataract	Eye disease, by which light is passed through the lens poorly.
ciliary body	Controls the accommodation of the eye and produces the aqueous humour that fills the space between the lens and the cornea
chorioallantoic membrane	a vascular membrane found in eggs
choroid	Layer of blood vessels between the retina and sclera. It supplies blood to the outer retina.
cornea	Transparent front part of the eye.
fovea	Center of the macula. It has the highest density of photoreceptor cells.
Glaucoma	Eye disorder, in which the optic nerve suffers damage.
hemorrhage	A bleeding
ILM	Internal limiting membrane, boundary between the retina and the vitreous body.
iris	Diaphragm that controls the amount of light that enters the eye.
keratomileusis	Surgical improvement of the refractive state of the cornea.
lens	Focuses the image on the retina. The focal length is set via the ciliary muscle in the ciliary body.
limbus	Border of the cornea and the sclera.
macula	Responsible for central vision. The diameter is approximately 2.5 mm.
ora serrata	Serrated junction between the retina and the ciliary body.
plasminogen	A protein that helps dissolve blood clots.
posterior	Back part of the eye.
pupil	Hole in the center of the iris that light passes through.
Rectus muscle	Muscles that move the eye
retina	Light sensitive layer of photoreceptor cells as well as neuronal and support structures.
sclera	Opaque, white outer layer of the eye.
strabismus	Crossed-eye
vitreous humour	Clear, gel like liquid that fills the space between the lens and the retina.

References

- [1] D. Albert and M. Lucarelli. *Clinical Atlas Procedures in Ophthalmic Surgery*. Atlanta, GA: AMA, 2004.
- [2] H. C. Allen, D. R. Guyer and S. L. Fine. Macular Hole, *Survey of Ophthalmology*, 42(5):393-416, 1998.
- [3] B. Allf and E. Juan. In vivo cannulation of retinal vessels, *Graefe's Archive for Clinical and Experimental Ophthalmology*, 255(3):221-225, 1988.
- [4] W. T. Ang, C. N. Riviere and P. K. Khosla. An active hand-held instrument for enhanced microsurgical accuracy. *MICCAI*, pages 878 – 886, 2000.
- [5] D. A. Atchison, C. E. Jones, K. L. Schmid, N. Pritchard, J. M. Pope, W. E. Strugnell and R. A. Riley. Eye Shape in Emmetropia and Myopia, *IOVS*, 45:3380-3386, 2004.
- [6] ATI Industry Automation, *Multi-axis force/torque sensor*, 2007.
- [7] L. J. M. van den Bedem. *Realization of a demonstrator slave for robotic minimally invasive surgery*. PhD thesis, Technische Universiteit Eindhoven, 2010, ISBN 9789038623009.
- [8] L. J. M. van den Bedem, R. Hendrix, P.C.J.N. Rosielle, M. Steinbuch and H. Nijmeijer. Design of a minimally invasive surgical teleoperated master-slave system with haptic feedback, *International Conference on Mechatronics and Automation (ICMA)*, pages 60-65, 2009.
- [9] J. Black and G. Hastings. *Handbook of Biomaterial Properties*, Springer Verlag, 1998, ISBN 978-0-412-60330-3.
- [10] T. L. Brooks. Telerobotic response requirements, *IEEE International Conference on Systems, Man and Cybernetics*, pages 113-120, 1990.
- [11] G. C. Burdea. *Force and touch feedback for virtual reality*. John Wiley & Sons, Inc., 1996, ISBN 0471021415.
- [12] J. T. Busby, M. C. Hash and G. S. Was. The relationship between hardness and yield stress in irradiated austenitic and ferritic steels, *Journal of Nuclear Materials*, 336(2-3):267-278, 2005.
- [13] M. Butter, A. Rensma, J. van Boxsels, S. Kalisingh, M. Schoone, M. Leis, G.J. Gelderblom, G. Cremers, M. de Wilt, W. Kortekaas, A. Thielmann, K. Cuhls, A. Sachinopoulou and I. Korhonen. *Robotics for healthcare, Final report*, 2008.
- [14] M. W. Charles and N. Brown; Dimensions of the human eye relevant to radiation protection. *Physics in Medicine and Biology*, 20(2):202 – 218, 1975.

- [15] S. Charles, H. Das, T. Ohm, C. Boswell, G. Rodriguez, R. Steele, and D. Istrate. Dexterity-enhanced telerobotic microsurgery. *International Conference on Advanced Robotics (ICAR)*, pages 5-10, 1997.
- [16] A. P. Ciardella, Y. L. Fisher, C. Carvalho, J. S. Slakter, R. G. Bryan, J. A. Sorenson, R. F. Spaide, K. B. Freund, D. R. Guyer and L. A. Yannuzzi. Endoscopic vitreoretinal surgery for complicated proliferative diabetic retinopathy. *Retina*, 21(1):20 – 27, 2001.
- [17] Curexo Technology Corporation, June 2011. <http://www.robodoc.com>
- [18] H. Das, H. Zak, J. Johnson, J. Crouch and D. Frambach. Evaluation of a telerobotic system to assist surgeons in microsurgery. *Computer Aided Surgery*, 4(1):15 – 25, 1999.
- [19] J.F.P. Deller, A.D. O'Connor and A. Sosby. X-ray measurement of the diameters of the living eye. *Proceedings of the Royal Society Biological Sciences*, pages 456–467, 1947.
- [20] U.S. Department of Defense Human Factors Engineering Technical Advisory Group. *Human engineering design data digest*. Pages 72-75, April 2000.
- [21] S. M. Donelson and C. C. Gordon. 1995 *Matched anthropometric database for U.S. Marine corps Personnel: summery and statistics*. Massachusetts, 1996.
- [22] DORC International bv., *New Generation 25 Gauge Instrumens*, 2010.
- [23] C. Eckardt. Transconjunctival suturless 23-gauge vitrectomy. *VitroTech Online, DORC International bv.*, 9(1):32–50, 2006. <http://www.dorc.nl/vitreotech>.
- [24] D. Engel, J. Raczowsky and H. Worn. A safe robot system for craniofacial surgery. *IEEE International Conference on and Automation (ICRA)*, 2:2020- 2024, 2001.
- [25] F. Faude and P. Wiedemann. Vitreoretinal endoscope for the assessment of the peripheral retina and the ciliary body after large retinectomies in severe anterior pvt. *International Ophthalmology*, 25(1):53 – 56, 2004.
- [26] B. Fei, W. Sing Ng, S. Chauhan and C. K. Kwoh. The safety issues of medical robotics, *Reliability Engineering & System Safety*, 73(2):183-192, 2001.
- [27] B. Fei, W. Sing Ng and C. K. Kwoh. The hazard identification and safety insurance control (HISIC) for medical robot, *Engineering in Medicine and Biology Society, 2000. Proceedings of the 22nd Annual International Conference of the IEEE* , 4:3022-3026, 2000.
- [28] B. Graf, M. Hans, J. Kubacki and R.D. Schraft. Robotic Home Assistant Care-O-bot II. *IEEE Engineering in Medicine and Biology Society and the Biomedical Engineering Society*, 2002.
- [29] J.H. Graham. Research issues in robot safety. *IEEE International Conference on Robotics and Automation (ICRA)*, pp.1854-1855 vol.3, 1988
- [30] P.K. Gupta, P.S. Jensen and E. de Juan. Surgical forces and tactile perception during retinal microsurgery. *Medical Image Computing and Computer-Assisted Intervention, Lecture Notes in Computer Science*, pp. 1218–1225, 1999.
- [31] B. Hannaford. A design framework for teleoperators with kinesthetic feedback. *IEEE Transactions on Robotics and Automation*,, vol.5, no.4, pp.426-434, 1989.
- [32] Harmonic Drive, *Precision in Motion*, 2010.
- [33] R. Hendrix. *Robotically assisted eye surgery: A haptic master console*. PhD thesis, Technische Universiteit Eindhoven, 2011, ISBN: 978-90-386-2442-6
- [34] R. Hendrix, P.C.J.N Rosielle and H. Nijmeijer. Design of a haptic master interface for robotically assisted vitreo-retinal eye surgery. *International Conference on Advanced Robotics*, pages.1-6, 2009.

- [35] Y. Ida, N. Sugita, T. Ueta, Y. Tamaki, K. Tanimoto and M. Mitsuishi. Microsurgical robotic system for vitreoretinal surgery, 2011. Published online, www.springerlink.com.
- [36] Intuitive Surgical, Inc., May 2011. <http://www.intuitivesurgical.com>.
- [37] I. Iordachita, Z. Sun, M. Balicki, J. Kang, S. Phee, J. Handa, P. Gehlbach, and R. Taylor, A sub-millimetric, 0.25 mm resolution fully integrated fiber-optic force-sensing tool for retinal microsurgery, *International Journal of Computer Assisted Radiology and Surgery (IJCARS)*, 4 (4):383–390, 2009.
- [38] A.D. Jagtap and C.N. Riviere. Applied force during vitreoretinal microsurgery with handheld instruments. *26th Annual IEEE International Conference of the Engineering in Medicine and Biology Society*, pages 2771-2773, 2004
- [39] P.S. Jensen, P.K. Gupta and E. de Juan Jr. Quantification of microsurgical tactile perception. *Engineering in Medicine and Biology, 1999. 21st Annual Conf. and the 1999 Annual Fall Meeting of the Biomedical Engineering Society BMES/EMBS Conference*, 1999.
- [40] P. Kazanzides. Safety design for medical robots. *IEEE Annual International Conference of the Engineering in Medicine and Biology Society*, pages 7208-7211, 2009.
- [41] M. Kilchenman and M. Goldfarb. Force saturation, system bandwidth, information transfer, and surface quality in haptic interfaces. *IEEE International Conference on Robotics and Automation (ICRA)*, 2:1382- 1387, 2001.
- [42] K. Krøyer, O. M. Jensen and M. Larsen., Objective Signs of Photoreceptor Displacement by Binocular Correspondence Perimetry: A Study of Epiretinal Membranes, *IOVS*, 46:1017-1022, 2005
- [43] R. Kumar, P. Berkelman, P. Gupta, A. Barnes, P.S. Jensen, L.L. Whitcomb and R.H. Taylor. Preliminary experiments in cooperative human/robot force control for robot assisted microsurgical manipulation. *IEEE International Conference on Robotics and Automation (ICRA)*, 1:610-617, 2000
- [44] D.S. Kwon, K. Y. Woo, S. K. Song, W. S. Kim and H. S. Cho. Microsurgical telerobot system. *IEEE/RSJ International Conference on Intelligent Robots and Systems (IROS)*, 2:945–950, 1998.
- [45] J. C. Locke and W. R. Morton. Further studies of the viscosity of aspirated human vitreous fluid: with special reference to its use in retinal detachment surgery. *Transactions of the American Ophthalmological Society*, 63:129-145, 1965.
- [46] H. Logan Brooks Jr. Macular hole surgery with and without internal limiting membrane peeling. *Ophthalmology*, 107(10):1939-1948, 2000.
- [47] Maquet Getinge Group, *Operating table system, Alphamaquet 1150*, www.maquet.com, 2010
- [48] P. Massin, C. Allouch, B. Haouchine et al. Optical coherence tomography of idiopathic macular epiretinal membranes before and after surgery. *American Journal of Ophthalmology*, 130:732–739, 2000.
- [49] Maxon Motor. *High precision drives and systems*, 2010/2011.
- [50] H.C.M. Meenink, *Surgical Robot*, Patent: NL233598 (2009)
- [51] H. C. M. Meenink, R. Hendrix, P. C. J. N. Rosielle, M. Steinbuch, H. Nijmeijer and M. D. de Smet. A master-slave robot for vitreo-retinal eye surgery. *Proceedings of the 10th International Conference of the European Society for Precision Engineering & Nanotechnology (EUSPEN)*, 2:408 – 411, 2010.

- [52] H. C. M. Meenink, P. C. J. N. Rosielle, M. Steinbuch and M. D. de Smet. Instrument manipulator for a master-slave robot for vitreo-retinal ophthalmic surgery. *International Conference of Society for Medical Innovation and Technology (SMIT)*, page 53, 2009.
- [53] H. C. M. Meenink, P. C. J. N. Rosielle, M. Steinbuch and M. D. de Smet. A slave robot for vitreo-retinal ophthalmic surgery. *International Conference of Society for Medical Innovation and Technology (SMIT)*, 2010.
- [54] B. Mitchell, J. Koo, M. Iordachita, P. Kazanzides, A. Kapoor, J. Handa, G. Hager, and R. Taylor. Development and Application of a New Steady-Hand Manipulator for Retinal Surgery. *IEEE International Conference on Robotics and Automation*, pages 623-629, 2007
- [55] M. Moriyama, K. Ohno-Matsui, K. Hayashi, N. Shimada, T. Yoshida, T. Tokoro and I. Morita. Topographic Analyses of Shape of Eyes with Pathologic Myopia by High-Resolution Three-Dimensional Magnetic Resonance Imaging, *Ophthalmology*, 2011.
- [56] T. Nakano, N. Sugita, T. Ueta, Y. Tamaki and M. Mitsuishi. A parallel robot to assist vitreoretinal surgery. *International Journal of Computer Assisted Radiology and Surgery*, 4(6):517 – 526, 2009
- [57] C.S. Nickerson. *Engineering the mechanical properties of ocular tissues*, PhD thesis, California Institute of Technology, 2005.
- [58] Nippon Thompson CO., IKO, *Micro linear way LWL*, cat-57143, 2005.
- [59] H. Okudera, S. Kobayashi, K. Kyoshima, H. Saito and R. Mochizuki. “Three-dimensional Hi-vision system for microneurosurgical documentation based on wide-vision telepresence system using one camera and one monitor.” *Neurologia medicochirurgica*, pages 719-721, 1993.
- [60] Orfit, *Efficast® high precision masks for head, neck and shoulders*, www.orfit.com, 2011
- [61] J.R. Phillips and N.A. McBrien. Form deprivation myopia: elastic properties of sclera. *Ophthalmic Physiological Optics*, 15:357-362, 1995.
- [62] J. Pransky, ROBODOC — surgical robot success story. *Ind Robot*, 24:231–23, 1997.
- [63] J.S. Pulido, M.E. Zobitz and K.N. An. Scleral penetration force requirements for commonly used intravitreal needles. *Eye*, 21:1210–121, 2007.
- [64] M. Raja, S. Anshuman, R. Rajeev, K. Sannapaneni and K. Baruch. Faster visual recovery after 23-Gauge vitrectomy compared with 20-Gauge vitrectomy. *Retina*, 30:1511-1514, 2010
- [65] Reliance, Precision Mechatronics LLP, *Precision motion control components & mechatronic assemblies*, 2006.
- [66] C. N. Riviere, R.S. Rader, and P. Khosla, Characteristics of hand motion of eye surgeons, *19th Annual Conference of the IEEE Engineering in Medicine and Biology Society*, pages 1690 – 1693, 1997.
- [67] S. Rizzo, F. Patelli, D.R. Chow, *Essentials in Ophthalmology: Vitreo-retinal Surgery, Progress III*. Springer-Verlag Berlin Heidelberg, 2009, ISBN 978-3-540-69461-8.
- [68] S. Rizzo, F. Genovesi–Ebert, S. Murri, C. Belting, A. Vento, F. Cresti, M. Palla and E. Di Bartol. 25 Gauge Sutureless Vitrectomy and Standard 20 Gauge Pars Plana Vitrectomy in Idiopathic Epiretinal Membrane Surgery: A Comparative Study. *Graefe’s Archive for Clinical and Experimental Ophthalmology*, 244(4):472-479.
- [69] S. Rizzo, F. Genovesi-Ebert and A.J. Augustin. Small-Gauge Incision Techniques: The art of wound construction. *Retina today*, Jan/Feb 2009.
- [70] P. C. J. N. Rosielle and E. A. G. Reker. *Constructieprincipes 1 - bedoeld voor het nauwkeurig bewegen en positioneren*, Lecture notes 4007 (in Dutch), TU/e, 2000.

- [71] R. B. Rusu, W. Meeussen, S. Chitta and M. Beetz. Laser-based perception for door and handle identification. *IEEE International Conference on Advanced Robotics (ICAR)*, pages 1 – 8, 2009.
- [72] C. Schaeffer and T. May. Care-O-bot: A System for Assisting Elderly or Disabled Persons in Home Environments. *In Proceedings of AAATE-99*, Düsseldorf, 1999
- [73] Schaeffler Technologies GmbH & Co. KG, *Technisches Taschenbuch*, May 2002.
- [74] M. D. de Smet and M. E. Carlborg, Managing severe endophthalmitis with the use of an endoscope. *Retina*, 25:976-98, 2005.
- [75] M. D. de Smet and M. Mura. Minimally invasive surgery - endoscopic retinal detachment repair in patients with media opacities. *Eye*, 22:662 – 665, 2008.
- [76] W. E. Smiddy, R. G. Michels and W. R. Green. Lens and peripheral retinal relationships during vitrectomy. *Retina*, 11(2):199 – 203, 1991.
- [77] Spitznas M. Motorized teleguided stereotactic micromanipulator for vitreous microsurgery. *Arch Ophthalmol* 101:623-630, 1983.
- [78] Steinmeyer GmbH, *Miniature ball screws*, 2003.
- [79] M. K. Tameesh, R. R. Lakhanpal, et al., Retinal vein cannulation with prolonged infusion of tissue plasminogen activator (t-PA) for the treatment of experimental retinal vein occlusion in dogs, *American Journal of Ophthalmology*, 138(5):829-839, 2004.
- [80] R.H. Taylor and D. Stoianovici. Medical robotics in computer-integrated surgery. *IEEE Transactions on Robotics and Automation*, 19(5):765- 781, 2003.
- [81] R.H. Taylor, H.A. Paul, P. Kazanzides, B.D. Mittelstadt, W. Hanson, J. Zuhars, B. Williamson, B. Musits, E. Glassman and W.L. Bargar. Taming the bull: safety in a precise surgical robot. *Fifth International Conference on Advanced Robotics, ICAR*, 1:865-870, 1991.
- [82] M. Tenorth, U. Klank, D. Pangercic and M. Beetz. Web-Enabled Robots. *Robotics & Automation Magazine, IEEE* , 18(2):58-68, 2011
- [83] T. Ueta, Y. Yamaguchi, Y. Shirakawa, Taiga N, et. Al., Robot-Assisted Vitreoretinal Surgery: Development of a Prototype and Feasibility Studies in an Animal Model, *Ophthalmology*, 116(8):1538-1543, August 2009.
- [84] A. Uneri, M.A. Balicki, J. Handa, P. Gehlbach, R.H. Taylor and I. Iordachita. New steady-hand Eye Robot with micro-force sensing for vitreoretinal surgery. *3rd IEEE RAS and EMBS International Conference on Biomedical Robotics and Biomechatronics (BioRob)*, pages 814-819, 2010.
- [85] S. B. Vohra and P. A. Good. Altered globe dimensions of axial myopia as risk factors for penetrating ocular injury during peribulbar anaesthesia. *British Journal of Anaesthesia*, (2): 242-245, 2000.
- [86] M. Waibel, M. Beetz, J. Civera, R. D’Andrea, J. Elfring; D. Gálvez-López, K. Häussermann, R. Janssen, J.M.M. Montiel, A. Perzylo, B. Schießle, M. Tenorth, O. Zweigle and R. van de Molengraft, “RoboEarth,” *Robotics & Automation Magazine, IEEE*, 18(2):69-82, June 2011.
- [87] W. Wei, R. E. Goldman, H. F. Fine, S. Chang and N. Simaan. Performance evaluation for multi arm manipulation of hollow suspended organs. *IEEE transactions on robotics*, 25(1):147 – 157, 2009.
- [88] W. Wei, R. E. Goldman, N. Simaan, H. F. Fine and S. Chang. Design and theoretical evaluation of micro-surgical manipulators for orbital manipulation and intraocular dexterity. *IEEE International Conference on Robotics and Automation (ICRA)*, pages 3389 – 3395, 2007.

- [89] Wilkins JR, Puliafito CA, Hee MR, et al. Characterization of *epiretinal membranes* using optical coherence tomography. *Ophthalmology*, 103:2142–2151, 1996.
- [90] H. Yamanobe, M. Tagami, T. Komori, M Ito. Reliability of Flexible Flat Cables with Excellent Bending Property, U.D.C. 621.315.213-418: 620.177.6-192.
- [91] P.N. Youssef, N. Sheibani and M.D. Albert. Retinal light toxicity, *Eye*, 25(1):1-14, 2011.
- [92] Y. Sato, Takako Isomae, Macular hole surgery with internal limiting membrane removal, air tamponade, and 1-day prone positioning, *Japanese Journal of Ophthalmology*, 47(5):503-506, Sep-Oct 2003.

Appendix A

Anatomical terms of location

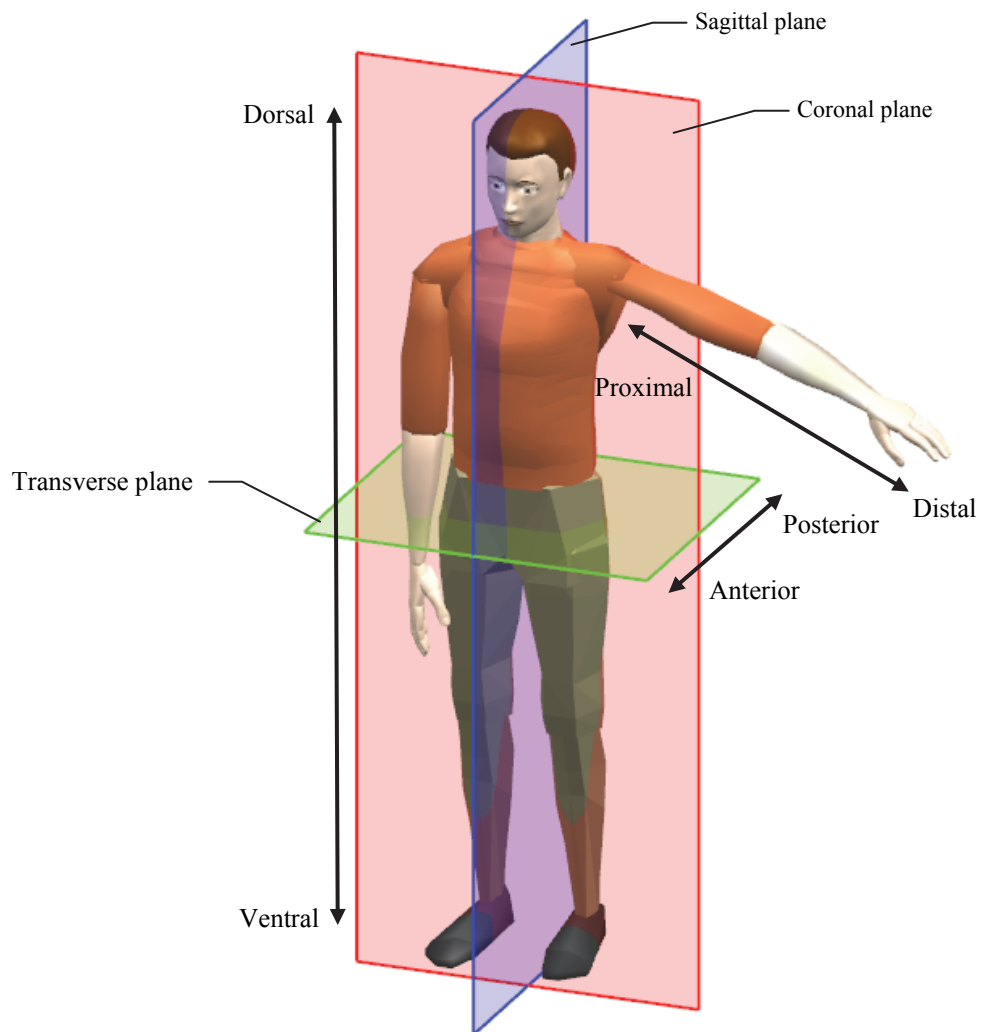


Figure A. 1/ The anatomical terms of location.

Calculations of the Θ -manipulator

B.1 Resistance to manipulate Θ

The resistance to rotate the Θ -DoF in the eye depends on the rolling resistance of the ball bearing, the friction torque with the cannula and the viscous friction resistance. The resistance of the roller bearing is estimated on an axial bearing preload $F_a = 10$ N, the bearing raceway diameter $r_{race} = 8.5$ mm and the estimated rolling resistance $\eta_b = 0.1\%$.

$$T_{fr.b} = F_a r_{race} \eta_b = 0.085 \text{ Nmm} \quad (\text{B.1})$$

The resistance of the friction between the instrument and cannula due to the sclera squeezing the cannula, is based on the calculation of a thick walled pressure vessel. Here, the tangential direction of the sclera is considered as the radial thickness of the wall (for r_0). The strain of tissue after penetrating is typically $\epsilon_{scl} = 30\%$, the modulus of elasticity of the sclera is not univocal [61] but maximal $E_{scl} = 3.5$ MPa.

The stress (on the instrument) in the sclera due to strain will be:

$$\sigma_{scl} = E_{scl} \epsilon_{scl} = 1.05 \text{ MPa} \quad (\text{B.2})$$

The pressure at the instrument, assuming that the outer radius of the sclera $r_0 = 3$ mm and the inner $r_i = 0.3$ mm will be:

$$p_{inst} = \sigma_{scl} \frac{(r_0^3 - r_i^3)}{(r_0^3 + r_i^3)} = 1.047 \text{ MPa} \quad (\text{B.3})$$

With the thickness of the sclera, $t = 1$ mm [14], the pressure surface is:

$$A = 2\pi r_{out} t = 1.88 \text{ mm}^2 \quad (\text{B.4})$$

The coefficient of friction is considered to be $\mu = 0.1$, for a contact with a moisture film, by which the applied friction torque will be:

$$T_{fr.scl} = p_{inst} A r_{out} \mu = .059 \text{ Nmm} \quad (\text{B.5})$$

The viscous friction of the vitreous humour is determined by:

$$T_{vis} = 4\pi r_{inst}^2 L_{inst} \eta_{vitr.h.} \omega = 5.65 \cdot 10^{-10} \text{ Nm} \quad (\text{B.6})$$

With $r_{instr} = 0.3 \text{ mm}$ the radius of instrument's tube, $L_{instr} = 25 \text{ mm}$ the length of the instrument, $\eta_{vitr.h.} = 2 \cdot 10^{-3} \text{ Ns/m}^2$ the viscosity of the vitreous humour [45] and $\omega = 10 \text{ rad/s}$ the approximate angle velocity. The viscous friction torque is a fraction of the resistance of the bearing and the friction with the trocar and therefore can be neglected.

With neglecting the low torque of T_{vis} , this results in a total resistance torque of:

$$T_{\Theta r} = T_{fr.scl} + 2T_{fr.b} = 0.176 \text{ Nmm} \quad (\text{B.7})$$

In practice, a free run torque of $T_{free} = 0.072 \text{ Nmm}$ is measured.

B.2 Θ -bearing calculation

The Θ -bearing design is based on dimensions derived by the calculation method in [73]. The parameters on which the bearing is based are presented in Table B. 1.

Table B. 1/ Parameters of the Θ -bearing.

Parameter		Description
$R_{11} = R_{12}$	0.35 mm	Ball radius bi-directional
R_{21}	8 mm	Bearing inner raceway radius
R_{22}	-0.4 mm	Raceway groove radius (negative for concave shape)
E	200 GPa	Young's modulus for stainless steel
ν	0.24	Poisson ration for stainless steel
n	13	Number of balls
α	45°	Contact angle
F_z	10 N	Axial preload force
F_c	1.09 N	Normal contact force per ball
ξ	2.3	Calculation coefficient from Table 8.17.1 in [73]
η	0.544	Calculation coefficient from Table 8.17.1 in [73]
ψ/ξ	0.922	Calculation coefficient from Table 8.17.1 in [73]

The effective curvature is calculated by:

$$\Sigma(r^{-1}) = r_{11}^{-1} + r_{12}^{-1} + r_{21}^{-1} + r_{22}^{-1} = 3.34 \text{ mm}^{-1} \quad (\text{B.8})$$

With factor $\cos(\tau)$, calculation coefficients ξ , η and ψ/ξ are derived from Table 8.17.1 in [73], these are presented in Table B. 1. $\cos(\tau)$ is calculated by:

$$\cos(\tau) = \frac{(r_{11}^{-1} - r_{12}^{-1} + r_{21}^{-1} - r_{22}^{-1})}{\Sigma(r^{-1})} = 0.79 \quad (\text{B.9})$$

The elliptic bi-directional lengths of the contact surface are calculated via C.3 and C.4. Here, a is the length in axial direction and b the length in tangential direction.

$$a = \xi \sqrt[3]{\frac{3F_c(1-\nu^2)}{\Sigma(r^{-1})E}} = 38 * 10^{-3} \text{ mm} \quad (\text{B.10})$$

$$b = \eta \sqrt[3]{\frac{3F_c(1-\nu^2)}{\Sigma(r^{-1})E}} = 9.1 * 10^{-3} \text{ mm} \quad (\text{B.11})$$

The Hertzian contact stress for an elliptic contact surface is calculated by:

$$\sigma_{hz} = \frac{1}{\eta\xi} \sqrt[3]{\frac{3F_c E^2 (\Sigma(r^{-1}))^2}{8\pi^3 (1-\nu^2)^2}} = 1525 \text{ MPa} \quad (\text{B.12})$$

For the 52 Rockwell C bearing raceway, the Hertzian stress of 1525 MPa is well within acceptable limits (2780 MPa [12][73]).

To determine the axial bearing stiffness, the compression is calculated first. Per contact this is:

$$\delta = \frac{\psi}{\zeta} \sqrt[3]{\frac{9F_c^2 \Sigma(r^{-1})(1-\nu^2)^2}{8E^2}} = 3.66 * 10^{-4} \text{ mm} \quad (\text{B.13})$$

With 4 times δ and the contact angle, the total axial displacement becomes $f_{bz} = 1.0 * 10^{-3} \text{ mm}$. As $\Delta\delta$ decreases with the increase of F_c , the stiffness is calculated over an increase of 1% of F_c . This results in a stiffness of $c_{bz} = 1580 \text{ N/mm}$.

Calculations of the Z-manipulator

C.1 Finite element analysis of the 2-DoF Z-carriage suspension

Tetrahedral 3D elements are used. The overall element size is set to 0.5 mm. For the struts, the size is adjusted to 0.1 mm, which results in 3 elements over the thickness. The mounting surface to the Z-carrier is used for the fixing constraint. Loads are applied to the mounting surface (and edges) of the carriage. Figure C. 1 shows the stiffness finite element analysis (FEA) in all six degrees of freedom. In Table C. 1 the corresponding overload analysis is presented. Axes correspond to modeling reference. Herein, X is the longitudinal axis of the carriage, Y the normal axis and Z the perpendicular sideways axis.

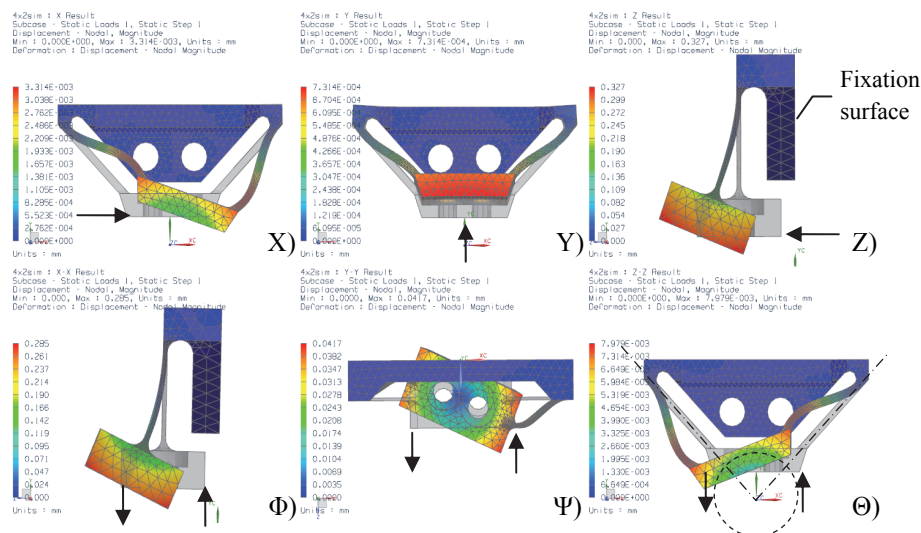


Figure C. 1/ FEA stiffness analysis of the 2-DoF Z-carriage suspension in six degrees of freedom. Loads applied correspond to Table C. 1.

The X and Y degree of freedom must be stiff (the Z DoF and the DoF normal to carriage). The others are desired to be compliant, not to overload the LWL linear way carriage. Table C. 1 shows the rotation/displacement values at which the carriage would be overloaded. For Z, Φ and Ψ these values cannot be reached and are presented illustratively. The Θ stiffness is relatively high, but considered not to be that relevant, because it is unlikely there will be much difference in height along the raceway grinding direction. Furthermore, the initial Θ mounting misalignment is eliminated by the slight oversized mounting holes, to attach the 2-DoF Z-carriage suspension to the Z-carrier.

Table C. 1/ Misalignment values to overload the LWL micro linear way

	Force/Torque	Deflection	Stiffness	Overload at:	Image
X	1 N	1.1 μm	910 N/mm	N/a	(X)
Y	1 N	0,73 μm	1370 N/mm	0.048 mm	(Y)
Z	1 N	327 μm	3,05 N/mm	21.6 mm*	(Z)
Φ	3 Nmm	0.197 rad	15.2 Nmm/rad	4.39 rad*	(Φ)
Ψ	5 Nmm	0.122 rad	40.9 Nmm/rad	2.20 rad*	(Ψ)
θ	5 Nmm	1.9 mrad	2627 Nmm/rad	0.026 rad	(Θ)

*A fictive statement, as this rotation/displacement cannot be achieved.

C.2 Finite element analysis of the 2-DoF Z-nut suspension

To validate the design of the 2-DoF Z-nut suspension, a finite element analysis is used. Four DoF are made compliant and the strength in those directions is analyzed. Its design uses four similar leaf springs. Therefore, only one leaf spring is analyzed in X and Φ direction (Figure C. 2). The maximum misalignment is limited to $\Phi = \pm 0.5^\circ$ and $X = 0.15 \text{ mm}$. This is well within the machining accuracies of the parts that can

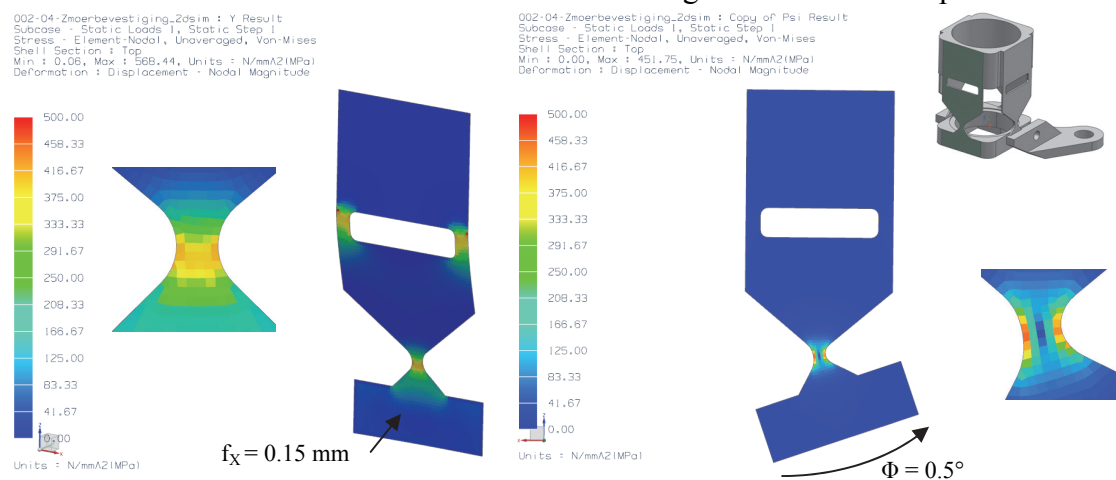


Figure C. 2/ FEA analysis of the 2-DoF Z-nut suspension in X and Φ direction.

cause misalignment of the Z-nut and leadscrew. 2D elements are used, with a size of 0.1 mm to create 5 elements over the thickness of the hinge. The leaf spring is constrained at the top, where the leaf spring is fixed to the model. A displacement is set to the lower end. The maximum stress is about $\sigma_X = 400$ MPa for the maximum displacement in X-direction and $\sigma_\Phi = 450$ MPa for the rotation in Φ -direction. This is below the yield stress of $\sigma_{0.2} = 550$ MPa of stainless steel AISI 420.

C.3 Relation between forces during an instrument change

In the procedure of changing instruments, an instrument is fixated to the bi-stable instrument clamp and/or to the instrument holder at the container. Figure C. 3 shows a schematic representation of the forces acting on the instrument during an instrument change, with:

- F_{Cc} : the axial force when the bi-stable clamp is closed,
- F_{Co} : the axial force when the bi-stable clamp is opened,
- F_{hr} : the axial force of the instrument pushing against the rim at the holder,
- F_{frh} : the friction force of the instrument to the holder,
- F_{ftl} : the friction force of the instrument to the leaf spring,
- F_{sp} : the force of the spring.

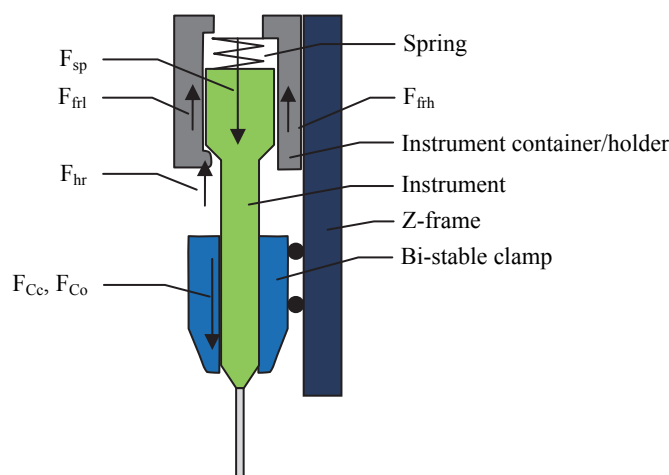


Figure C. 3/ Schematic representation of the forces acting on the instrument during an instrument change.

When an instrument is taken from the holder, F_{Cc} must be higher than sum of the forces at the holder:

$$F_{Cc} > 2F_{hr} + F_{frh} - F_{sp} \quad (C.1)$$

When the bi-stable clamp is opened, leaving the instrument in the holder:

$$F_{Co} < 2F_{hr} + F_{frh} - F_{sp} \quad (C.2)$$

In C.1 and C.2 F_{frh} is not included, because when the instrument touches the rim, it is assumed the leaf springs lose contact with the instrument. Further, when the instrument is in the holder, the spring must be able to push the instrument down against the rim, but the rim must keep the instrument inside the holder:

$$F_{frh} + 2F_{frl} < F_{sp} \quad (C.3)$$

$$2F_{hr} + F_{frh} > F_{sp} \quad (C.4)$$

As a break loose safety measure, the axial clamping force is set to $F_{Cc} = 2$ N (Section 4.4.2). When the bi-stable clamp is in open position, the instrument goes in freely, as it has a running fit. To ensure its operation, it is assumed F_{C0} can be up to 0.5 N. F_{frh} , F_{frl} and F_{rh} depend on the leaf spring's radial preload force (F_r) and the coefficient of friction between the container and the instrument ($\mu_h = 0.10$ for UHMWPE with PPSU). The friction force on with the rim (F_{rh}), also depends on the rim and instrument contact angle (α_{rim}). Parameters F_r , α_{rim} and μ_h are chosen and designed as such to get:

- $F_{hr} = 1.4$ N
- $F_{frh} = 0.14$ N
- $F_{frl} = 0.14$ N
- $F_{sp} = 0.6$ N

Analysis of the parallelogram mechanism

D.1 Finite element analysis of the parallelogram mechanism

Two parts in the parallelogram mechanism have elastic hinges, these are: the Ψ -drive A-arm and the motor/bearing housing. Obviously, these elastic elements may not fail and therefore their design is determined by use of Finite Element Analysis (FEA).

Ψ -drive A-arm

The Ψ -drive A-arm has two leaf springs, which each consist of two elastic hinges and a stiffened middle part (Figure 4.19). The hinges have a thickness of 0.1 mm and a radius of 1.5 mm. The leaf springs have a length of 10 mm and a height of 7 mm. A maximum lateral misalignment of 0.2 mm is used, which is well within the part accuracy of modern tooling methods. This relates to a lateral deflection of $f_Y = 0.17$ mm, which results in a leafspring rotation of 1° . This corresponds to a leadscrew rotation of 0.13° . The maximum lateral deflection is limited by an end limit stop.

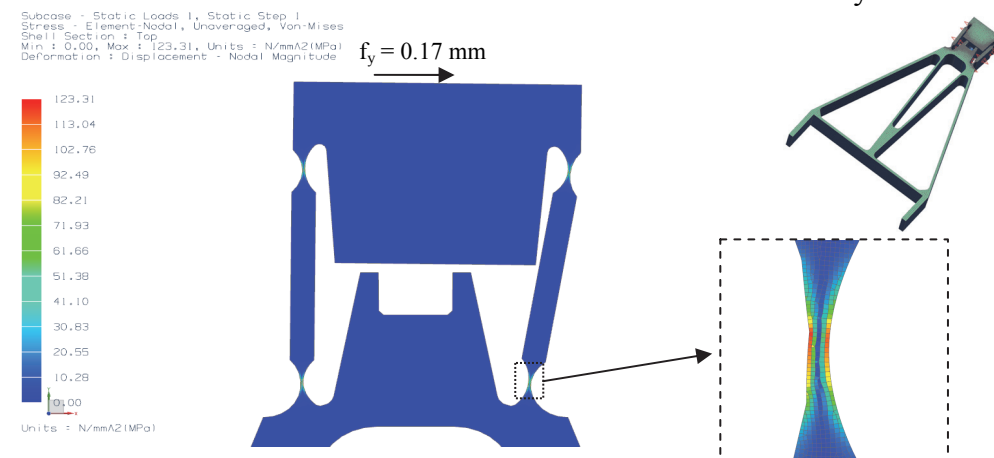


Figure D. 1/ Von Mises FEA of the Ψ -drive A-arm hinges. The maximal Von Mises stress at $f_Y = 0.17$ mm is $\sigma_{VM} = 120$ MPa.

Rectangular 2D elements are used, by which the element size at the hinges is adjusted to create five elements over the thickness. The Von Mises stress at maximum deflection is $\sigma_{VM} = 120$ MPa (Figure D. 1), which is within the yield stress of $\sigma_{0.2} = 260$ MPa of the material used: Aluminium 6082.

Ψ -drive motor/bearing housing

The hinges at the Ψ -drive motor/bearing housing are analyzed in the same way. The FEA result is shown in Figure D. 2. Rectangular 2D elements are used, which size is adjusted at the hinge, to create five elements over the thickness. The hinge has a radius of 1.5 mm and a thickness of 0.18 mm. De maximal rotation is limited by the gap width that creates the hinge and is about 1° . The gap width is 0.15 mm and is set as the displacement.

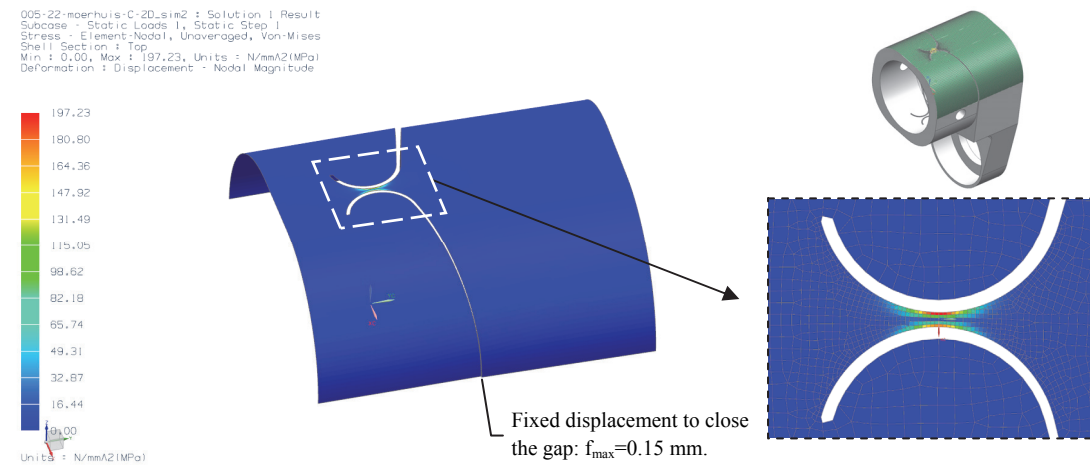


Figure D. 2/ Von Mises FEA at maximum rotation of the hinge in the motor/bearing housing of the Ψ -drive.

At maximum angular deflection, the maximum Von Mises stress is about $\sigma_{vm} = 195$ MPa, which is within $\sigma_{0.2} = 260$ MPa of the material used: Aluminium 6082. The actual maximum angular deflection is defined by the lateral displacement of the Ψ -drive A-arm. By this rotation of 0.13° , the Von Mises stress is $\sigma_{vm} = 25$ MPa.

Φ and Ψ stiffness analysis of the parallelogram mechanism

Here, the results are presented of the Φ and Ψ stiffness analysis of the parallelogram mechanism. The FEA is constructed as discussed in Section 4.6. For the Φ analysis, a load in Y-direction, $F_Y = 10$ N (chosen for practicality, normally $F_Y < 1$ N), is applied at a height of 62.5 mm to the Z-frame. A rotation of $\Phi = 740$ μ rad and a shift sideways of $Y = 40$ μ m, can be derived from the FEA result (Figure E. 1). This results in a stiffness of $k_\psi = 0.84 \cdot 10^6$ Nmm/rad and $c_Y = 250$ N/mm.

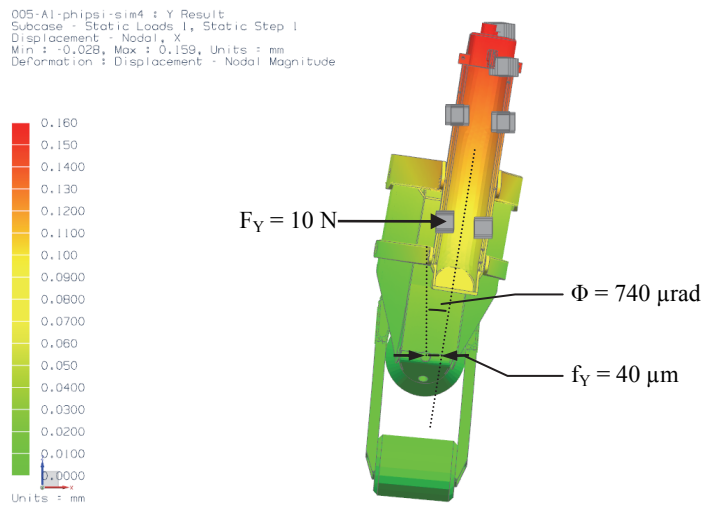


Figure E. 1/ Stiffness analysis in Φ -direction; a load in Y-direction applied at a height of 62.5 mm results in a deflection in Y-direction and a rotation about the Φ -axis.

In a similar fashion the stiffness in Ψ -direction is analyzed (Figure E. 2). Here, the load is applied in X-direction. From the FEA, a rotation of $\Psi = 150 \mu\text{rad}$ and displacement of $f_X = 20 \mu\text{m}$ are derived. The stiffness in Ψ and X direction is respectively $k_\Psi = 4.20 \cdot 10^6 \text{ Nmm/rad}$ and $c_X = 500 \text{ N/mm}$.

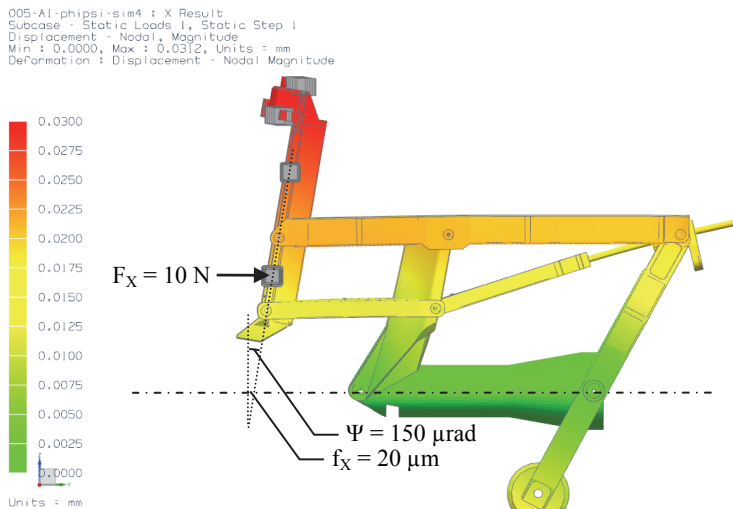


Figure E. 2/ Stiffness analysis in Ψ -direction; a load in X-direction applied at a height of 62.5 mm results in a deflection in X-direction and a rotation about the Φ -axis.

Samenvatting

Vitreo-retinale chirurgie heeft betrekking op operaties aan het glasachtig lichaam en aan het netvlies in het oog. Ingrepen bestaan uit het verwijderen van het glasvocht, het verwijderen van een membraan van het netvlies en/of het herstellen van een netvliesloslating. Operaties worden uitgevoerd op een minimaal invasieve wijze, waarbij dunne naaldachtige instrumenten via kleine incisies in het oog worden gebracht. De te gebruiken instrumenten worden met de hand bediend in vier graden van vrijheid rond het toegangspunt tot het oog. Deze vrijheidsgraden zijn: twee rotaties om de tip van het instrument zijwaarts te bewegen, een axiale translatie en een rotatie rond de lengte as van het instrument. Het bedienen van bijvoorbeeld een pincetje of schaarje aan de punt van het instrument, kan worden beschouwd als een vijfde vrijheidsgraad.

De chirurg staat voor verschillende uitdagingen bij het handmatig uitvoeren van vitreo-retinale procedures. Een vaste hand en nauwkeurige instrumentbewegingen zijn vereist bij het opereren van delicaat weefsel van slechts enkele micrometers dik. Hierbij kan de chirurg maximaal twee instrumenten tegelijk hanteren. Zijwaartse bewegingen worden gespiegeld door het rotatiepunt op het toegangspunt tot het oog en geschaald afhankelijk van de insteekdiepte. Operatiekrachten die uitgeoefend worden op het instrument, liggen over het algemeen onder de menselijke gevoelsgrens. Hierdoor heeft de chirurg enkel visuele feedback, verkregen via een microscoop of een endoscopisch systeem. Deze beide optische systemen dwingen de chirurg te werken in een statische en onergonomische zithouding. Hoewel de kennis en vaardigheid van de chirurg in de loop van zijn carrière verbetert, zal het toenemen van handtrillingen hem op hogere leeftijd beperken om operaties uit te voeren.

Een robotisch systeem in de vorm van een master-slave systeem vergroot de mogelijkheden van een chirurg. De slave robot wordt boven het oog geplaatst en voert de daadwerkelijke operatie uit door de instrumenten te hanteren. De instrumenten worden gemanipuleerd door instrumentmanipulators. Deze worden bediend door de chirurg via haptische pennen vanuit de master. Door middel van elektronische hardware en softwarematige regelalgoritmen zijn de master en slave met elkaar verbonden. Met robotische ondersteuning is het mogelijk om: handtrillingen te filteren,

bewegingen op te schalen of krachten versterkt terug te koppelen naar de master. Daarnaast kan een ergonomische werkhouding worden aangeboden. Deze mogelijkheden kunnen de handelingen van de chirurg vereenvoudigen en zijn loopbaan verlengen. Dit proefschrift richt zich op het ontwerp en realisatie van een slave robot voor vitreo-retinale oogchirurgie.

De slave robot heeft twee hoofd componenten: de instrumentmanipulatoren en het passieve ondersteunende systeem hiervan. Het heeft een compact, lichtgewicht en eenvoudig te installeren ontwerp en is volledig uitgerust voor een complete operatie. Eisen en eigenschappen van de slave robot zijn gebaseerd op handmatig uitgevoerde operaties, gesprekken met oogartsen en analyses van de menselijke anatomie en vitreo-retinale ingrepen.

Het passieve ondersteunende systeem creëert een stijve verbinding tussen de instrumentmanipulator, de patiënt en de operatie tafel. Met behulp van instelmogelijkheden kunnen de instrumentmanipulatoren, voorafgaand aan de operatie, op het oog gepositioneerd worden. Een deel van het ondersteunend systeem is geïntegreerd in de hoofdsteen van de patiënt. Hieraan worden, via de zijkant, de ondersteunende manipulator armen bevestigd. Afhankelijk van het te opereren oog (bijv. het linker oog), wordt een lage ondersteunende arm aan de operatie zijde van het hoofd geplaatst (links) en een hoge arm aan de overstaande zijde (rechts). Hierbij reikt de instrumentmanipulator op de hoge arm, over het hoofd en de neus naar het te opereren oog. Het compacte, lichtgewicht en eenvoudig te installeren ontwerp draagt bij aan een korte installatietijd en snelle verwijdering in geval van een complicatie. Om een operatiebereik te krijgen soortgelijk aan dat van handmatige uitgevoerde operaties, is de lay-out van de instrumentmanipulatoren geoptimaliseerd.

Tenminste twee instrumentmanipulatoren worden gebruikt voor bimanuele operaties. Additionele manipulatoren kunnen worden gebruikt voor niet continu actieve instrumenten, zoals een endoscoop of een illuminator. Evenals bij de handmatig uitgevoerde operaties, hebben de instrumentmanipulatoren vier vrijheidsgraden. Operatiekrachten worden gemeten en teruggekoppeld naar de haptische pennen. De instrumentmanipulator is ontworpen op hoge stijfheid, is spelingsvrij en heeft een lage weerstand om dun weefsel te opereren met een hoge nauwkeurigheid. Iedere manipulator is uitgerust met een instrument wisselsysteem, waarmee het instrument op een snelle en veilige manier gewisseld kunnen worden. Een compact ontwerp maakt het operatiegebied toegankelijk en laat ruimte voor de microscoop boven het oog.

In het ontwerp van de slave robot zijn verschillende veiligheidsmaatregelen verwerkt, zoals een “quick release” mechanisme voor de instrumentmanipulatoren en een extra veiligheidspal op de klemmen die het ondersteunende systeem fixeren. Er zijn extra veiligheidsmaatregelen voorgesteld, zoals een beschermkap over de instrumentmanipulatoren en parallel lopende regelalgoritmen. Voor de veiligheid van de patiënt is, met behulp van een kunststof masker, een methode voorgesteld om het hoofd te fixeren aan de hoofdsteen tijdens een operatie.

Dankwoord

Het ontwerpen van een robot zoals beschreven in dit proefschrift, kun je niet alleen. Verschillende mensen hebben mij ondersteund om tot dit resultaat te komen.

Als eerste wil ik Nick Rosielle bedanken. Van jou heb ik de afgelopen jaren ontzettend veel geleerd over de kunst van *Constructie Principes*. Ik vond het erg plezierig en een grote eer om in jouw lab en onder jouw begeleiding dit project te mogen volbrengen. Ik heb erg veel respect en bewondering voor je onuitputtende bron van kennis, ideeën, oplossingen, verhalen en anekdotes.

Ik ben erg trots en vind het een hele eer dat ik dit schitterende project in de groep van prof. Maarten Steinbuch heb mogen realiseren. Maarten, bedankt voor je vertrouwen in mij en voor het feit dat je me de kans voor dit promotietraject hebt gegeven. Ik bewonder je om je kennis en kunde (in zo ongeveer alles), maar vooral ook vanwege je positieve houding en je onuitputtelijke enthousiasme, waarmee je mensen weet te motiveren. Jij hebt altijd het overzicht over het project gehad, waarin ik de vrijheid kreeg om onderzoek te doen en me te ontplooien.

Prof. Marc de Smet (AMC UvA, Montchoisi Clinic), jou wil ik bedanken voor het wegwijs maken in de oogheelkunde, het bespreken van al mijn ideeën en vragen, en het geven van de nodige feedback op mijn werk. Ik vond het altijd erg boeiend om de wereld van de techniek samen te brengen met die van de geneeskunde. Mensen met een vooruitziende blik zoals jij, zijn daarbij onmisbaar.

De slave robot voor vitreo-retinale chirurgie is gerealiseerd door Michiel van Gorp (TU/e GTD). Michiel, bedankt voor de prettige samenwerking. Het is fijn te weten dat er een vakbekwaam persoon staat aan wie je je ontwerp over kunt dragen. Michiel is iemand die begrijpt wat je wenst. Je weet zeker dat hetgeen hij realiseert, ook echt goed is. Verder wil ik iedereen van de GTD bedanken die Michiel hierbij ondersteund of geholpen hebben, met name Mariëlle vanwege haar uitstekende vonkwerk.

Verder wil ik Prof. Henk Nijmeijer, naast het beoordelen van mijn proefschrift, ook bedanken voor de prettige samenwerking binnen het projectteam.

Dr. Erik van Oosterhout (CZE) wil ik bedanken voor het lezen van mijn proefschrift, geven van additionele feedback op medisch gebied, de hulp bij de speurtocht naar patiëntveiligheid en het uitdragen van het project bij het Nederlandse Oogheelkundig Genootschap.

Directe (oud)collega's uit het Constructies en Mechanismen lab en natuurlijk ook uit de DCT groep: Simon, Geert-Jan, Raimondo, Chris, Rens, Roger, Kees V., Kees M., George, Gerrit, Ruud en alle anderen die ik niet genoemd heb, wil ik bedanken voor de samenwerking. In het bijzonder wil ik Ron Hendrix bedanken voor alle adviezen en voor de prettige samenwerking binnen het EyeRHAS project. Linda van den Bedem wil ik bedanken voor een luisterend oor en de gezellige gespreksstof. Geertje Janssen, Lia Neervoort en Petra Aspers bedank ik voor hun ondersteuning tijdens de afgelopen jaren.

De mensen die er voor hebben gezorgd dat de instrumentmanipulators uitgerust zijn met een uniek stukje elektronica zijn Ruud van den Bogaert, Arthur Ketels en Richard Ketels (KSMF).

Zonder financiering is een project al EyeRHAS niet mogelijk. Daarom wil ik dan ook Lou Hulst, Casper Langerak, Eddy Schipper en Annette Steggerda bedanken van SenterNovem/Agentschap NL.

Project partner TNO heeft een belangrijke rol gespeeld. Zonder de themamiddag over medische technologie was dit project waarschijnlijk niet tot stand gekomen. Een woord van dank gaat dan ook uit naar Pieter Kappelhof, Ian Saunders, Jeroen Heijmans, Michiel Oderwald, Bart Dirkx en Bas de Kruif voor het opzetten en het leiden van dit project. Ook Sandy, Fokko, Irene, Gert en Raymond wil ik bedanken voor hun input in het project.

Alle leden van de begeleidingscommissie wil ik via deze weg graag bedanken voor de interesse, kritische blik, de vele op- en aanmerkingen en alle andere input bij de halfjaarlijkse bijeenkomsten.

Tenslotte wil ik mijn familie bedanken voor alles wat ze voor mij gedaan hebben en natuurlijk de steun in de afgelopen vier jaren. Met jullie steun ben ik deze uitdaging aangegaan en heb ik het succesvol kunnen afronden. Pa en Ma, Joost en Femke, Gerrit en Janny, Karien en Esmee bedank ik hiervoor. Joost, mede door ons motto: "bij ons is nog nooit iets niet gelukt", is ook dit proefschrift tot een mooi resultaat gekomen. In het bijzonder wil ik mijn lieve vriendin Anne bedanken. Het is prettig om een fijne baan te hebben, maar niets gaat boven een fijn thuis. Al die credits zijn voor jou. Jij bent er altijd om plezier mee te maken en om op terug te vallen. De laatste maanden heb je veel voor mij moeten opvangen. Alle tijd en aandacht die je de afgelopen maanden voor mij hebt gegeven, ga ik dubbel en dwars inhalen!

Thijs Meenink

Steenderen, september 2011.

Curriculum Vitae

Thijs Meenink was born on June 11, in 1982, Steenderen, the Netherlands. After graduating secondary school in 2000 at the Baudartius College in Zutphen the Netherlands, he studied Automotive Engineering at the Hogeschool Arnhem en Nijmegen in Arnhem the Netherlands. He graduated in 2004 and received his B.Eng. degree in Product Development. In 2004, he started the Mechanical Engineering study at Eindhoven University of Technology in Eindhoven, the Netherlands. He received his M.Sc. degree in 2007 within the Constructions and Mechanisms group, as a part of the Control Systems Technology section. The M.Sc. thesis was entitled: “The design of an instrument manipulator for a Master- μ Slave Robot to perform eye surgery.”. In 2007 he started as a PhD student at Eindhoven University of Technology. As a result he designed a slave system for vitreo-retinal eye surgery. Results of that work are presented in this thesis.

